2011

Post-translational Modifications, Structure and Function of Human Lens Crystallins

Chinwe Asomugha
University of Alabama at Birmingham

POST-TRANSLATIONAL MODIFICATIONS, STRUCTURE AND FUNCTION OF HUMAN LENS CRYSTALLINS

by

CHINWE OBIOMA ASOMUGHA

OM P. SRIVASTAVA, CHAIR
KENT T. KEYSER
ALECIA K. GROSS
DENNIS J. PILLION
DAVID R. WHIKEHART

A DISSERTATION

Submitted to the graduate faculty of The University of Alabama at Birmingham,
in partial fulfillment of the requirements for the degree of
Doctor of Philosophy

BIRMINGHAM, ALABAMA

2011

POST-TRANSLATIONAL MODIFICATIONS, STRUCTURE AND FUNCTION OF HUMAN LENS CRYSTALLINS

CHINWE O. ASOMUGHA

VISION SCIENCES

ABSTRACT

Cataract is an opacification of the lens causing reduction in vision over time. It is one of the leading causes of vision loss among adults age 55 and older. The lens is a transparent structure that focuses incoming light onto the retina for visual perception. It has a high protein content, attributed mainly to water-soluble proteins known as crystallins. With age, crystallins undergo post-translational modifications (PTMs) that alter their structural and/or functional properties and, in turn, lead to cataract formation.

The purpose of this research was to take a top-down approach in understanding changes in lens proteins with age, starting with determining the overall changes in crystallins occurring in cortical and nuclear regions of the lens, followed by determining effects of PTMs (deamidation and truncation) on structural/functional properties of αB-crystallin, and concluding with studies of molecular properties of individual N-terminal domain (NTD), core domain (CD), and C-terminal extension (CTE) of αA- and αB-crystallins. In the first study, a combination of laser capture microdissection (LCM), 2-D Difference Gel Electrophoresis (2-D DIGE), and Matrix-Assisted Laser Desorption/Ionization Time-of-Flight (MALDI-TOF) and Electrospray Ionization Quadripole Linear Ion-Trap Liquid Chromatography (ESI-QTRAP LC-MS/MS) mass spectrometry were used to map and identify the *in situ* protein profile and PTMs of crystallins in the cortical and nuclear regions of aging human lenses. Crystallin fragmentation resulting from truncation began in the cortical region and continued into

the nuclear region, whereas aggregation was predominantly observed in the nuclear region.

One way to study the effects of PTMs is to create mutants that mimic *in vivo* modifications (i.e., truncation and deamidation) and examine their altered structural and functional properties. In the second study, the structural and functional properties of deamidated, N- or C-terminally deleted, and deamidated plus N- or C-terminally deleted mutants of αB-crystallin were analyzed. Relative to WT αB, the N146 deamidation and N-terminal deletion caused greater structural and functional changes in the crystallin. In the third study the molecular properties of NTD, CD, and CTE constructs of αA- and αB-crystallins were analyzed. The individual α-crystallin regions exhibited varied biophysical properties and each region alone retained some level of chaperone function.

Keywords: Lens, Crystallins, Cataract, Chaperone, Deamidation, Post-translational modifications

DEDICATION

To Daddy and Mommy, Mr. Lawrence C. Asomugha, Sr and Mrs. Ekele E. Asomugha. Thank you for your eyes that see me for me, your ears that listen to the good and the bad, your hands that hold even from afar, your feet that are always ready to move to action, and your hearts that love me through it all. Thank you for being praying parents.

To my brothers, Lawrence Jr (Junior) and Chimela O'kezie (Kez); aka the "A" boys. Need I say more? Thank you for encouraging me in your own quiet ways, and for always having my back when it counted.

To the extended family and church family, I am grateful for your continuous support and genuine concern.

We've come a long way family, and I thank God for each of you.

ACKNOWLEDGMENTS

I would like to thank my committee members for their willingness to serve, for making themselves available to me, and for their valuable input and contributions. Thank you to my advisor, Dr. Om Srivastava, for giving me the opportunity to work in an area of research I was initially unfamiliar with. All in all, I have grown as a person and as a scientist having passed through your lab. To Dr. Kent Keyser, who will forever be referred to as "the reason I came to Vision Sciences," thank you for taking a chance on me after our brief encounter at ARVO in 2005, for thinking enough of me that I would fit into the program, and for always opening your office door. I thank Dr. Alecia Gross, who has become my personal "Jillian Michaels" in this process, caring to see me succeed and willing to whip me into gear if needed, so that I could go forth and "dream." To Dr. Pillion and Dr. Whikehart, thank you for your commitment and for trekking up the hill and juggling your schedules to serve. You all have helped me stay afloat in uncharted waters.

I am forever indebted to Dr. Ratna Gupta, who has guided me from near and far. Your hard work and effort, which sometimes went unacknowledged, were not lost on me. Thank you for seeing my strengths and for working with me to minimize my weaknesses. For your genuine friendship and for treating me as another "sister," I am ever grateful.

Thank you to the rest of the Srivastava lab members, past and present, – Mrs. Kiran Srivastava, Dr. Mauro Chaves, and Roy Joseph – that directly and indirectly motivated me to finish. Thank you for your contributions.

I cannot forget to thank staff members in the department. Ms. Linda Phillips, thank you for your ever encouraging words. You had a knack for saying something uplifting even without knowing I needed to hear it, and we shared some really good laughs too. Dr. Ramona Hart, you have been a point of contact and a great reference since before I officially arrived. Thank you for letting me harass you with every possible odd question about what needed to be done, from day one. Your statement, "Let me know if there's anything I can do to help," was more than just words, and was made manifest in your many actions on my behalf. Thank you to Mr. David Parkinson. From the first joke I heard you crack, I knew we would get along. Thanks for keeping me laughing every time I crossed your path and for always pointing out the brighter side of things. Your humor was equally balanced by your organization and willingness to find a resolution to any given issue. Mr. Clifford Kennon, I cannot say thank you enough. You have been a true friend in every sense and another "big brother." Thank you for helping with everything from UAB issues to car maintenance issues, and for always allowing me to come in your office when I was "having a moment."

A big thank you to my fellow graduate students, colleagues, and friends within the department, across departments, and across state lines, with whom I could share the struggles of graduate student life; you know who you are. We've shared many laughs, ideas, and vented to one another at times. Best wishes to each of you going forward.

Once again, to my family who continue to hold me up when my legs feel too weak to stand, thank you.

TABLE OF CONTENTS

Page

LIST OF TABLES

Table *Page*

IDENTIFICATION OF CRYSTALLIN MODIFICATIONS IN THE HUMAN LENS CORTEX AND NUCLEUS USING LASER CAPTURE MICRODISSECTION AND CYDYE LABELING

STRUCTURAL AND FUNCTIONAL ROLES OF DEAMIDATION OF N146 AND/OR TRUNCATION OF N- OR C-TERMINI IN HUMAN αB-CRYSTALLIN

CHARACTERIZATION OF PROPERTIES OF N-TERMINAL DOMAIN, CORE DOMAIN, AND C-TERMINAL EXTENSION OF αA- AND αB-CRYSTALLINS

LIST OF FIGURES

Figures *Page*

INTRODUCTION

IDENTIFICATION OF CRYSTALLIN MODIFICATIONS IN THE HUMAN LENS CORTEX AND NUCLEUS USING LASER CAPTURE MICRODISSECTION AND CYDYE LABELING

STRUCTURAL AND FUNCTIONAL ROLES OF DEAMIDATION OF N146 AND/OR TRUNCATION OF N- OR C-TERMINI IN HUMAN αB-CRYSTALLIN

CHARACTERIZATION OF PROPERTIES OF N-TERMINAL DOMAIN, CORE DOMAIN, AND C-TERMINAL EXTENSION OF αA- AND αB-CRYSTALLINS

LIST OF ABBREVIATIONS

2-DE	Two dimensional electrophoresis
2D-DIGE	Two dimensional – difference gel electrophoresis
2D-PAGE	Two dimensional – polyacrylamide gel electrophoresis
αA	alpha A
αB	alpha B
ANS	8-anilino-1-naphthalene sulfonate
CyDye	Sulfonated indocyanine dye
CP49	Phakinin
Da	Dalton
DTT	Dithiothreitol
ESI-QTRAP LC/MS/MS	Electrospray Ionization Quadripole Linear Ion-Trap Liquid Chromatography
HMW	High molecular weight
IEF	Isoelectric focusing
IgG	Immunoglobin G
IPG	Immobilized pH gradient gel
IPTG	Isopropyl β-D-1-thiogalactopyranoside
kDa	Kilodalton
LCM	Laser capture microdissection
LMW	Low molecular weight

MALDI-TOF	Matrix-assisted laser desorption ionization – time of flight
MALS	Multi-angle light scattering
mL	Milliliter
mM	Millimolar
M_r	Molecular weight
nm	Nanometer
PCR	Polymerase chain reaction
PTMs	Post-translational modifications
SDS-PAGE	Sodium dodecyl sulfate – polyacryamide gel electrophoresis
μg	Microgram
μm	Micrometer
V	Volt
WI	Water-insoluble
WS	Water-soluble
WT	Wild type

GLOBAL INTRODUCTION

Background and Significance

Lens

The human lens is a biconvex, transparent avascular structure located in the anterior segment of the eye (Figure 1). Because it is avascular, it is nourished by the aqueous humor, a clear liquid within the anterior segment. Essential nutrients, such as glucose, diffuse in through Na^+/K^+ ATPase pumps located in lens epithelial cells and waste diffuses out at the equatorial regions. Glucose metabolism is the primary source of energy for the lens, and occurs mainly via anaerobic respiration. Suspensory ligaments known as zonules suspend the lens between the anterior and posterior chambers of the eye. These zonular fibers attach to the lens near its equator and connect it to the ciliary body, whose muscles relax and contract, causing the lens to change shape and curvature. By changing its curvature, the lens is able to focus objects at various distances, a process known as accommodation. It is through accommodation that the lens accomplishes it main purpose, which is to focus incoming light onto the retina for visual processing (Andley, 2007; Bloemendal et al., 2004; Harding, 1997).

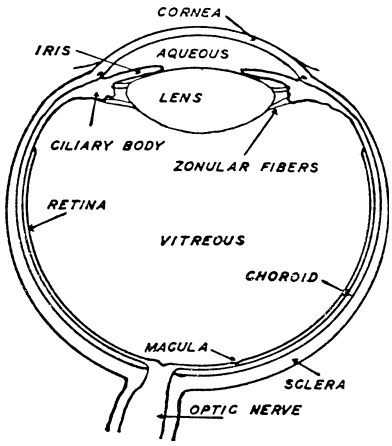

Figure 1 - Sketch of the human eye. The lens functions to focus incoming light onto the retina at the back of the eye

Note: From "Viewing molecular mechanisms of ageing through a lens" by J. J. Harding, 2002, *Ageing Research Reviews*, *1(3)*, p. 466. Copyright 2002 by Elsevier Science Ireland, Ltd. Reprinted with permission.

A collagenous capsule makes up the outermost non-cellular layer of the lens. On the anterior surface of the lens is a single layer of simple cuboidal epithelial cells, which are the progenitors of the lens fiber cells (Figure 2). Epithelial cells continuously divide and move toward the equator, where they elongate into fiber cells, and each new layer of cells is placed outside slightly older cells (Duncan, Wormstone, & Davies, 1997; Harding, 1997). During elongation and compression into the nucleus, cell nuclei and organelles are lost, which allows for lens transparency. The lack of cell and protein turnover in the lens tissue means that nuclear fiber cells, as well as nuclear lens proteins, exist from birth to death. This also means that over time lens structural proteins, known as crystallins, are susceptible to undergoing post-translational modifications (PTMs) that cause changes in their structure and function.

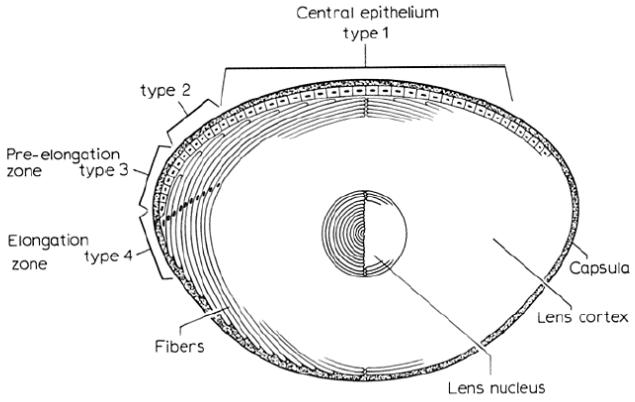

Figure 2 – Schematic of the lens. Epithelial cells divide, travel toward the equator, and elongate during the process of differentiating into fiber cells, with the oldest fiber cells forming the nucleus and less mature fiber cells making up the cortex.

Note: From "Lens differentiation. Crystallin synthesis in isolated epithelia from calf lenses" by A. J. Vermorken, J. M. Hilderink, W. J. van de Ven, and H. Bloemendal, 1978, *J Cell Biol, 76*, p. 176. Copyright 1978 by Rockefeller University Press. Reprinted with permission.

Crystallins

Crystallins are a group of soluble, globular, structural proteins that account for almost 90% of the total protein content of the lens. The crystallins are grouped into two major classes: α-crystallins, which are present in both epithelial and fiber cells, and βγ-crystallins, which are synthesized in the fiber cells (Harding, 1997). α-Crystallin serves as both a structural and functional protein in the lens, due to its chaperone-like activity, whereas βγ-crystallins serve as structural proteins. As structural proteins, α-, β-, and γ-crystallins contribute to lens transparency and refractive power mainly because of their short-range interactions *in vivo* (Andley, 2007; Bloemendal et al., 2004; Harding, 1997). Thus, they assist in providing a clear path for light passing through the lens to be focused onto the retina.

Of the crystallins, α-crystallin is the most abundant and, therefore, a major contributor to lens transparency. α-Crystallin has been reported to account for 30-50% of total lens protein within mature lens fiber cells. It exists *in vivo* as a large heterogeneous oligomer of ~800 kDa composed of two ~20 kDa subunits, αA and αB, in a 3:1 ratio. α-Crystallins belong to a family of small heat shock proteins (sHSPs), made of 12-43 kDa monomers that mostly form larger oligomers of 150-800 kDa. Like other sHSPs, α-crystallin contains a highly conserved α-crystallin domain sequence of 80-100 residues (αA= residues 64-140; αB= residues 67-150), and independently folded N-terminal domain (αA= residues 1-63; αB= residues 1-66), and a flexible unstructured C-terminal extension (αA= residues 141-173; αB= 151-175) (Harding, 1997) (Figure 3). Members of small heat shock protein family are known to be stress-inducible proteins that show molecular chaperone activity, whereby they sequester unfolded or improperly folded proteins and prevent their aggregation and interaction with other proteins in order to maintain transparency (Andley, 2007; Bloemendal et al., 2004). α-Crystallin has been shown to have chaperone activity (Horwitz, 1992). αA and αB distributions vary such that αA is lens-specific while αB is more widely expressed, especially in the brain, heart, and muscle (Bhat & Nagineni, 1989; Bloemendal et al., 2004; de Jong, Caspers, & Leunissen, 1998).

αA:
MDVTIQHPWF KRTLGPFYPS RLFDQFFGEG LFEYDLLPFL SSTISPYYRQ
SLFRTVLDSG ISEVRSDRDK FVIFLDVKHF SPEDLTVKVQ DDFVEIHGKH
NERQDDHGYI SREFHRRYRL PSNVDQSALS CSLSADGMLT FCGPKIQTGL
DATHAERAIP VSREEKPTSA PSS

αB:
MDIAIHHPWI RRPFFPFHSP SRLFDQFFGE HLLESDLFPT STSLSPFYLR
PPSFLRAPSW FDTGLSEMRL EKDRFSVNLD VKHFSPEELK VKVLGDVIEV
HGKHEERQDE HGFISREFHR KYRIPADVDP LTITSSLSSD GVLTVNGPRK
QVSGPERTIP ITREEKPAVT AAPKK

Figure 3 – Amino acid sequences of human WT αA and WT αB lens crystallins. Amino acids labeled in green identify the N-terminal domain (WT αA residues no. 1-63 and WT αB residues no. 1-66), in black identify the core domain (WT αA residues no 64-140 and WT αB residues no. 67-150), and in blue identify the C-terminal extension (WT αA residues no. 141-173 and WT αB residues no. 151-175). Red labeled amino acids are the deamidation sites (WT αA residues no. 101 and 123; WT αB residues no. 78 and 146) where Asn (N) is deamidated to Asp (D).

β-crystallins are oligomers of ~ 40-200 kDa composed of ~ 25-35 kDa subunits, while γ-crystallins are monomers of 20 kDa. The major difference between β- and γ-crystallins is that the β-crystallins contain N-terminal extensions, and basic β-crystallins have additional C-terminal extensions (Bloemendal et al., 2004). There are six primary gene products of the β-crystallins: basic βB1, βB2, βB3 and acidic βA3/A1, βA2, and βA4, which are further divided based on size into β-high (βH) and β-low (βL) fractions. The mammalian genome contains 7 γ-crystallins (γA, γB, γC, γD, γE, γF, and γS), however γA, γB, γC, γD, and γS are the only ones present in humans (Bloemendal et al., 2004; Harding, 1997;). Both β and γ crystallins are found primarily in the lens (Harding, 1997).

Post-translational Modifications

Over time, lens crystallins undergo post-translational modifications. These PTMs that occur with aging are thought to be a causative factor in the development of human cataracts because of their effects on protein structure, solubility, and interactions (Bloemendal et al., 2004, Horwitz, 1992). It is believed that these modifications lead to conformational changes and unfolding or improper folding of α-, β-, and γ-crystallins, which further lead to their aggregation and cross-linking. Several PTMs have already been identified in human lenses, including truncation, deamidation, phosphorylation, and oxidation (Gupta & Srivastava, 2004a; Gupta & Srivastava, 2004b; Hanson, Hasan, Smith, & Smith, 2000; Lampi, Amyx, Ahmann, & Steel, 2006; Lampi et al., 1998; Takemoto & Boyle, 1998; Takemoto, 1998; Srivastava & Srivastava, 2003), to name a few, and have been shown to alter crystallin stability, solubility, and function. Deamidation of Asn and Gln residues has repeatedly been identified as the most commonly occurring modification (Hains & Truscott, 2007; Harms et al., 2004; Takemoto, 1998a; Takemoto, 1998b; Lampi, 1998, Ma et al., 1998; Wilmarth et al., 2006), but there appears to be a greater prevalence of deamidated Gln residues in human crystallins. Deamidation of Asn-101 and Asn-123 in human αA-crystallin and deamidation of Asn-146 in human αB-crystallin alter both structural and functional properties of these crystallins, even affecting the ability of αA-crystallin to oligomerize with αB-crystallin (Gupta, 2004a; Gupta 2004b). β- and γ-crystallin oligomerization and solubility has also been shown to be adversely affected by deamidation which increases βB1 tendency to aggregate, destabilizes βB2 dimers and decreases solubility of γS-crystallin (Harms et al., 2004; Lapko, Purkis, Smith, & Smith, 2002; Lampi et al., 2006).

It seems possible that deamidation, with its addition of a negative charge to a once neutral amide, causes protein unfolding and exposure of buried surfaces that leave the protein more accessible to further deamidation and other modifications, leading to eventual insolubility.

Truncation is another frequently occurring modification in the human lens. Both the N- and C-termini truncation of α-crystallin has been detected, though C-terminal truncation is more common in the human lens (Ma et al., 1998), along with N-terminal truncation of βB1, βB2 and βA3/A1 (Lund, Smith, & Smith, 1996; Ma et al., 1998; Smith, Sun, Smith, & Green, 1992; Srivastava, 2003). Studies in our lab have also demonstrated that truncation of specific motifs (motif III and IV) in human lens βA3-crystallin destabilizes its structure, and suggested that the N-terminal domain was more stable than the C-terminal extension (Gupta et al., 2006). As with deamidated crystallin-species, fragmented crystallins, resulting from various truncations, are also increasingly present in the water-insoluble fraction of aging and cataractous human lens as compared to the water-soluble fraction (Hanson et al., 2000; Harrington, McCall, Huynh, Srivastava, & Srivastava, 2004; Lund et al. 1996). The presence of αB- but not αA-crystallin in the water-insoluble urea-insoluble fraction suggests that αB-crystallin has a major role in crystallin insolubility (Harrington, Srivastava, & Kirk, 2007). α-Crystallins are also known to function as molecular chaperones, as established by Horwitz (1992) and the C-terminal extension of α-crystallin is particularly involved in its ability to chaperone other proteins (Takemoto, Emmons, & Horowitz, 1993). It is important then to understand the effects of truncation particularly of α-crystallin and its chaperone function as it is an essential part of understanding aggregation and insolubility of crystallins.

Recent studies in our lab have shown that deamidation of both asparagines (N101 and N123) is more crucial than truncation of N- and C-termini in maintaining chaperone function of αA-crystallin, however, both the N- and C-termini are still important to chaperone activity (Gupta 2004b, Chaves, Srivastava, Gupta, & Srivastava, 2008).

Some modifications can be important to protein function, such as phosphorylation, while others are a consequence of aging and stress (i.e. oxidative stress, UV-exposure). Conversely, *in vivo* point mutations such as those of a highly conserved Arg at equivalent positions in αA (R116C) and αB (R120G), located in the α-crystallin domain, have caused structural changes that lead to hereditary cataracts (Bova et al., 1999; Cobb & Petrash, 2000; Kumar, Ramakrishna, & Rao, 1999; Liu et al., 1999). However, certain modifications such as deamidation and truncation of the native protein alter protein structure and/or function and cause aggregation. Aggregation and cross-linking of crystallins, resulting from age-related post-translational modifications and leading to the formation of insoluble products, have been linked to cataract development.

Cataract

Cataracts are one of the leading causes of blindness in the world (Bloemendal et al., 2004). A cataract is generally defined as an opacity or cloudiness of the lens. Many studies suggest that cataract development is due to mutations or post-translational modification of lens crystallins that result in incorrect folding and eventually formation of insoluble aggregates of α-, β-, and γ-crystallins. Protein-protein interactions are altered as a result of aggregation. Such changes in protein structure affect protein function and thereby disturb the short-range interactions that maintain lens transparency (Andley,

2007; Bloemendal et al., 2004; Harding, 2002). Although much work has been done, the actual molecular mechanism by which age-related cataractogenesis occurs appears to be multifactoral and, therefore, has not been solidified as yet.

Overall Goal and Hypothesis

Overall Goal

The overall goal of this study was to determine the molecular mechanism of cataractogenesis in human lens and clarify the role of post-translational modifications such as deamidation and truncation on the structural and functional properties of α-crystallins.

Overall Hypothesis

Post-translational modifications such as deamidation and/or truncation increase with age and alter both structural and functional properties of α-crystallins leading to their aggregation.

Specific Aims and Hypotheses

Specific Aim 1

Map the *in situ* protein profile and post-translational modifications in cortical and nuclear regions of normal aging human lenses.

Specific Aim 1 Rationale

Much of the work on crystallins has been accomplished using *in vitro* studies (Hanson et al., 2000; Lampi et al., 1998; Lampi et al., 2006; Lapko et al., 2002;

Takemoto, 1998a; Takemoto, 1998b; Srivastava, 2003). *In vivo* studies of human lenses have used paraffin-embedded tissue, which has less physiological relevance than frozen human lens tissue sections (Boyle & Takemoto, 1997; Harding, Chylack, Susan, Lo, & Bobrowski, 1983). LCM and 2-D Difference Gel Electrophoresis (2D-DIGE) are two relatively new analytical techniques that allow isolation of specific tissues/cells and identification of proteins at low concentrations (Banks et al., 1999; Espina et al., 2006; Kondo & Hirohshi, 2007; Simone, Bonner, Gillespie, Emmert-Buck, & Liotta, 1998; Simone, Paweletz, Charoneau, Petricoin, & Liotta, 2000).

Specific Aim I Hypothesis

The *in situ* protein profile of normal aging human lenses should show increased presence of post-translationally modified crystallin species in the nuclear region as compared to the cortical region.

Specific Aim II

Determine the effect of deamidation and/or truncation on the protein structure and chaperone function of human αB-crystallin.

Specific Aim II Rationale

Deamidation of α-crystallins is one of the most commonly occurring post-translational modifications that occur during aging and cataract development (Bloemendal et al., 2004; Hains, & Truscott, 2007; Ma et al., 1998; Takemoto, 1998a; Takemoto, 1998b;). N- and C-terminal truncations are also post-translational

modifications that occur commonly in α-crystallins with age (Hanson et al., 2000; Lund et al., 1996; Ma et al., 1998). Literature has already established that αB-crystallin is a better chaperone than αA-crystallin, it is more prevalent in various tissues apart from the lens, and it has been associated with several neurodegenerative diseases. Previous studies in Dr. Srivastava's lab have identified deamidation of Asn *in vivo* and studied its effects on structure and function of αB-crystallin *in vitro* (Gupta, 2004a; Gupta, 2004b Srivastava, 2003). Deamidation of Asn146 in αB-crystallin altered structural and functional properties more compared to deamidation of Asn 78 (Gupta, 2004a). However, these studies have not looked at the effects of both deamidation and truncation of the αB-crystallin. Similar studies from this lab have looked at such effects on αA-crystallin (Chaves, Srivastava, Gupta, & Srivastava, 2008). The relative significance of deamidation and/or truncation on structure and function of human αB-crystallin is presently unknown.

Specific Aim II Hypothesis

Deamidation and/or truncation will alter both structural and functional properties of αB-crystallin. Comparative analysis of effects of deamidation and/or truncation on αB-crystallin will help understand their effects on stability and chaperone activity of the crystallin, as well as provide further insight into the molecular mechanism of cataractogenesis.

Specific Aim III

To determine chaperone activity and biophysical properties of N-terminal domain, Core domain, and C-terminal extension proteins of αA- and αB-crystallins.

Specific Aim III Rationale

The target protein-binding region of αA- and αB-crystallins seems to reside between the N-terminal and the Core domains **(**Bhattacharyya, Udupa, Wang, & Sharma, 2006; Narberhaus, 2002; Reddy, Kumar, & Kumar, 2006; Sharma, Kumar, Kumar, & Quinn, 2000**)**. However, variations in study results suggest that virtually every region of α-crystallin is vital for its chaperone function (Bhattacharyya et al., 2006; Derham et al., 2001; Ghosh, Estrada, & Clark, 2005; Muchowski, Wu, Liang, Adam, & Clark, 1999; Reddy et al., 2006; Sharma et al., 2000).

Specific Aim III Hypothesis

Mutations, such as truncation, to any of these regions (i.e., the N-terminal domain, Core domain, and/or C-terminal extension) will affect both their biophysical properties and chaperone function.

IDENTIFICATION OF CRYSTALLIN MODIFICATIONS IN THE HUMAN LENS CORTEX AND NUCLEUS USING LASER CAPTURE MICRODISSECTION AND CYDYE LABELING

by

CHINWE O. ASOMUGHA, RATNA GUPTA, and OM P. SRIVASTAVA

Molecular Vision; 16: 476-494

Format adapted and errata corrected for dissertation

Abstract

Purpose

With aging, lens crystallins undergo post-translational modifications (PTMs) and these modifications are believed to play a major role in age-related cataract development. The purpose of the present study was to determine the protein profiles of crystallins and their PTMs in the cortical and nuclear regions within an aging human lens to gain a better understanding about changes in crystallins as fiber cells migrate from cortical to nuclear region.

Methods

Laser capture microdissection (LCM) was used to select and capture cells from cortical and nuclear regions of 12 μm, optimum cutting temperature (OCT) compound-embedded frozen lens sections from a 69-year-old human lens. Proteins were extracted and then analyzed by 2-D difference gel electrophoresis (2-D DIGE) with sulfonated indocyanine dye (CyDye) labeling. Crystallin identities and their PTMs were then determined by Matrix-Assisted Laser Desorption/Ionization Time-of-Flight (MALDI-TOF) and Electrospray Ionization Quadripole Linear Ion-Trap Liquid Chromatography (ESI-QTRAP LC-MS/MS) mass spectrometry.

Results

Crystallin fragments (M_r <20 kDa) were present in both cortical and nuclear regions, while high molecular weight (HMW) aggregates (M_r > 35 kDa) were mostly localized in the nuclear region. HMW complexes contained a relatively large number of truncated and modified β-crystallins, compared to α- and γ-crystallins, and two lens-specific intermediate filaments, CP49 (phakinin) and filensin. Modified α-crystallins were in low

abundance in the nuclear region compared to the cortical region. Several PTMs, including deamidation, oxidation, phosphorylation, ethylation, methylation, acetylation, and carbamylation, were identified in virtually all crystallins and CP49. The data provide the first report of human lens crystallin profiling by a combination of LCM, 2D-DIGE, and mass spectrometric analysis.

Conclusions

The results suggested that as the fiber cells migrate from cortical region to the nuclear region, the crystallin degradation begins in the cortical region and continues in the nuclear region. However, a greater number of the HMW complexes exist mainly in the nuclear region.

Introduction

Crystallins (α, β, and γ) are structural proteins whose ability to form soluble oligomers in high concentrations, along with their specific short-range interactions, increase the refractive power of the lens and maintain lens transparency [1,2]. α-Crystallin is a large heterogenous oligomer, present in both epithelial and fiber cells, and composed of two primary gene products, αA- and αB-crystallin. In the β/γ-crystallin superfamily, β-crystallin has seven primary gene products – four acidic (βA1-, βA2-, βA3-, and βA4-crystallin) and three basic (βB1-, βB2-, and βB3-crystallin) – while there are seven γ-crystallins (γA- to γF- and γS-crystallin), with only γA-, γB-, γC-, γD-, and γS-crystallin present in humans [3-5]. As a member of a larger small heat shock protein (sHSP) superfamily, α-crystallin functions as a molecular chaperone [6] to prevent non-specific aggregation of improperly folded or denatured proteins [7,8], and is therefore believed to play a critical role in maintaining lens transparency.

Post-translational modifications (PTMs) that occur with aging are thought to be one of the causative factors in human cataract development because of their effects on crystallin structure and interactions. Recent genetic studies clearly demonstrated that the association of human inherited autosomal dominant, congenital zonular or nuclear sutural cataracts with misfolded proteins or prematurely terminated crystallins was the result of truncation at the translational level [9-11]. Several PTMs have already been identified in human lenses, including deamidation [12,13], oxidation of Trp, Met, and His residues [14,15], disulfide bonding [16], glycation [17], transglutaminase-mediated cross-linking [18], methylation [19], phosphorylation, and truncation of crystallins, and have been shown to alter crystallin stability, solubility, and function [19-22]. However, deamidation has been identified as the most commonly occurring modification [12,13,23-25].

Cataractous lenses have previously shown selective insolubilization of βA3/A1- and βB1-crystallin fragments and relatively greater truncation, deamidation of Asn residues, and oxidation of Trp [26,27]. This was consistent with earlier studies which showed that a major fraction of water soluble (WS) protein in adult human lens is composed of modified crystallin species, specifically truncated βB1- and βA3/A1-crystallin, and that almost all human crystallins are subject to deamidation [24,28]. Studies have also concluded that the major modifications distinguishing WS- and water insoluble (WI)-crystallins were increased, which included disulfide bonding, oxidation of Met, deamidation of Gln and Asn, truncation of both NH_2- and COOH- termini of αA- and αB-crystallin, and backbone cleavage [29,30]. All of the above-mentioned studies used homogenized lens extracts. However, since homogenization of lenses in buffered solutions often solubilizes only part of the lens proteins [29], such studies that require

whole tissue homogenates may not accurately represent molecular events taking place in the cortical and nuclear regions. Further, how the distribution of modified crystallin species changes during migration of fiber cells from the cortical to the nuclear region within an aging human lens has not been investigated. Consequences of the above mentioned PTMs on crystallin structure and function have been investigated extensively, but mainly with in vitro studies. For example, results have shown various modifications including deamidation at specific sites altered structural and oligomeric properties of βB1-, βB2- and other crystallins [22,30,31], as well as the chaperone activity of both αA- and αB-crystallin [20,21]. Our recent studies have shown that deletion of the COOH-terminal extension, but not the NH_2-terminal domain, led to the insolubilization of αA-crystallin [32].

As an alternative approach to above in vitro studies, we used laser capture microdissection (LCM) and two-dimensional difference gel electrophoresis (2D-DIGE), which allow comparative expression following isolation of specific tissue/cells from the same tissue or identical regions of diseased versus normal specimens [33-36]. LCM is a one-step microdissection technique for acquiring cells from specific regions of tissue sections under direct visualization, while maintaining structural integrity and morphology. Therefore, it allows for in situ studies that correlate to in vivo events and decreases the likelihood of generating in vitro artifacts by minimizing tissue manipulation during sample acquisition [37]. Early LCM studies have shown that the LCM process itself does not alter samples [37]. This technique has mostly been used in studies investigating cancers in various tissues like the human brain [38], cervix [33], kidney [33], bladder [39], prostate [40], and colon [41], a small number of which have followed

LCM with protein analysis rather than DNA/RNA analysis. Studies also identified the spatial distribution of modified and unmodified proteins using two-dimensional electrophoresis (2-DE) of microdissected tissue regions [42-44]. Preliminary proteomic studies have shown compatibility of LCM with two-dimensional PAGE (2-D PAGE) to examine protein profiles of selected tissues, and often noted enrichment of some proteins compared to analyses of whole tissues [33,37,44]. However, crystallins and their modifications have not been analyzed using LCM, although PTMs of human αA-crystallin alone have been successfully studied using manual microdissection [45]. The study correlated increased truncation and modification of αA-crystallin with lens fiber cell age and depth within the lens.

Development of a multiplexing fluorescent electrophoresis method, 2D-DIGE, has been an advancement in 2-D PAGE [40,46] that allows labeling of 2–3 samples with different dyes, including an internal control, which is a pool of all samples that were individually labeled. All samples can be run on a single 2-D gel to minimize gel-to-gel variation and the number of gels required for one experiment. The ability to multiplex different sulfonated indocyanine dye (CyDye) DIGE Fluor minimal dye-labeled samples on the same gel means that the different samples will be subject to exactly the same 1st and 2nd dimension running conditions. Consequently, the same protein labeled with any of the CyDye DIGE Fluor minimal dyes and separated on the same gel will migrate to the same position on the 2D-gel and overlay. Again, this limits experimental variation and ensures accurate within-gel matching. Recent studies in cancer proteomics have applied 2D-DIGE analysis to LCM-acquired samples and have found it to be a powerful tool suitable for mass spectrometric protein identification [35].

To avoid the pitfalls of studying PTMs in human crystallins using whole lens homogenates, the present study used both LCM and 2D-DIGE to identify the regional distribution of crystallins and their PTMs in cortex and nucleus with age of a single lens. The present study reports a novel finding that truncation of crystallins begins in the cortical region and progressively extends to the nuclear region, while crystallin aggregation mainly occurs in the nucleus. These changes in crystallins represent those that occur during fiber cell migration from the periphery (cortex) to the central region (nucleus) with aging.

Methods

Tissue preparation and sectioning

Intact frozen normal human donor lenses, stored at −80 °C following excision from globes, were provided by Dr. Christine Curcio (UAB Department of Ophthalmology, Birmingham, AL). The lenses did not show any opacity and therefore were considered normal. Lenses were collected and transported on dry ice, then stored at −80 °C before use. Two lenses, one from a 65- and the other from 69-year-old donor, were thawed, embedded directly in optimum cutting temperature (OCT) compound (Tissue-Tek®; Sakura Finetek, Torrance, CA) at −20 °C, and tissue blocks were cut into 12 μm sections using a Shandon Cryotome E (ThermoFisher Scientific, Kalamazoo, MI). The multiple sections acquired were from anterior, equatorial, and posterior regions of the lenses. Individual sections were mounted onto PALM® polyethylene naphthalate (PEN) membrane slides (Carl Zeiss MicroImaging GmbH, Germany) and/or Fisherbrand Superfrost glass slides (Fisher Scientific, Pittsburgh, PA). Slides were stored at −80 °C before performing laser capture microdissection (LCM).

Laser capture microdissection

Just before microdissection, slides containing frozen sections were quick-thawed to room temperature, then fixed and dehydrated using a graded series of alcohols and cleared in xylene as follows: 70% ethanol (15 s), 95% (15 s), 100% (15 s), and xylene (5 min). The sections were then air-dried.

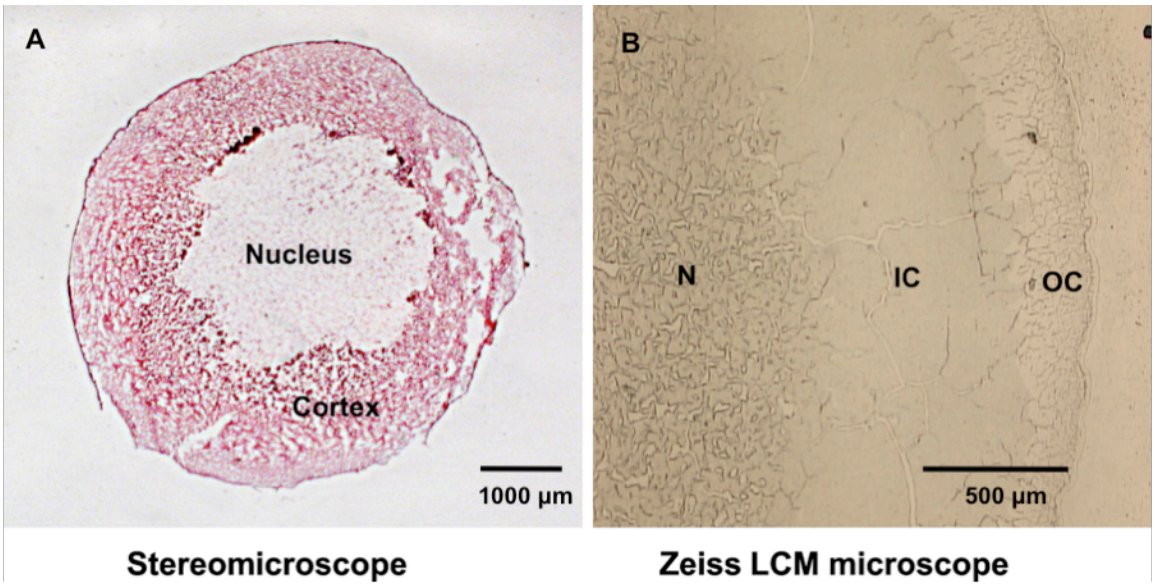

Note: From "Identification of crystallin modifications in the human lens cortex and nucleus using laser capture microdissection and CyDye labeling" by Asomugha et al., 2010, *Mol Vis, 16*, p. 476. Copyright 2010 by Molecular Vision. Reprinted with permission.

Figure 1. Tissue section of a human lens. **A**: Whole tissue section (12 µm) of 69-year-old lens stained with hematoxylin and eosin, as seen under a stereomicroscope with 4× magnification. All three major regions are present in this section, however the nucleus stained more faintly because of possible increased hydrophobicity of the proteins in this region. **B**: Unstained section showing the three major lenticular regions: Nucleus (N), Inner Cortex (IC), and Outer Cortex (OC), as seen during LCM with the Zeiss/PALM Microbeam microscope at its lowest magnification of 2.5×.

Cells from either three or two major lenticular regions – outer cortex, inner cortex, and nucleus, or outer and inner cortex combined and nucleus alone (Figure 1) – were microdissected (Zeiss/PALM Microbeam; Carl Zeiss) by outlining regions of

interest and pressure catapulting selected objects using the Auto LPC software function. Pulses of a high quality UV-A laser beam (<1 μm spot size) cut and eject/catapult selected objects into individual PALM® adhesive cap microfuge tubes (Carl Zeiss). Microfuge tubes containing captured tissue were transported on dry ice and stored at −80 °C before processing.

Protein extraction

Following microdissection, samples were processed for desired types of electrophoretic analysis. For SDS–PAGE, captured tissue from each of three regions, stated above, was individually solubilized in Buffer A (50 mM Tris-HCl, pH 7.8, 1 mM phenylmethylsulphonyl fluoride [PMSF], 1 mM iodoacetamide, 1 mM dithiothreitol [DTT]), then microcentrifuged (13,400× g, 10 min, 4 °C) (Eppendorf Centrifuge 5415R; Eppendorf of North America, Westbury, NY). Protein concentration was measured by absorbance at 280 nm using a NanoDrop® ND-1000 Full Spectrum (200–750 nm) Spectrophotometer (NanoDrop Technologies Inc., Wilmington, DE).

For 2D-DIGE and 2-D PAGE analyses, captured tissue was extracted using extraction buffer (EB; 7.8 M urea, 2.2 M thiourea, 2.2% [v/v] pharmalyte, pH 3–10 [Amersham, Hercules, CA], 1.1% [v/v] protease inhibitor cocktail [Sigma Aldrich, St. Louis, MO]), followed by addition of detergent (40% [v/v] -[(3-Cholamidopropyl)dimethylammonio]-1-propansulfonate [CHAPS]). The buffer solubilized both soluble and insoluble proteins from lens sections. Samples were then reduced with 5 mM tributylphosphine (TBP; Sigma) and alkylated with 20 mM 4-vinylpyridine (4-VP; Sigma). Pharmalytes were removed from 2D-DIGE samples by

exchange of EB with DIGE exchange buffer (DExB; 7 M urea, 2 M thiourea, 30 mM Tris, 4% [w/v] CHAPS) using a Millipore Centrifugal filter with a membrane cutoff of 10 kDa. Protein was then quantified using a 2-D Quant Kit (GE Healthcare Biosciences, Piscataway, NJ) and labeled as described below.

SDS–PAGE analysis

Equal amounts of protein (10 μg) from three lenticular regions (outer cortical, inner cortical, and nuclear regions) were analyzed by one-dimensional sodium dodecyl sulfate – PAGE (SDS–PAGE) [47], and gels were stained with Coomassie blue R250 stain (Fisher). Individual protein bands were excised and processed for Matrix-Assisted Laser Desorption Ionization-Time of Flight (MALDI-TOF) mass spectrometric analysis. Samples were destained using three washes of 25 mM ammonium bicarbonate (ABC)/50% acetonitrile and were digested with trypsin (12.5 ng/μl) plus 50 mM ABC for 16 h at 37 °C. Peptides were extracted with two washes in a 50/50 solution of 5% formic acid and 100% acetonitrile, dried in a Savant Speed Vac Concentrator (Forma Scientific, Millford, MA), and resuspended in 10 μl of 0.1% formic acid (FA). Peptides were desalted using C18 Zip Tips™ (Millipore, Bradford, MA) and further analyzed by MALDI-TOF mass spectrometry.

2D-DIGE analysis

CyDye DIGE Fluor minimal dyes are very useful for multicolor analysis and also specially developed to be size and charge matched specifically for Ettan DIGE Systems (GE Healthcare). The protein samples and the internal standard are each labeled with a

different CyDye DIGE Fluor minimal dye, after which these labeled samples are combined, run on an isoelectric focusing (IEF) gel in the first dimension, and separated by SDS–PAGE in the second dimension (GE Healthcare). Proteins from cortical and nuclear regions were separated by 2D-DIGE. First dimension IEF was performed by active rehydration of an 11 cm immobilized pH gradient gel (IPG) strip, pH 5–8. This was performed at 500V with rehydration buffer (7M urea, 2M thiourea, 2% [v/v] pharmalyte, pH 3–10) and using a PROTEAN IEF System (Bio-Rad, Hercules, CA). An internal standard, containing pooled cortical and nuclear proteins was labeled with Cy2, cortical proteins from both outer and inner cortex were labeled with Cy3, and nuclear proteins were labeled with Cy5. Technical replicates, created by dye-swapping the labeled samples, were also run. This was followed by desalting at 300 V for 4 h and focusing at 3,500 V for 9 h. Focused strips were equilibrated for 15 min before running the second dimension with equilibration buffer containing 6M urea, 50 mM Tris-HCl, pH 8.8, 2% SDS, 30% glycerol, and 0.01% bromophenol blue.

In the second dimension, proteins were separated by SDS–PAGE using 23×20 cm 15% polyacrylamide gels. IPG strips were immobilized at the top of second dimension slab gels using 1% low-melt agarose in 3× running buffer containing bromophenol blue (24 mM Tris-HCl, 192 mM glycine, 1% SDS, 0.01% bromophenol blue), which was added as a tracking dye. Second dimension gels were run for 1 h at 1 W/gel, and then at 15 W/gel for 6 h. Gels were post-stained with SYPRO Ruby protein gel stain (Bio-Rad) and imaged with a Typhoon 9400™ scanner (GE Healthcare). Image analysis was done using DeCyder™ v6.5 software (GE Healthcare) accompanying the Typhoon™ 9400 scanner (GE Healthcare).

Gels were secondarily post-stained with Coomassie blue stain (Fisher) to increase visibility for manual spot picking. Individual excised spots were destained, trypsin-digested, and extracted similarly to samples processed for MALDI-TOF analysis, as described above. Supernatants were also dried down in a speed vac (Forma Scientific) and resuspended in 10 μl of 0.1% formic acid. Peptides were analyzed by Electrospray Ionization Quadrupole Linear Ion-Trap Liquid Chromatography Mass Spectrometry (ESI-QTRAP LC-MS/MS).

2-D PAGE analysis

Proteins from the nuclear region alone were separated by 2-D PAGE. Similarly to samples from 2D-DIGE, the first dimension IEF and second dimension SDS–PAGE were performed using an 11 cm IPG strip, pH 5–8, but without CyDye labeling. The gel was post-stained with Coomassie blue stain (Fisher) and imaged.

Identification of lens proteins

MALDI-TOF and ESI-QTRAP LC-MS/MS analyses were performed at the Comprehensive Cancer Center Mass Spectrometry Shared Facility of the University of Alabama at Birmingham (Birmingham, AL). Individual protein bands or spots were manually excised from SDS–PAGE, 2D-PAGE, and 2D-DIGE gels that were post-stained with Coomassie blue R250 (Fisher) for identification purposes, and subjected to processing for mass spectrometric analysis. The polyacrylamide pieces containing individual spots were destained with three consecutive washes with a mixture of 50% 25 mM ammonium bicarbonate/50% acetonitrile for 30 min. Next, the samples were

washed for 10 min with 25 mM ammonium bicarbonate before digestion with trypsin (12 ng/μl; sequencing grade from Roche) for 16 h at 37 °C. Peptide solutions were then extracted using 100 μl of a 50/50 solution of 5% formic acid and acetonitrile for 30 min. Supernatants were collected and dried to dryness in a Savant Speed Vac Concentrator (Forma Scientific). Samples were resuspended in 10 μl of 0.1% formic acid. Tryptic peptides extracted from the SDS–PAGE gel bands were mixed in 1:10 dilutions with a mixture of α-cyano-4-hydroxycinnamic acid (CHCA; 5 mg/ml; Sigma) matrix dissolved in acetonitrile: 0.1% trifluroacetic acid (1:1). C18 Zip Tips (Millipore) were used to desalt peptide mixtures before applying samples to the MALDI-TOF 96×2 well target plates. Samples were applied to a MALDI-TOF 96-well target plate (Applied Biosystems, Foster City, CA), air-dried, and analyzed using Voyager DE-Pro scanning from 900 to 4000 m/z in positive ion mode (Applied Biosystems). Spectra were then analyzed using Voyager Explorer software, and peptide masses were entered into the Matrix Science: MASCOT database for identification of peptides. The MALDI-TOF identity of proteins was established by using the NCBInr database from Matrix Science. Tryptic peptides extracted from 2D-DIGE and 2-D PAGE gel spots and bands were analyzed using an ABI 4000 QTRAP LC-MS/MS Mass Spectrophotometer (Applied Biosystems). Five microliters per sample of trypsin digested peptides were injected into the spectrophotometer and eluted off of a capillary C-18 reverse-phase column using an H_2O/acetonitrile gradient, then fragmented in the QTRAP. Columns were washed between sample analyses. For identification, the resulting spectra were processed using Analyst Software (Applied Biosystems), and all data were subjected to a MASCOT server peptide-sequencing search against all known mammalian proteins found in the

NCBI and Unihuman2 protein databases. Peptide identifications from the MASCOT search were accepted for peptides scoring 40 and above within each protein identification of a given spot. Identifications were performed, and scoring criteria were set with the help of a qualified mass spectrometry specialist in the Comprehensive Cancer Center - Mass Spectrometry and Proteomics shared facility at the University of Alabama at Birmingham (Birmingham, AL).

Results

Laser microdissection and protein identification following SDS–PAGE

To determine the crystallin profile of a normal human aging lens using LCM and 2D-DIGE, it was necessary to first acquire intact sections of appropriate thickness from the human lenses (Figure 1). Acquiring intact 12 μm sections was technically difficult because the water content and high protein concentration of the lens make the tissue harder and brittle when frozen. During tissue embedding, OCT does not infiltrate the tissue and become miscible with the water, therefore some cracking was visible during sectioning. After considerable trial and error, the technique was standardized and 12 μm intact sections were recovered (see Methods for details). These lens sections were used for LCM initially to recover tissue constituting the outer cortical, inner cortical and nuclear regions. Later, tissue from outer and inner cortical regions were combined and referred to as the cortical region (see below). This pooling was done because the GE Healthcare 2D-DIGE protocol suggested that approximately 40 μg of total protein was needed to efficiently label them with CyDyes. An initial extraction of proteins from a single 12 μm section of a 65 year-old normal human lens was performed to estimate how many lens sections were needed to acquire sufficient quantity of protein from each of the

three lens regions (i.e., outer cortical, inner cortical and nuclear regions). As shown in Table 1, LCM of the 12 μm sections from 65 year-old or 69 year-old lenses yielded protein ranging from 0.6 to 2 μg/section from the outer cortical region, 13–15 μg/section from the inner cortical region, and 12–15 μg/section from the nuclear region.

Table 1. Quantities of protein recovered by LCM from outer cortex, inner cortex, and nuclear regions in 12 μM sections of human lens.

Lenses	Number of sections	Outer cortex Total Protein (μg)	Inner cortex Total Protein (μg)	Nucleus Total Protein (μg)
65-year-old	6	12	78	70
69-year-old	12	7	182	182

Note: From "Identification of crystallin modifications in the human lens cortex and nucleus using laser capture microdissection and CyDye labeling" by Asomugha et al., 2010, *Mol Vis, 16*, p. 476. Copyright 2010 by Molecular Vision. Reprinted with permission.

MALDI-TOF analysis of individual protein bands from the SDS-gel revealed the presence of αA- and αB-crystallins (spectral data not shown) in the outer cortical region, βA3-crystallin in both the inner cortical and nuclear regions, and a truncated βA3 species in the nuclear region (Figure 2). Although initial findings spurred further analysis, additional preliminary experiments proved that it was difficult to obtain sufficient amounts of protein from the outer cortical region (Table 1).

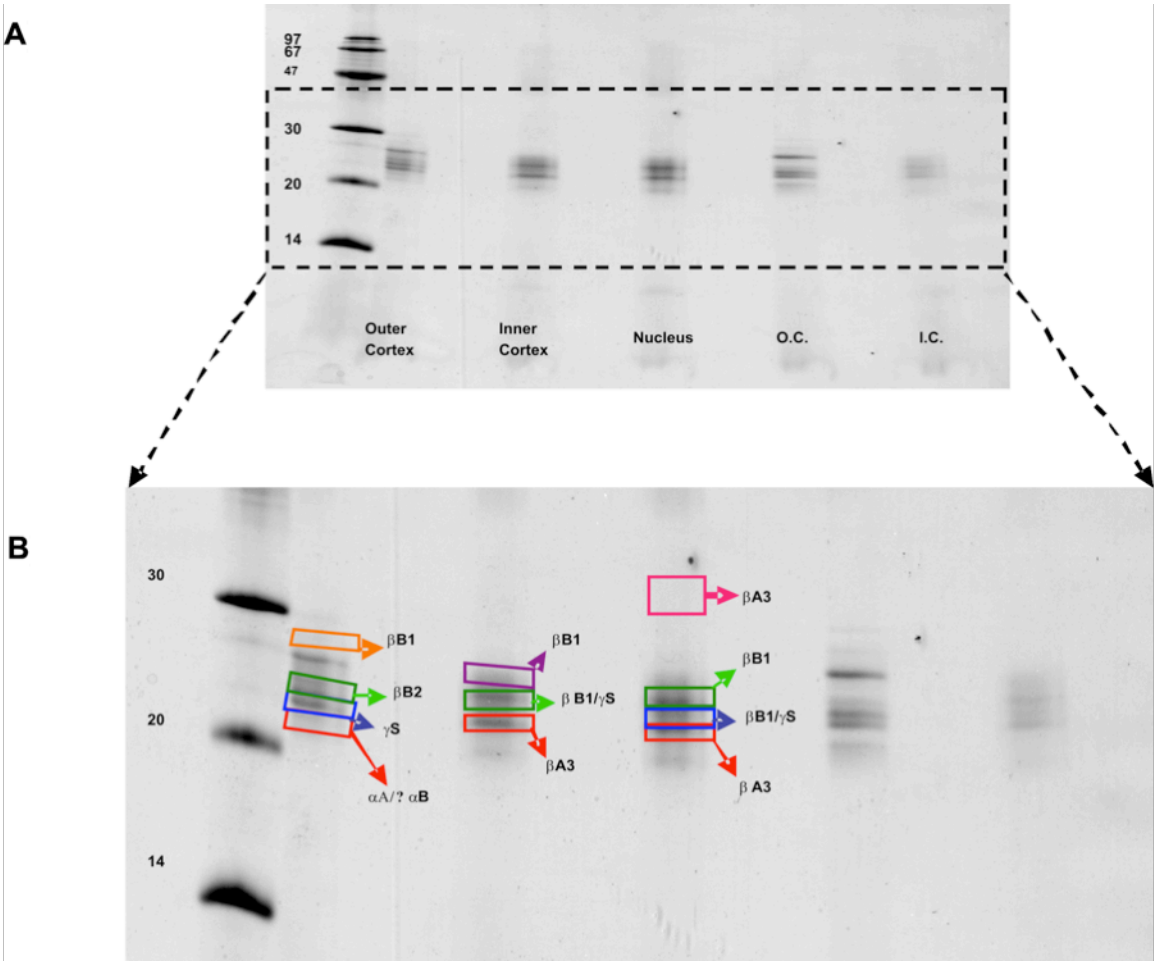

Note: From "Identification of crystallin modifications in the human lens cortex and nucleus using laser capture microdissection and CyDye labeling" by Asomugha et al., 2010, *Mol Vis, 16*, p. 476. Copyright 2010 by Molecular Vision. Reprinted with permission.

Figure 2. Separation of 65-year-old human lens proteins using 15% polyacrylamide gel by SDS-PAGE analysis and identification of excised bands by MALDI-TOF mass spectrometry. **A**: SDS-PAGE image of proteins in three lenticular regions with Coomassie Blue R250 staining showing mostly LMW species. Samples from the outer and inner cortices were repeated in the last two lanes on the right side of the gel. **B**: Expanded image seen in **A**. Boxes outline the bands excised for mass spectrometric analysis and crystallin identifications of excised bands were based on MALDI-TOF data.

In the lens sections, the cortical tissue (both inner and outer cortex) constitutes ~30%–40% of the lens tissue section, whereas the nuclear region constitutes ~60%–70% (Figure 1). Because of low protein recovery, the tissues from both inner and outer cortical

regions, although captured separately, were pooled and referred to as the cortical region in subsequent experiments.

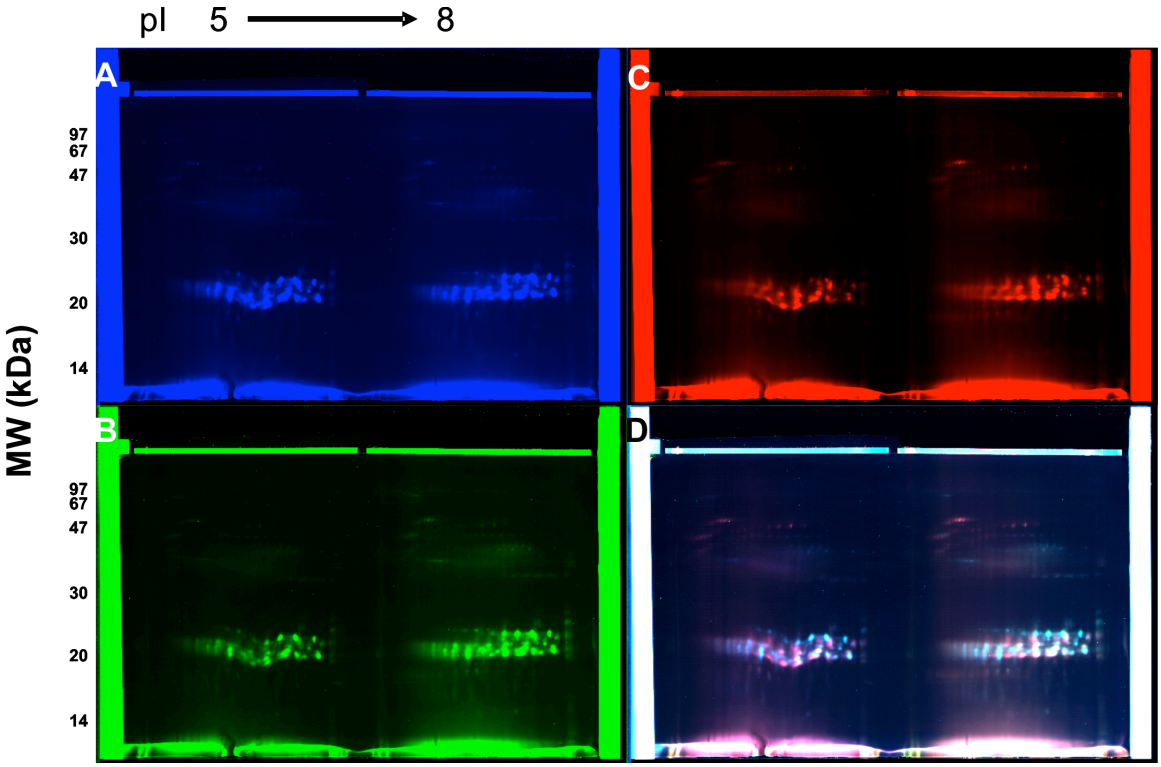

Note: From "Identification of crystallin modifications in the human lens cortex and nucleus using laser capture microdissection and CyDye labeling" by Asomugha et al., 2010, *Mol Vis, 16*, p. 476. Copyright 2010 by Molecular Vision. Reprinted with permission.

Figure 3. Typhoon-scanned fluorescence images from a 2D-DIGE of a 69-year-old human lens. Equal concentrations of protein (20 mg) from the cortex and nucleus were labeled with different fluorescent dyes and analyzed by 2D-DIGE. **A**: Internal standard labeled with Cy2 (Ex 488 nm, Em 520 nm). **B**: Cortical proteins (outer and inner cortex pooled) labeled with Cy3 (Ex 532 nm, Em 580 nm). **C**: Nuclear proteins labeled with Cy5 (Ex 633 nm, Em 670 nm). **D**: Overlay of **A**, **B**, and **C**. Spots fluorescing white are protein species present in both cortex and nucleus, while those fluorescing blue and red are localized to the corresponding regions as show in **B** and **C**, respectively.

Detection of proteins in cortical and nuclear regions

Tissue samples, selectively collected by LCM from the cortical and nuclear regions of a 69-year-old normal human lens, were used for analysis by 2D-DIGE.

Following protein extraction (see Methods), equal amounts of protein (20 μg) from each region, along with an internal standard (pooled proteins from the two regions), were labeled with different fluorescent dyes (Cy2 – internal standard, Cy3 – cortical region, Cy5 – nuclear region). Figure 3A shows the internal standard labeled with Cy2 (Excitation at 488 nm, Emission at 520 nm), 3B shows the cortical proteins labeled with Cy3 (Excitation at 532 nm, Emission at 580 nm), and 3C shows nuclear proteins labeled with Cy5 (Excitation at 633 nm, Emission at 670 nm). Figure 3D is an overlay of the images and identifies white fluorescing protein spots common to both cortical and nuclear regions, whereas red and blue fluorescing spots were from nuclear and cortical regions, respectively.

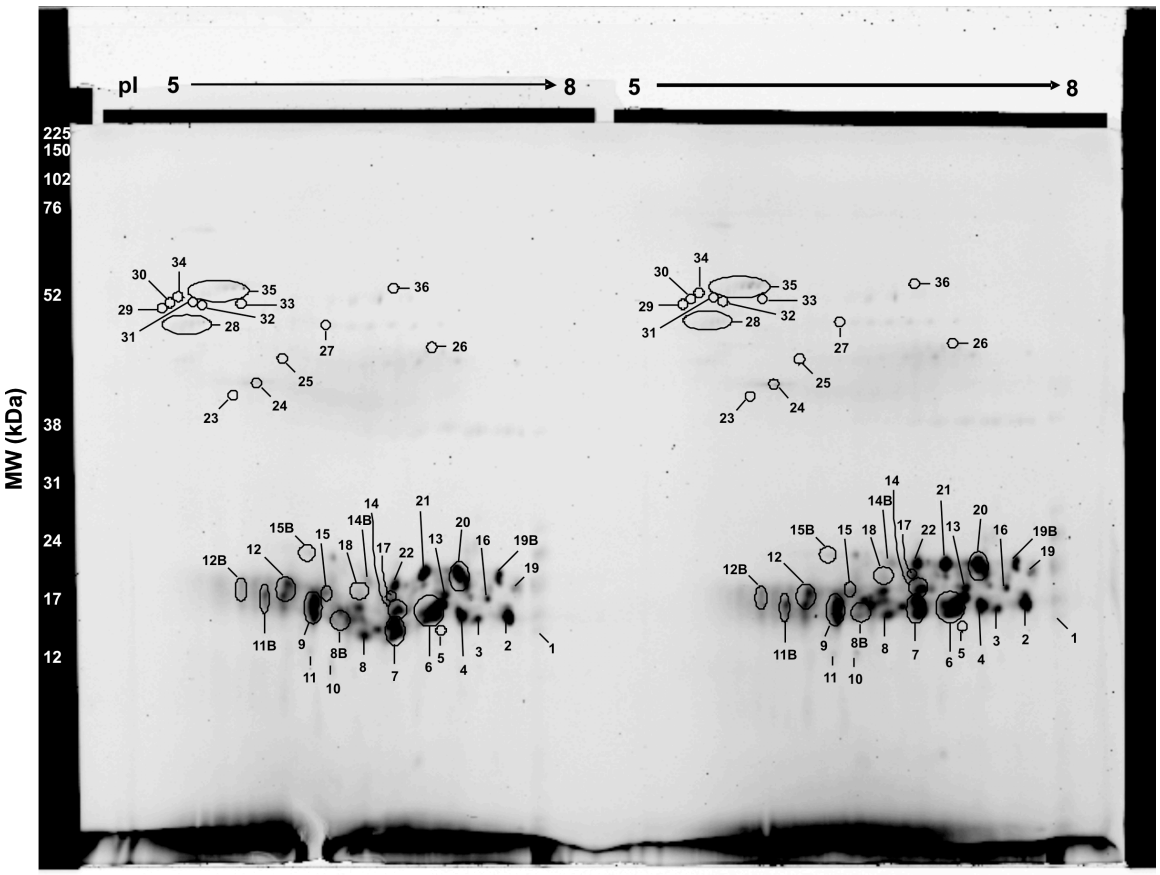

Note: From "Identification of crystallin modifications in the human lens cortex and nucleus using laser capture microdissection and CyDye labeling" by Asomugha et al., 2010, *Mol Vis, 16*, p. 476. Copyright 2010 by Molecular Vision. Reprinted with permission.

Figure 4. Coomassie blue-stained gel from 2D-DIGE of 69-year-old human lens. The gel was stained with Coomassie blue R250 for the purpose of manually picking the individually labeled spots (circled and numbered by ESI-QTRAP LC-MS/MS. The gels in this figure are technical replicates so corresponding spots were picked and pooled for identification.

Protein and PTM identification in 2-D gel electrophoresis

To identify the crystallin species present in individual spots of cortical and nuclear regions, the 2D-DIGE gel was secondarily stained with Coomassie blue (Figure 4). Each labeled spot was manually excised and processed for analysis by Q-TRAP LC-MS/MS (see Methods). The mass spectrometric data were tabulated and spots were distributed into the following three categories based on their molecular weights (M_r): (1) Crystallin fragments (M_r <20 kDa), (2) Intact crystallins (M_r 20–35 kDa), and (3) High molecular weight (HMW) proteins (M_r >35 kDa; Table 2). A total of 36 spots were observed with identification of spots 1–11B as crystallin fragments, spots 12–22 as intact crystallins, and spots 23–36 as HMW proteins (Figure 4 and Table 2). Table 2 provides a summary of crystallin species present in each excised spot and their relative localizations in the two lenticular regions, while Appendix 1 shows the amino acid sequences of their tryptic peptides as identified by ESI-QTRAP LC-MS/MS. Spots 1–11B contained tryptic fragments of αA-, αB-, βA3-, βA4-, βB1-, βB2-, βB3-, γB-, γC-, γD-, and γS-crystallin (Table 2). Taken together, the results shown in Table 2 and Appendix 1 suggested that truncation of α-, β-, and γ-crystallins begins in the cortical region. Spots 12–22 contained tryptic peptides of αA-, αB-, βA3-, βA4-, βB1-, βB2-, βB3-, γB-, γC-, γD-, and γS-crystallin (Table 2), but from the tryptic peptide sequences of spots 12–22, it was unclear

Table 2. Summary of crystallin species in spots from Coomassie-stained 2D-DIGE gel of 69-year-old human lens identified by ESI-QTRAP LC MS/MS

Spot number	Identification by Q-TRAP	M_r (kDa)	Localization
1	γD	<20	N > C
2	αA chain, αB	<20	N < C
3	αA chain, αB, βA3, βB3	<20	N < C
4	αB, βA3, βB1, γD	<20	N = C
5	αB, βA3, γD	<20	N > C
6	αA, αB, βA3, γD, γS	<20	N = C
7	αA, αB, βA3, βB1, βB2, γB, γS	<20	N = C
8	αB, βA3	<20	N = C
8B	αB, βA3	<20	N > C
9	αB, βA3, βA4	<20	N < C
10	αA, αB, βA3, βA4	<20	N < C
11	αA, βA3, βA4	<20	N > C
11B	αA, αB, βA4	<20	N < C
12	αA, γS	20 - 35	N < C
12B	αA, αB, βA3, βB1, βB2, γC, γS	20 - 35	N < C
13	αA, βA4, βB1, βB2, γS	20 - 35	N < C
14	βA3, βB1, γS	20 - 35	N = C
14B	βB2	20 - 35	N < C
15	βA3, βB1, βB2, βA4, γS	20 - 35	N = C
15B	βA3, βA4, βB2, γS	20 - 35	N < C
16	αA, βB1, βB2	20 - 35	N < C
17	truncated βB1 chain, βB1, βB2	20 - 35	N = C
18	βB1, βB2	20 - 35	N > C
19	αA chain, βB1, βB2	20 - 35	N > C
19B	αA, αB, βA3, βB2, βB4	20 - 35	N < C
20	αB, βA3, βB1, βB2, γS	20 - 35	N = C
21	αA, αB, βA3, βB1, βB2	20 - 35	N < C
22	αA	20 - 35	N < C
23	NI	>35	N > C
24	NI	>35	N > C
25	NI	>35	N > C
26	NI	>35	N < C
27	NI	>35	N > C
28	CP49	>35	N > C
29	NI	>35	N > C
30	NI	>35	N > C
31	NI	>35	N > C
32	NI	>35	N > C
33	NI	>35	N > C
34	NI	>35	N > C
35	αA, Filensin	>35	N > C
36	NI	>35	N > C

NI = Not Identified by mass spectrometry. Data from the "Localization" column was based on DIGE analysis.

whether these were intact crystallins. Additionally, DeCyder analysis software that accompanies the Typhoon scanner used to image the 2D-DIGE gels was also applied, with the help of a qualified specialist in the Proteomics Core facility at UAB. Based on technical replicates and software analysis, Table 3 identifies relative fold differences in volume ratios of overlapping spots, in both cortical and nuclear regions, in the 2D-DIGE profile of a 69-year-old lens (Figure 3). DeCyder software analysis selectively identified only 22 out of 36 spots as statistically significant. Therefore, the values listed in the last column showed statistically significant differences ($p<0.05$) determined by the ratio of intensity of one fluorophore to another in overlapping spots (Table 3). DeCyder Differential In-gel Analysis (DIA) co-detects three images created from the internal standard and the two samples, and determines differences in the intensity of spots within the gel that are matched across all images (Figure 3). Significance was based on parameters for Student's *t*-test entered into the software. As seen in Table 3, among the crystallin fragments (M_r <20 kDa), spot 6 (containing fragments of αA-, αB-, βA3-, γD-, and γS-crystallin), spot 8B (containing fragments of αB- and βA3-crystallin), and spot 11 (containing fragments of αA-, αB-, and βA4-crystallin) showed a 1.2–3 fold greater abundance in the nuclear region compared to the cortical region. In contrast, spot 11B (containing fragments of αA-, αB-, and βA4-crystallin) showed roughly twofold greater abundance in the cortical region compared to the nuclear region. A similar analysis of intact crystallins with M_r 20–35 kDa showed differential distribution in the cortical and nuclear regions. Spot 12 (containing αA- and γS-crystallin), spot 12B (containing αA-, αB-, βA3-, βB1-, βB2-, γC-, and γS-crystallin), spot 14B (containing βB2-crystallin), and spot 15B (containing βA3-, βA4-, βB2-, and γS-crystallin) showed about twofold greater

abundance in the cortical region compared to the nuclear region. Spots 23–36, with M_r >35 kDa, represented crystallin multimers and showed greater abundance in the nuclear region compared to the cortical region.

Table 3. DeCyder software analysis hilighed statistically significant spots, based on technical replicates, differentially expressed in nuclear and cortical regions (p<0.05) from the 2D-DIGE gel of a 69-year-old lens (Figure 3) and crystalline species were then identified by ESI-QTRAP LC-MS/MS (Appendix 1).

Spot number	Crystallin Species	M_r (kDa)	Nucleus/Cortex
6	αA chain, αB, βA3, γD, γS	<20	1.24/1
8B	αB, βA3	<20	2.08/1
11	αA, βA3, βA4	<20	3.14/1
11B	αA, αB chain, βA4	<20	-1.61/1
12	αA, γS	20 - 35	-1.97/1
12B	αA, αB chain, βA3, βB1, βB2, γC, γS	20 - 35	-1.51/1
14B	βB2	20 - 35	-2.06/1
15B	βA3, βA4, βB2, γS	20 - 35	-2.21/1
17	Truncated βB1, βB2	20 - 35	2.01/1
23	NI	>35	3.00/1
24	NI	>35	2.17/1
25	NI	>35	2.84/1
26	NI	>35	-3.14/1
27	NI	>35	1.96/1
29	NI	>35	2.49: 1
30	NI	>35	3.09/1
31	NI	>35	2.18/1
32	NI	>35	3.42/1
33	NI	>35	3.58/1
34	NI	>35	3.65/1
35	αA, filensin	>35	3.91/1
36	NI	>35	3.40/1

Values given in the last column represent fold differences in abundance between nuclear and cortical regions, with the sign of the fold value representing up- or down-regulation. NI=Not identified by mass spectrometry because of low concentrations, although DeCyder determined relative abundance.

Note: From "Identification of crystallin modifications in the human lens cortex and nucleus using laser capture microdissection and CyDye labeling" by Asomugha et al., 2010, *Mol Vis, 16*, p. 476. Copyright 2010 by Molecular Vision. Reprinted with permission.

A major problem encountered in the 2D-DIGE experiment was identification of crystallins that existed as HMW protein spots with M_r >35 kDa. ESI-QTRAP LC-MS/MS analysis successfully identified both spot 28 containing CP49 and spot 35 that contained αA-crystallin and filensin (Tables 2 and 3), with spot 35 having almost a fourfold greater abundance in the nuclear region compared to the cortical region (Table 3). Identification of HMW protein spots 23–27, 29–34, and 36 failed because of their low protein concentrations (Figure 4). Therefore, protein yield was increased by extraction from a greater number of lens sections, and specifically from the nuclear region. Tissue from the nuclear region of 48 sections (12 μm) of a 69-year-old lens was captured by LCM and processed for standard 2D-gel electrophoresis. The 2D gel protein profile exhibited a pattern similar to that of the 2D-DIGE gel (compare protein profiles of gels in Figure 4 and Figure 5). However, unlike the 2D-DIGE gel, 39 spots were resolved and the HMW proteins appeared as non-descript bands that were labeled as numbers 38 and 39 (Figure 5). The appearance of non-descript bands was likely because the majority of proteins in the nuclear region are highly modified and cross-linked. Results showed that band 38 contained a mixture of αA-, αB-, βA3-, βA4-, βB1-, γB-, γC-, γD-, and γS-crystallins and CP49, whereas band 39 was a mixture of αA-, αB-, βA3-, βA4-, βB1-, βB2-, γB-, γC-, γD-, and γS-crystallin and both filensin and CP49 (Table 4). Table 5 shows the amino acid sequences of tryptic peptides of crystallin species identified in bands 38 and 39 of Figure 5.

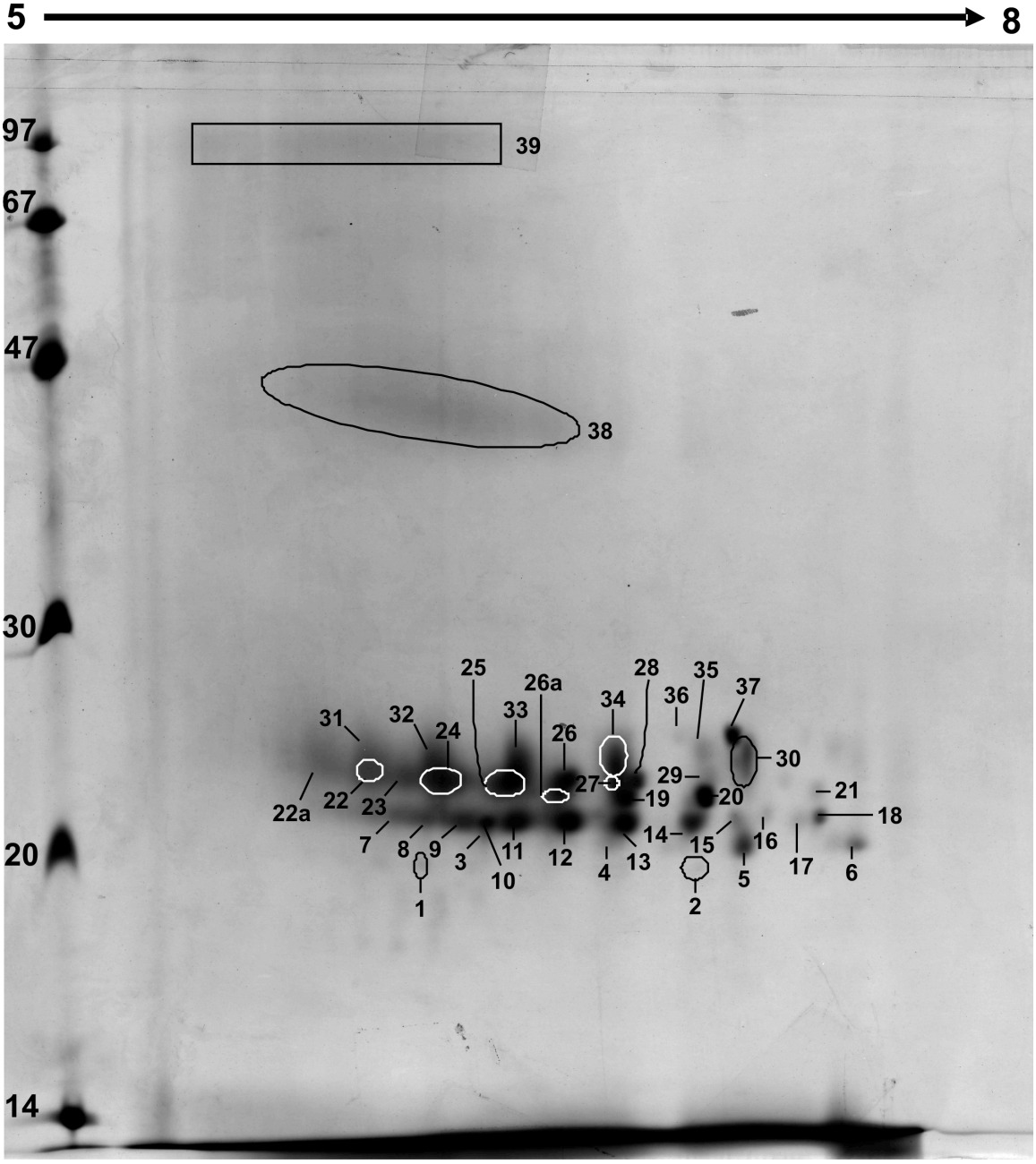

Note: From "Identification of crystallin modifications in the human lens cortex and nucleus using laser capture microdissection and CyDye labeling" by Asomugha et al., 2010, *Mol Vis, 16*, p. 476. Copyright 2010 by Molecular Vision. Reprinted with permission.

Figure 5. Standard 2D gel of a 69-year-old human lens. IEF was done in the first dimension using an 11 cm IPG strip, pH 5-8, followed by SDS-PAGE using a 15% polyacrylamide gel in the second dimension. The gel was stained with Coomassie blue R250, and shows a profile similar to 2D-DIGE gels of the same tissue. However, HMW (>35 kDa) aggregates are not distinguished as individual spots, rather they appeared as non-descript bands.

Table 4. Identification of crystallins present in the HMW bands of a 69-year-old lens following 2D-gel electrophoresis (Figure 5).

Band number	Identification by QTRAP
38	**αA, αB, βA3, βA4, βB1, γB, γC, γD, γS filensin**
39	**αA, αB, βA3, βA4, βB1, βB2, γB, γC, γD, γS CP49, filensin**

Note: From "Identification of crystallin modifications in the human lens cortex and nucleus using laser capture microdissection and CyDye labeling" by Asomugha et al., 2010, *Mol Vis, 16*, p. 476. Copyright 2010 by Molecular Vision. Reprinted with permission.

Q-TRAP analysis also identified several PTMs in crystallins including: αA-, αB-, βA3-, βA4-, βB1-, βB2-, γD-, and γS-crystallins, as well as CP49, which are summarized in Table 6. Table 6 and Appendix 1 show the amino acid sequences, specific modification sites within these tryptic sequences (see underlined amino acids), and PTMs (see brackets) of such modified proteins as those described. PTMs found in αA-crystallin species were present in both the cortical and nuclear regions. The same was true for αB-crystallin, except for a single oxidized M68 residue that was only present in the HMW region and, therefore, only found in the nuclear region. βA3-crystallin exhibited modifications that were found in both cortical and nuclear regions, however, deamidation of residues Q38, N40, and Q42 was seen only in the HMW proteins of the nuclear region. Among the crystallins, the fewest modifications were seen in βA4-crystallin, which contained only seven PTMs (i.e., two deamidations of residue N114, and five oxidations of residue M14). Unlike the PTMs seen in the α-crystallins, modifications of βB1-crystallin mostly occurred in the HMW proteins of the nuclear region, while only two modifications, deamidations of N68 and Q236, occurred in the lower molecular weight

(LMW) crystallins (<35 kDa). All the modified species of βB2-crystallin were found only in LMW proteins and the majority of the PTMs were deamidations, followed by oxidations, and ethylations. Among the γ-crystallins, γS-crystallin showed the most modifications. Oxidations of residues M70, M147, and W157 of γD-crystallin were all present only in HMW proteins. In contrast, several modifications were found in γS-crystallin, four of which were only seen in the HMW region (i.e., carbamylation of residue I8, deamidations of Q17 and Q93 residues, and one kynurenin at residue W163). Two of these γS-crystallin modifications, N-formylkynurenin at residue W163 and kynurenin at residue W163, were each seen only once in the whole crystallin profile determined from the 69-year-old human lens. Although both CP49 and filensin were identified, CP49 was found in HMW proteins of nuclear region with an oxidation of residue M175. The new PTMs identified in α-, β-, and γ-crystallin, not yet reported in the literature, are highlighted in Table 6.

Table 5. Crystallin species, sequences, and modifications in HMW bands from 2D gel of the nuclear region of a 69-year-old human lens identified by ESI-QTRAP LC-MS/MS (Figure 5).

Band number	α-Crystallin	β- and γ-Crystallin	CP49	Filensin
38	αA: #1 – 11 MDVTIQHPWFK [Acet(N-term);Oxi(M)]	βA3: #33 – 44 ITIYDQENFQGK [Deam(NQ)]		#78 – 90 LGELAGPEDALAR
	αA: #13 – 21 TLGPFYPSR	βA3: #33 – 45 ITIYDQENFQGKR [Deam(NQ)]		#99 – 106 VRDLEAER
	αA: #55 – 65 TVLDSGISEVR	βA3: #96 – 109 WDAWSGSNAYHIER		
	αA: #79 – 88 HFSPEDLTVK	βA3: #126 – 137 MTIFEKENFIGR Eth(N-term);Oxi(M)]		
	αA: #89 – 99 VQDDFVEIHGK	βA3: #197 – 211 EWGSHAQTSQIQSIR		
	αA: #146 – 157 IQTGLDATHAER	βA4: #14 – 25 MVVWDEDGFQGR [Oxi(M)]		
	αB: #12 – 22 RPFFPFHSPSR	βA4: #107 – 118 LTIFEQENFLGK [Deam(NQ)]		
		βA4: #178 – 192 EWGSHAPTFQVQSIR		
		βB1: #51 – 60 AAELPPGNYR		
		βB1: #61 – 72 LVVFELENFQGR		
		βB1: #73 – 86 RAEFSGECSNLADR [Phos(STY)]		
		βB1: #74 – 86 AEFSGECSNLADR		
		βB1: #111 – 118 GEMFILEK		
		βB1: #124 – 132 WNTWSSSYR [Deam(NQ)]		
		βB1: #136 – 143 LMSFRPIK		
		βB1: #151 – 160 ISLFEGANFK		
		βB1: #188 – 202 VSSGTWVGYQYPGYR [Oxi(HW)]		
		βB1: #203 – 214 GYQYLLEPGDFR		
		γB: #4 – 10 ITFYEDR		
		γB: #60 – 77 RGEYPDYQQWMGLSDSIR		
		γB: #155 – 164 FLDWGAPNAK		
		γC: #4 – 10 ITFYEDR		
		γC: #60 – 77 RGEYPDYQQWMGLSDSIR		
		γC: #116 – 122 FHLSEIR		
		γD: #2 – 10 GKITLYEDR		

		γD: #4 – 10 ITLYEDR γD: #60 – 77 RGDYADHQQWMGLSDSVR γD: #61 – 77 GDYADHQQWMGLSDSVR [Oxi(M)] γD: #81 – 89 LIPHSGSHR γD: #143 – 152 QYLLMPGDYR [Oxi(M)] γD: #154 – 163 YQDWGATNAR [Oxi(HW)] γS: #8 – 14 ITFYEDK [Eth(K)] γS: #8 – 19 ITFYEDKNFQGR [Cam(N-term);Deam(NQ)] γS: #42 – 52 VEGGTWAVYER γS: #73 – 79 WMGLNDR γS: #85 – 95 AVHLPSGGQYK [Deam(NQ)] γS: #147 – 154 GRQYLLDK γS: #149 – 155 QYLLDKK γS: #159 – 166 KPIDWGAA γS: #159 – 174 KPIDWGAASPAVQSFR [Deam(NQ);Oxi(HW)] γS: #159 – 175 KPIDWGAASPAVQSFRR		
39	αA: #1 – 11 MDVTIQHPWFK αA: #1 – 12 MDVTIQHPWFKR αA: #13 – 21 TLGPFYPSR αA: #55 – 65 TVLDSGISEVR αA: #79 – 88 HFSPEDLTVK αA: #89 – 99 VQDDFVEIHGK αA: #146 – 157 IQTGLDATHAER αB: #57 – 69 APSWFDTGLSEMR [Oxi(M)] αB: #73 – 82 DRFSVNLDVK αB: #83 – 92 HFSPEELKVK	βA3: #33 – 44 ITIYDQENFQGK [Deam(NQ)] βA3: #96 – 109 WDAWSGSNAYHIER [Deam(NQ)] βA3: #126 – 137 MTIFEKENFIGR [DeamNQ);Oxi(M)] βA3: #197 – 211 EWGSHAQTSQIQSIR βA4: #14 – 25 MVVWDEDGFQFR [Oxi(M)] βA4: #107 – 118 LTIFEQENFLGK βB1: #51 – 60 AAELPPGNYR βB1: #61 – 72 LVVFELENFQGR βB1: #73 – 86 RAEFSGECSNLADR [Phos(STY)] βB1: #111 – 118 GEMFILEK	#77 – 89 ALGISSVFLQGLR	#78 – 90 LGELAGPEDALAR #96 – 106 VRDLEAER

αB: #93 – 103 VLGDVIEVHGK

βB1: #111 – 123 GEMFILEKGEYPR
βB1: #124 – 132 WNTWSSSYR [Deam(NQ)]
βB1: #133 – 143 SDRLMSFRPIK
βB1: #136 – 143 LMSFRPIK
βB1: #136 – 150 LMSFRPIKMDAQEHK
βB1: #151 – 160 ISLFEGANFK
βB1: #171 – 182 APSLWVYGFSDR
βB1: #188 – 202 VSSGTWVGYQYPGYR [Deam(NQ);Oxi(HW)]
βB1: #203 – 214 GYQYLLEPGDFR
βB2: #109 – 120 IILYENPNFTGK
βB2: #146 – 160 VQSGTWVGYQYPGYR
βB2: #161 – 168 GLQYLLEK
βB2: #169 – 188 GDYKDSSDFGAPHPQVQSVR
βB2: #190 – 198 IRDMQWHQR
γB: #4 – 10 ITFYEDR
γB: #155 – 164 FLDWGAPNAK
γC: #4 – 10 ITFYEDR
γC: #116 – 122 FHLSEIR
γD: #4 – 10 ITLYEDR
γD: #143 – 152 QYLLMPGDYR
γD: #154 – 163 YQDWGATNAR
γS: #8 – 14 ITFYEDK [Eth(K)]
γS: #8 – 19 ITFYEDKNFQGR
γS: #73 – 79 WMGLNDR
γS: #85 – 95 AVHLPSGGQYK
γS: #159 – 174 KPIDWGAASPAVQSFR [Kyn(W);Oxi(HW)]
γS: #159 – 175 KPIDWGAASPAVQSFRR

Underlined amino acids mark sites of modification, and modifications are shown in brackets. Abbreviations Used: Acet – Acetylation; Cam – Carbamylation; Deam – Deamidation; Eth – Ethylation; Fkyn – Formylkynurenin=Double oxidation of Trp; Kyn – Kynurenin=Triple oxidation of Trp; Meth – Methylation; Oxi – Oxidation=Single oxidation; Phos – Phosphorylation; Sulph – Sulphone.

Note: From “Identification of crystallin modifications in the human lens cortex and nucleus using laser capture microdissection and CyDye labeling” by Asomugha et al., 2010, *Mol Vis*, *16*, p. 476. Copyright 2010 by Molecular Vision. Reprinted with permission.

Table 6. Compilation of PTMs found in crystallins and filaments in a 69-year-old human lens.

Crystallins/Filaments	Total Post-translational Modifications
αA	Acetylation: **M1** Ethylation: T13, H79, V89, I146 Methylation: H79, V89, Q90, I146, Q147, H154, R157 Oxidation: **M1**, **W9**, H154
αB	Acetylation: M1 Carbamylation: M1, **K92**, E164 Deamidation: N146 Ethylation: **H83**, **V93**, **Q108** Methylation: **H83** Oxidation: **M1**, W9, **W60**, **M68****
βA3	Carbamylation: K44, K131 Deamidation: **Q38**, N40**, **Q42****, N103, N133 Ethylation: W96, M126 Oxidation: W99, M126 Sulphone: M126
βA4	Deamidation: N114 Oxidation: M14
βB1	Deamidation: N68*, N125, Q197, Q236* Oxidation: W193 Phosphorylation: S81
βB2	Acetylation: A2 Deamidation: Q71, Q105, N114, N116, Q138, Q163, Q183 Ethylation: **I109**, **K121**, **G161** Formylkynurenin***: W85, W151 Oxidation: W82, **M122**, **H133**, **H135**, W151
γD	Oxidation: M70, M147, W157
γS	Carbamylation: I8** Deamidation: Q17**, Q93**, Q171 Ethylation: I8, K14, K159 Formylkynurenin***: W163 Kynurenin***: W163** Methylation: H87, K159 Oxidation: W163 Phosphorylation: S167
CP49	Oxidation: M175

The asterisk indicates modified species present only in LMW region. The double asterisk indicates modified species present only in HMW region. The triple asterisk indicates Oxidation=Single oxidation; Formylkynurenin=Double oxidation of Trp; Kynurenin=Triple oxidation of Trp. Newly identified PTMs are in bold.

Note: From "Identification of crystallin modifications in the human lens cortex and nucleus using laser capture microdissection and CyDye labeling" by Asomugha et al., 2010, *Mol Vis, 16*, p. 476. Copyright 2010 by Molecular Vision. Reprinted with permission.

Discussion

In this study, the experimental approach used a novel combination of LCM, 2D-DIGE, and mass spectrometric analysis. LCM separately recovered proteins from cortical and nuclear regions of a normal human lens, 2D-DIGE determined their comparative distribution, and mass spectrometric analysis determined the identity of crystallins and intermediate filament proteins, and their PTMs in the two regions. The results showed changes in crystallins in fiber cells that occur during their age-related migration from the cortical to nuclear region. Further, the LCM method for isolating cells of the above two regions from lens sections was relatively superior to a similar isolation procedure using sequential solubilization of different regions of a human lens (see Introduction). To minimize crystallin degradation and modification during protein processing, proteins from minimally manipulated tissue sections were fully solubilized in a buffer containing protease inhibitors and denaturating agents. Further, following sensitive 2D-DIGE detection, individual spots were identified based on their amino acid sequences by Q-TRAP LC-MS/MS method (Table 6 and Appendix 1).

Fluorescent dyes (Cy2, Cy3, and Cy5) used in this study, that generally label approximately 1%–2% of Lys residues in proteins, are very useful in determining differential distribution of proteins. CyDye DIGE Fluor minimal dyes contain an N-hydroxysuccinimidyl ester reactive group, which enables labeling of Lys residues within proteins, forming a covalent bond with the epsilon amino group to yield an amide linkage. The recommended concentration of fluor present in a protein labeling reaction ensures that fluor is limiting, and therefore approximately 1%–2% of Lys residues are labeled. As a result, CyDye DIGE Fluor minimal dyes will label only a small proportion

of each protein in a sample, hence the expression "minimal labeling" (GE Healthcare Biosciences). Further, minimal labeling of proteins does not affect mass spectrometric data because approximately 98% of protein remains unlabeled. This also means that the technology is not affected by post-translational modifications to Lys residues. For example, if a Lys residue is modified in a tryptic fragment, an adjacent Lys will be alternatively labeled by the dye.

Mass spectrometric analysis of labeled proteins separated by 2D-DIGE identified ~36 spots, which included crystallin fragments, intact crystallins, and crystallin aggregates (referred to as HMW proteins). In this study, only crystallin fragments with M_r >10 kDa were analyzed because a filter of 10 kDa was used during protein fractionation (see Methods). Among these, 22 protein spots showed statistically significant differences in abundance levels ($p<0.05$) between nuclear and cortical regions, as determined by DeCyder analysis.

The major findings of this study were: (A) crystallin fragments (M_r <20 kDa) were present in both cortical and nuclear regions, suggesting that the age-related migration of fiber cells from the cortical to nuclear region is accompanied by the truncation of crystallins in the cortical region and continues on in the nuclear region. (B) The HMW aggregates of crystallins (M_r >35 kDa) were present in a greater abundance in the nuclear region (i.e., ~3:1 fold difference ratio of nuclear:cortex, Table 3; $p<0.05$), suggesting that aggregation and/or cross-linking mostly occurred in the nuclear region. (C) The HMW complexes contained a relatively large number of truncated or modified β-crystallin species compared to α- and γ-crystallin, as well as two lens-specific intermediate filaments, CP49 and filensin. (D) The modified α-crystallins were found in

low abundance in the nuclear region compared to the cortical region suggesting their chaperone function was possibly compromised due to their truncation and aggregation with other crystallins. This could have potentially resulted in insolubilization of unchaperoned β- and γ-crystallin as seen by their greater abundance in the nuclear region. (E) Several different PTMs (deamidation, oxidation, phosphorylation, methylation, acetylation, ethylation, carbamylation, sulfonation, double and/or triple oxidation, and truncation) of crystallins (αA-, αB-, βA3-, βA4-, βB1-, βB2-, γB-, γC-, γD-, and γS-crystallin) and CP49 and filensin were identified. Some of these PTMs have been identified for the first time in crystallins. Our results show that all lens crystallins undergo post-translational modifications, and these changes would affect their appearance on a 2D-gel. Therefore, crystallins are changing in various directions, and the end result is a difference in overall size of their spot.

To our knowledge, this is the first report in human lens proteomic studies that has used sensitive techniques (LCM and 2D-DIGE) to differentiate the in situ regional distribution of crystallins and intermediate filament proteins in cortical and nuclear regions of the same lens. A previous report examined the distribution of both cortical and nuclear lens proteins in lenses of galgo, beef, cat, deer, rabbit, and chick [48] using a paper and starch gel electrophoretic method [49]. It mainly focused on the functional role of embryonic proteins and changes in their levels during adult life. The application of a combination of LCM, 2D-DIGE, and Q-TRAP LC-MS/MS had a major advantage in that it allowed high throughput analysis and rapid identification of proteins present in lens cortical and nuclear regions. LCM, however, is a time consuming and an expensive technique yielding only a limited amount of protein per 12 μm lens section (i.e., 0.6–2 μg

from outer cortical region, 13–15 μg from inner cortical region, and 12–15 μg from the nuclear region, Table 1). To overcome this limitation, cellular proteins from 12 and 48 lens sections were captured by LCM to analyze cortical and nuclear regions, respectively. For LCM, 60–65 h of operation time was consumed, and therefore it became an expensive method for recovering the desired amount of proteins. However, as was evident from the results, the captured cells yielded enough protein for the 2D-DIGE analysis and for the determination of statistically significant differences in abundance in the two lens regions. Additionally, the recovery of sufficient quantities of HMW protein complexes (M_r >35 kDa) from the nuclear region (Table 2, Table 4, and Table 5) was more time-consuming and challenging relative to recovery of crystallins with M_r <35 kDa from both cortical and nuclear regions. This was because of the existence of HMW proteins at lower levels relative to other crystallin species. Further improvement of the LCM technology, specifically increasing the laser power to cut and catapult a greater number of cells from thicker sections, will make it more cost-effective.

Because PTMs of crystallins are believed to be causative factors for cataract development, we hypothesized that their identification would provide clues regarding the age-related changes in crystallins as cells progressively move from the periphery to the center of the lens. Although several earlier reports have described PTMs in crystallins [12-17,22-25,50-53], it is not clear whether they are localized in cortical or nuclear regions or both.

The presence of truncated and aggregated acidic/basic β-crystallin was relatively higher both in cortical and nuclear regions than α-crystallin, suggesting that β-crystallins were more susceptible to modifications during aging. The β-crystallins showed PTMs in

the following decreasing order: deamidation > oxidation > ethylation > carbamylation/ formylkynurenin > phosphorylation/sulphonation/acetylation (Table 6). However, the oxidation of αA- and αB-crystallin occurred more frequently than other PTMs. αA-Crystallin also exhibited maximum methylation compared to other crystallins, which has been reported for the first time here. Another interesting finding was that only truncated forms of βB2-crystallin were present in both nuclear and cortical regions, suggesting that modified βB2-crystallin is more susceptible to degradation than other β-crystallins. Further, mass spectrometric analysis showed that truncated crystallins with M_r <20 kDa were recovered from both cortical and nuclear regions (Table 2, spot numbers 1 to 11B), and these spots were considered as crystallin fragments. DeCyder analysis also showed that certain crystallin fragments were more abundant in the cortical region compared to the nuclear region, suggesting a greater truncation of certain crystallins in the cortical region relative to the nuclear region.

NH_2-terminal acetylation, a widespread PTM in eukaryotes and viruses compared to prokaryotes [54], is believed to protect proteins against proteolytic degradation by aminopeptidases. More than two decades ago, Driessen et al. [55] reported the presence of NH_2-terminally acetylated α/β-crystallins in calf lens, while others reported it in human [25] and chicken lenses [56]. However, its lenticular localization was still unknown. Our results showed for the first time that NH_2-terminally acetylated αA- and αB-crystallins are present in both cortical and nuclear regions of human lens. NH_2-terminal acetylation (e.g., M1 acetylation) was reported earlier in human αA- and αB-crystallins in water soluble and insoluble fractions using whole lens extracts [25]. Lin et al. [57] have reported in vivo acetylation at Lys 70 in human αA-crystallin and proposed

that it may affect its chaperone function. Similarly, acetylation at Ala 2 in βB2-crystallin, as shown in the present study, may alter surface charge, protein conformation and intermolecular interaction. The functional significance of NH_2-terminal acetylation is presently unknown but since NH_2-termini of αA- [32] and αB-crystallin (Asomugha and Srivastava, unpublished results) play a major role in maintaining structural integrity and solubility, acetylation of NH_2-termini may therefore alter oligomeric structure and affect chaperone function.

Deamidation, which induces a net "charge-change" by conversion of a neutral amide group to an acidic group in asparaginyl and glutaminyl residues of crystallins, alters structural and functional properties. Although the deamidated α-crystallins were absent in the HMW complex, they were present as crystallin fragments (M_r <20 kDa). This study identified a significant number of deamidated β-crystallin species in the HMW complex of the nuclear region, suggesting that these deamidated crystallin species aggregate with aging. Also, deamidation was identified as one of the major and most abundantly occurring PTMs in β-crystallins, with greater deamidation of Gln residues than Asn residues as reported earlier by Hains et al. [23]. βA3-crystallin with deamidation of Q38, N40, Q42, N103, and N133 residues were identified, but only species with deamidations at Q38, N40, and Q42 were present in the nuclear region. Furthermore, deamidations of N40, N103, and N133 sites in βA3-crystallin have been reported for the first time. We also identified novel and previously unreported deamidation sites in other β-crystallins (βA4 – N114; βB1 – N68, N125, Q197, Q236; βB2 – Q71, Q105, N114, N116, Q138, Q163, Q183). While deamidated βA4- and βB1-crystallin were present in both cortical and nuclear regions, deamidated βB2-crystallin

was present only in the cortical region. Although the effects of different deamidations reported for the first time is presently unclear, previous reports by Lampi et al. [22], along with ourselves [20,21], have demonstrated deleterious effects of specific deamidations of Asn and Gln residues on structural/functional properties of crystallins. Understanding the effects of the above-mentioned deamidations would provide insight into the mechanism of crystallin destabilization and their age-related aggregation.

Another major PTM identified in the present study was oxidation of M, H, and W residues. Again, β-crystallin showed relatively greater levels of oxidatively modified species than α-crystallin. Oxidation of M68 in αB-crystallin was observed, as reported previously in both WS- and WI-protein fractions of aging and cataractous human lenses [26,27]. Additional oxidation sites observed were: αA – M1, W9, H154; αB – M1, W9, W60, M68; βA3 – W99, M126; βA4 – M14; βB1 – W193; βB2 – W85, M122, H133, H135, W151; γS – W163. Because methionine oxidation might occur during sample handling, some of the observed Met oxidations could be artifacts. These oxidized crystallin species were present in both the crystallin fragment fraction (M_r <20 kDa) and the aggregated crystallin fraction (M_r >35 kDa). Although it was unclear if truncation and aggregation of crystallins were results of their oxidation, their presence in the above two fractions was a hallmark of the aging process. Oxidized γD-crystallin (oxidized at M70, M147, and W157 residues) was present in the HMW complex and was localized only in the nuclear region, suggesting that the oxidation of γD-crystallin resulted in its aggregation in the nuclear region. A previous report [58] showed that γ-crystallins migrated as aggregated species if not boiled with SDS-gel loading buffer. That study used in vitro synthesized γ-crystallins, unlike this study, but whether this was a factor in the

present study was not determined. Our findings of doubly- and triply-oxidized W (formylkynurenin and kynurenin) observed in βB2-crystallin residues W85 and W151 [59] and W163 residue of γS-crystallin further suggest that oxidation of W might lead to aggregation of β- and γ-crystallins. Present literature suggests that UVA-exposure induces production of reactive oxygen species, which oxidizes M, H and W residues of crystallins and would result in their structural alterations and aggregation. For example, triply-oxidized W residues in these crystallins may have reacted with either the ground state molecular oxygen to form $^1O_2$ or with amino acids to produce free radicals, which might have resulted in the presence of modified species in the HMW complex.

Phosphorylation, a known developmental regulatory element in a variety of proteins including lens crystallins, was found to be associated with aging [60]. An interesting finding of the present study was that only S81 and S167 residues of βB1- and γS-crystallins, respectively, were identified as phosphorylated species in the HMW complex of the nuclear region. Several phosphorylated sites in αB-crystallin have been previously reported and some of these were present in a cataractous lens [30]. At present, the effects of phosphorylation on aggregation properties of βB1- and γS-crystallins are not known.

The present study demonstrated carbamylation of M, E, K, and I residues in human αB-, βA3- and γS-crystallins. All these carbamylation sites in the crystallins have been identified for the first time, with the exception of the K92 residue in αB-crystallin identified as a carbamylation site in calf lens [19].

In summary, we have identified several new PTM sites in crystallins and intermediate filament proteins in the cortical and/or nuclear regions. We also showed that

truncation of crystallins began in the cortex and continues in the nuclear region, whereas crystallin aggregation is mostly localized in the nuclear region. The study showed that α-, β-, and γ-crystallins exhibited several sites of deamidation (N and Q), oxidation (M, H, W), methylation (H, V, Q, I, R and K) and carbamylation (M, E, K and I), and these modified species were present in both cortical and nuclear regions of an aging lens. Together these PTMs might disrupt the net charges and conformations of the crystallins, and lead to protein degradation, aggregation, or both. Because deamidation [20,21,32] and oxidation [4,14] have been shown to affect chaperone activity of α-crystallins, the apparent loss of α-crystallin chaperone function with aging might leave β- and γ-crystallins more susceptible to degradation and aggregation. Additionally, we have successfully performed the proteomic analysis of a human lens by tissue microdissection, 2D-DIGE separation and mass spectrometric analysis. These methods would be helpful in the future in analyzing cataractous lenses to distinguish age-related events from those occurring during cataract development. Because of the use of only two lenses, it remains to be seen whether these relative changes in crystallins in cortical versus nuclear regions are universal.

Acknowledgements

We thank Martha Robbins for editorial assistance. We also thank Dr. Andra Frost and Natalya Frolova (Laser Capture Microdissetion Laboratory, UAB, Birmingham, AL) for training and access to the LCM equipment, Dr. Mike Frost (Department of Vision Sciences, UAB, Birmingham, AL) for his assistance in 2D-DIGE protocol, Landon Wilson and Richie Herring (Comprehensive Cancer Center - Mass Spectrometry and

Proteomics shared facility of UAB, Birmingham, AL) for assistance with mass spectrometric analysis and 2D-DIGE gel analysis, respectively. Support for these studies was provided by PHS grants EY06400, P 50 AT00477, and P 30 EY03039 and a grant from the Alabama EyeSight Foundation.

References

1. Delaye M, Tardieu A. Short-range order of crystallin proteins accounts for eye lens transparency. Nature. 1983;302:415–7.
2. Ponce A, Sorensen C, Takemoto L. Role of short-range protein interactions in lens opacifications. Mol Vis. 2006;12:879–84.
3. Andley UP. Crystallins in the eye: function and pathology. Prog Retin Eye Res. 2007;26:78–98.
4. Bloemendal H, de Jong W, Jaenicke R, Lubsen NH, Slingsby C, Tardieu A. Ageing and vision: structure, stability and function of lens crystallins. Prog Biophys Mol Biol. 2004;86:407–85.
5. Harding JJ. Lens. In: Harding, JJ, editor. Biochemistry of the Eye. London: Chapman & Hall; 1997. p. 94–134.
6. Horwitz J. α-Crystallin can function as a molecular chaperone. Proc Natl Acad Sci USA. 1992;89:10449–53.
7. Derham BK, Harding JJ. Effect of aging on the chaperone-like function of human α-crystallin assessed by three methods. Biochem J. 1997;328:763–8.
8. Muchowski PJ, Bassuk JA, Lubsen NH, Clark JI. Human αB-crystallin. J Biol Chem. 1997;272:2578–82.

9. Cohen D, Bar-Yosef U, Levy J, Gradstein L, Belfair N, Ofir R, Joshua S, Lifshitz T, Carmi R, Birk OS. Homozygous CRYBB1 deletion mutation underlies autosomal recessive congenital cataract. Invest Ophthalmol Vis Sci. 2007;48:2208–13.
10. Ferrini W, Schorderet DF, Othenin-Girard P, Uffer S, Heon E, Munier FL. CRYBA3/A1 gene mutation associated with suture-sparing autosomal dominant congenital nuclear cataract: a novel phenotype. Invest Ophthalmol Vis Sci. 2004;45:1436–41.
11. Lu S, Zhao C, Jiao H, Kere J, Tang X, Zhao F, Zhang X, Zhao K, Larsson C. Two Chinese families with pulverulent congenital cataracts and deltaG91 CRYBA1 mutations. Mol Vis. 2007;13:1154–60.
12. Takemoto L, Boyle D. Determination of the in vivo deamidation rate of asparagines-101 from alpha-A crystallin using microdissected sections of the aging human lens. Exp Eye Res. 1998;67:119–20.
13. Takemoto LJ. Quantitation of asparagines-101 deamidation from alpha-A crystallin during again of the human lens. Curr Eye Res. 1998;17:247–50.
14. Andley UP, Clark JA. Generation of oxidants in the near UV photooxidation of human lens alpha-crystallin. Invest Ophthalmol Vis Sci. 1989;30:706–13.
15. McDermott M, Chiesa R, Roberts JE, Dillon J. Photooxidation of specific residues of α-crystallin. Biochemistry. 1991;30:8653–60.
16. Spector A. The search for a solution to senile cataracts. Procter lecture. Invest Ophthalmol Vis Sci. 1984;25:130–45.
17. Nagaraj RH, Sell DR, Prabhakaram M, Ortwerth BJ, Monnier VM. High correlation between pentosidine protein crosslinks and pigmentation implicates ascorbate

oxidation in human lens senescence and cataractogenesis. Proc Natl Acad Sci USA. 1991;88:10257–61.

18. Lorand L. Transglutaminase mediated cross-linking of proteins and cell aging: the erythrocyte and lens models, In: Zappia V, editor. Advances in post-translational modifications of proteins and aging. New York: Plenum Press; 1988. p. 79–94.
19. Lapko VN, Smith DL, Smith JB. In vivo carbamylation and acetylation of water soluble human lens alpha B-crystallin lysine 92. Protein Sci. 2001;10:1130–6.
20. Gupta R, Srivastava OP. Deamidation affects structural and functional properties of human αA-crystallin and its oligomerization with αB-crystallin. J Biol Chem. 2004;279:44258–69. a.
21. Gupta R, Srivastava OP. Effect of deamidation of asparagines 146 on functional and structural properties of human lens αB-crystallin. Invest Ophthalmol Vis Sci. 2004;45:206–14. b.
22. Lampi KJ, Amyx KK, Ahmann P, Steel EA. Deamidation in human lens βB2-crystallin destabilizes the dimmer. Biochemistry. 2006;45:3146–53.
23. Hains PG, Truscott RJW. Post-translational modifications in the nuclear region of young, aged, and cataract human lenses. J Proteome Res. 2007;6:3935–43.
24. Ma Z, Hanson SRA, Lampi KJ, David LL, Smith DL, Smith JB. Age-related changes in human lens crystallins identified by HPLC and mass spectrometry. Exp Eye Res. 1998;67:21–30.
25. Wilmarth PA, Tanner S, Dasari S, Nagalla SR, Riviere MA, Bafna V, Pevzner PA, David LL. Age-related changes in human crystallins determined from comparative

analysis of post-translational modifications in young and aged lens: does deamidation contribute to crystalline insolubility? J Proteome Res. 2006;5:2554–66.

26. Harrington V, McCall S, Huynh S, Srivastava K, Srivastava OP. Crystallins in water soluble-high molecular weight protein fractions and water insoluble protein fractions in aging and cataractous human lenses. Mol Vis. 2004;10:476–89.
27. Harrington V, Srivastava OP, Kirk M. Proteomic analysis of water insoluble proteins from normal and cataractous human lenses. Mol Vis. 2007;13:1680–94.
28. Srivastava OP, Srivastava K. Existence of deamidated αB-crystallin fragments in normal and cataractous human lenses. Mol Vis. 2003;9:110–8.
29. Hanson SR, Hasan A, Smith DL, Smith JB. The major in vivo modifications of the human water-insoluble lens crystallins are disulfide bonds, deamidation, methionine oxidation and backbone cleavage. Exp Eye Res. 2000;71:195–207.
30. Lund AL, Smith JB, Smith DL. Modifications of the water-insoluble human lens α-crystallins. Exp Eye Res. 1996;63:661–72.
31. Kim YH, Kapfe DM, Boekhorst J, Lubsen NH, Bachinger HP, Shearer TR, David LL, Feix JB, Lampi KJ. Deamidation, but not truncation decreases the urea stability of a lens structural protein, βB1-crystallin. Biochemistry. 2002;41:14076–84.
32. Chaves JM, Srivastava K, Gupta R, Srivastava OP. Structural and functional roles of deamidation and/or truncation of N- or C-termini in human αA-crystallin. Biochemistry. 2008;47:10069–83.
33. Banks RE, Dunn MJ, Forbes MA, Stanley A, Pappin D, Naven T, Gough M, Harnden P, Selby PJ. The potential use of laser capture microdissection to selectively obtain

distinct populations of cells for proteomic analysis – preliminary findings. Electrophoresis. 1999;20:689–700.

34. Espina V, Wulfkuhle JD, Calvert VS, VanMeter A, Zhou W, Coukos G, Geho DH, Petricoin EF, 3rd, Liotta LA. Laser-capture microdissection. Nat Protoc. 2006;1:586–603.
35. Kondo T, Hirohashi S. Application of highly sensitive fluorescent dyes (CyDye DIGE Fluor saturation dyes) to laser microdissection and two-dimensional difference gel electrophoresis (2D-DIGE) for cancer proteomics. Nat Protoc 2006. 12940–56. 17406554
36. Simone NL, Paweletz CP, Charboneau L, Petricoin EF, 3rd, Liotta LA. Laser capture microdissection: beyond functional genomics to proteomics. Mol Diagn. 2000;5:301–7. a.
37. Craven RA, Banks RE. Laser capture microdissection and proteomics: possibilities and limitation. Proteomics. 2001;1:1200–4.
38. Mouledous L, Hunt S, Harcourt R, Harry J, Williams KL, Gutstein HB. Navigated laser capture microdissection as an alternative to direct histological staining for proteomic analysis of brain samples. Proteomics. 2003;3:610–5.
39. Simone NL, Bonner RF, Gillespie JW, Emmert-Buck MR, Liotta LA. Laser-capture microdissection: opening the microscopic frontier to molecular analysis. Trends Genet. 1998;14:272–6.
40. Simone NL, Remaley AT, Charboneau L, Petricoin EF, 3rd, Glickman JW, Emmert-Buck MR, Fleisher TA, Liotta LA. Sensitive immunoassay of tissue cell proteins procured by laser capture microdissection. Am J Pathol. 2000;156:445–52. b.

41. Lawrie LC, Curran S, McLeod HL, Fothergill JE, Murray GI. Application of laser capture microdissection and proteomics in colon cancer. Mol Pathol. 2001;54:253–8.

42. Grey AC, Schey KL. Distribution of bovine and rabbit lens α-crystallin products by MALDI imaging mass spectrometry. Mol Vis. 2008;14:171–9.

43. Lampi KJ, Ma Z, Hanson SRA, Azuma M, Shih M, Shearer TR, Smith DL, Smith JB, David LL. Age-related changes in human lens crystallins identified by two-dimensional electrophoresis and mass spectrometry. Exp Eye Res. 1998;67:31–43.

44. Craven RA, Totty N, Harnden P, Selby PJ, Banks RE. Laser capture microdissection and two-dimensional polyacrylamide gel electrophoresis. Evaluation of tissue preparation and sample limitations. Am J Pathol. 2002;160:815–22.

45. Colvis C, Garland D. Posttranslational modification of human αA-crystallin: correlation with electrophoretic migration. Arch Biochem Biophys. 2002;397:319–23.

46. Tannu NS, Hemby SE. Two-dimensional fluorescence difference gel electrophoresis for comparative proteomics profiling. Nat Protoc. 2006;1:1732–42.

47. Laemmli UK. Cleavage of structural proteins during the assembly of the head of bacteriophage T4. Nature. 1970;227:680–5.

48. Maisel H, Goodman M. Analysis of cortical and nuclear lens proteins by a combination of paper and starch gel electrophoresis. Anat Rec. 1965;151:209–15.

49. Smithies O. Zone electrophoresis in starch gels: group variations in the serum proteins of normal human adults. Biochem J. 1955;61:629–41.

50. Gupta R, Srivastava K, Srivastava OP. Truncation of motifs III and IV in human lens βA3-crystallin destabilizes the structure. Biochemistry. 2006;45:9964–78.

51. Harms MJ, Wilmarth PA, Kapfer DM, Steel EA, David LL, Bachinger HP, Lampi KJ. Laser light-scattering evidence for an altered association of βB1-crystallin deamidated in the connecting peptide. Protein Sci. 2004;13:678–86.

52. Lapko VN, Purkis AG, Smith DL, Smith JB. Deamidation in human γS-crystallin from cataractous lenses is influenced by surface exposure. Biochemistry. 2002;41:8638–48.

53. Lapko VN, Smith DL, Smith JB. Methylation and carbamylation of human gamma-crystallins. Protein Sci. 2003;12:1762–74.

54. Shearer D, Ens W, Standing K, Valdimarsson G. Posttranslational modifications in lens fiber connexins identified by Off-Line-HPLC MALDI-Quadrupole Time-of-Flight mass spectrometry. Invest Ophthalmol Vis Sci. 2008;49:1553–62.

55. Driessen HPC, Ramaekers FCS, Vree Egberts WTM, Dodemont HJ, de Jong WW, Tesser GI, Bloemendal H. The function of N^{α}-acetylation of the eye-lens crystallins. Eur J Biochem. 1983;136:403–6.

56. Wilmarth PA, Taube JR, Riviere MA, Duncan MK, David LL. Proteomic and sequence analysis of chicken lens crystallins reveals alternate splicing and translational forms of βB2 and βA2 crystallins. Invest Ophthalmol Vis Sci. 2004;45:2705–15.

57. Lin PP, Barry RC, Smith DL, Smith JB. In vivo acetylation identified at lysine 70 of human lens αA-crystallin. Protein Sci. 1998;7:1451–7.

58. Bhat SP, Spector A. A simple method to characterize gamma-crystallin synthesized in vitro. Exp Eye Res. 1984;39:317–23.

59. MacCoss MJ, McDonald WH, Saraf A, Sadygov R, Clark JM, Tasto JJ, Gould KL, Wolters D, Washburn M, Weiss A, Clark JI, Yates JR., 3rd Shotgun identification of protein modifications from protein complexes and lens tissue. Proc Natl Acad Sci USA. 2002;99:7900–5.

60. Spector A, Chiesa R, Sredy J, Garner W. cAMP-dependent phosphorylation of bovine lens α-crystallin. Proc Natl Acad Sci USA. 1985;82:4712–6.

STRUCTURAL AND FUNCTIONAL ROLES OF DEAMIDATION OF N146 AND/OR TRUNCATION OF N- OR C-TERMINI IN HUMAN αB-CRYSTALLIN

by

CHINWE O. ASOMUGHA, RATNA GUPTA, OM P. SRIVASTAVA

In preparation for *Molecular Vision*

Format adapted for dissertation

Abstract

Purpose

The purpose of the study was to determine the relative effects of deamidation and/or truncation on the structural and functional properties of αB-crystallin.

Methods

Using wild-type (WT) αB-crystallin and the αB deamidated mutant (i.e., αB N146D), we generated N-terminal domain deleted (residues no. 1-66; αB-NT), deamidated plus N-terminal domain deleted (αB N146D-NT), C-terminal extension-deleted (residues no. 151-175; αB-CT), and deamidated plus C-terminal extension-deleted (αB N146D-CT) mutants. All of the proteins were purified and their structural and functional (chaperone activity) properties were determined and compared to WT αB-crystallin.

Results

The desired deletions in the αB-crystallin mutants were confirmed by matrix-assisted laser desorption/ionization time-of-flight (MALDI-TOF) mass spectrometric analysis. The homomers of αB-CT and its deamidated form (αB N146D-CT) became water insoluble, whereas the αB N146D, αB-NT, and αB N146D-NT species remained water-soluble. CD spectroscopic studies revealed that the mutants with deletion of N- and C-termini or deamidation showed increased β-sheet and decreased in α-helical contents with the exception of αB N146D-CT, which showed a substantial increase in α-helix and decrease in β-sheet content. Results of intrinsic Trp fluorescence suggested little change in Trp microenvironment of αB N146D relative to WT αB, but substantial alterations on

deletion of C-terminal extension or a combination of this deletion plus deamidation. ANS binding results showed that, relative to WT αB structure, the N146 deamidation, C-terminal extension deletion or a combination of this deamidation and deletion resulted in a relatively compact structure, whereas the N-terminal domain deletion and a combination of this deletion plus deamidation resulted in a relaxed structure. All the αB-mutants showed even higher molecular mass ranging from 1.2×10^6 to 3.1×10^6 Da, relative to WT αB with a molecular mass of 5.8×10^5 Da. Chaperone activity across all αB species decreased in the following order: WTαB > αB N146D-CT > αB N146D-NT > αB-NT > αB-CT > αB N146D. Specifically, substantial losses in chaperone activity (only 10% to 20% protection) were seen in αB N146D, αB-NT, and αB-CT. However, in the species with the combination of deamidation plus N- or C-terminal deletion, the percent protection increased to about 24% in αB N146D-NT and about 40% in αB N146D-CT.

Conclusions

Although all mutants also formed oligomers even after deamidation, deletion of either N-terminal domain or C-terminal extension or a combination of these deletions and deamidation, their structural properties were substantially altered. The results suggested that the N-terminal domain is relatively more important than the C-terminal extension for the chaperone function of αB. The non-deamidated N146 residue, N-terminal domain and C-terminal extension are also of critical importance to the maintenance of αB-crystallin chaperone activity.

Introduction

The α-, β-, and γ-crystallins are the major components of the vertebrate eye lens and their interactions lead to maintenance of the refractive properties of the lens, as well as lens transparency. Of the crystallins, α-crystallin accounts for almost half of the total lens protein and exists in vivo as an ~800 kDa hetero-oligomer made up of αA- and αB-crystallin in a 3:1 ratio [1,2]. Unlike αA-, αB-crystallin is a stress-inducible sHSP [2,3] found in several organs other than the lens, such as the heart, skeletal muscle, and kidney [4,5]. In, the brain, αB has also been associated with neurological disorders such as Alzheimer's [6] and Parkinson's [7] diseases. As a member of the small heat shock protein (sHSP) family, α-crystallins also function as molecular chaperones [8] to protect proteins from physiological stress and bind improperly folded proteins to prevent their aggregation [3,9]. This chaperone function is thought to be a critical part of the maintenance of lens transparency.

Crystallins are long-lived proteins that must survive the lifetime of the lens and as such undergo post-translational modifications (PTMs) with age and cataract development. PTMs identified in the human lens include, but are not limited to, methionine oxidation, disulfide bond formation, deamidation of Asn and Gln residues, truncation of N- and C-termini, and backbone cleavage [10-12]. These PTMs, and others, are believed to alter protein structure and conformation and, in turn, the functional properties of the crystallins. Previous reports have shown that removal of 56 residues of the N-terminal domain and 32-34 residues of the C-terminal extension of both αA- and αB-crystallins, results in improper folding, diminished chaperone activity, and formation of trimers and tetramers [5,13,14].

Deamidation, which is a non-enzymatic process that introduces a negative charge by replacing a neutral amide group with a carboxylic group, has been reported as the most common PTM in several studies [15-20] and leads to protein destabilization and changes in solubility. The existence of deamidated fragments of αB-crystallin with N146 deamidation has been found in both normal and cataractous lenses [21]. Other recent studies from this lab also found that deamidation of N101 in αA-crystallin caused more pronounced changes in structural and functional properties than deamidation of N123 [22]. Likewise, deamidation of N146 had more pronounced effects on structural and functional properties of αB-crystallin than deamidation of N78 [23]. Similar findings of altered structure and function were seen in site-directed mutation studies of αB-crystallin [24], mutation of a conserved Arg residue (R120G) in the α-crystallin domain of αB-crystallin [25], as well as a study highlighting a novel mutation (D140N) in αB associated with the development of autosomal dominant congenital lamellar cataract [26]. Despite such studies, the role of deamidation in cataractogenesis is still unclear.

It has been suggested that deamidation of both Gln and Asn residues in proteins may serve as molecular clocks for biological events including protein turnover, development, and aging and provide a signal for degradation in order to regulate intracellular levels [27,28]. This may explain why deamidation has been found to be the most commonly occurring PTM, as stated above. Also, since both αA- and αB-crystallin are susceptible to N- and C-terminal degradation, and deamidation sites exist in or near these regions (i.e. N101 and N123 of αA-crystallin and N78 and N146 of αB-crystallin), deamidation may serve as signal for truncation of these termini. Additional studies have shown that truncation or mutation in the C-terminal extension of αB-crystallin cause

myofibrillar myopathies [28]. This raised the question of what were the relative effects of deamidation and/or truncation on the structural and functional properties of αA- and αB-crystallins. Therefore a recent study in this lab compared both deamidation and truncation of αA-crystallin and found that N123 deamidation, as well as truncation of N- and C-termini, altered the protein structure and were detrimental to chaperone function [29]. In the present study, we seek to answer the same question in αB-crystallin as to what are the relative effects of deamidation and/or truncation on the structural and functional properties of αB. Using wild-type (WT) αB-crystallin and the αB deamidated mutant (i.e., αB N146D), we generated N-terminal domain deleted (residues no. 1-66), deamidated plus N-terminal domain deleted, C-terminal extension deleted (residues no. 151-175), and C-terminal extension deleted mutants and compared structural and functional properties of these mutants to WT αB-crystallin.

Methods

Materials

The restriction endonucleases Bam HI and Sac I, the molecular weight protein markers and DNA markers were purchased from Amersham Biosciences (Piscataway, NJ), Invitrogen (Carlsbad, CA) and Promega (Madison WI), respectively. The T7 promoter, T7 terminator and other primers used in the study were obtained from Sigma-Aldrich (St. Louis, MO). Anti-Histidine-tagged mouse monoclonal primary antibody and goat anti-mouse IgG (H+L) horseradish peroxidase-conjugated secondary antibody were obtained from Calbiochem-EMD Biosciences (La Jolla, CA) and Thermo Scientific (Rockford, IL), respectively. Unless otherwise stated, all other molecular biology-grade

chemicals used in this study were purchased from Sigma or Fisher Scientific (Fair Lawn, NJ).

Bacterial Strains and Plasmids

The *E.coli* One Shot® TOP 10 cells and BL21 (DE3) bacterial strains were obtained from Invitrogen, and used for propagation and expression, respectively. The human, wild-type (WT) αB-crystallin cDNA cloned on a plasmid pDIRECT was received from Dr. Mark Petrash, University of Colorado, Denver, CO. Cells were propagated in Luria broth, and recombinant bacteria were selected using ampicillin.

Site-Specific Mutagenesis

Deamidation of an Asn (N) residue at position 146 to an Asp (D) residue was introduced in αB-cDNA using the Quickchange site-directed mutagenesis kit (Stratagene, La Jolla, CA) as described previously [23]. The deamidated αB DNA was used as a template, along with specific complementary primer pairs (Table 1), to generate the desired deleted or deamidated plus deleted αB-crystallin mutants, and the PCR products were ligated to a pET 100 Directional TOPO vector (Invitrogen). Recombinant human WT αB-crystallin and αB N146D were subcloned in the pET 100D TOPO vector to introduce a six His-tag at the N-terminus of the protein. The αB N-terminal domain (residue no. 1-66) or the C-terminal domain (residue no. 151-175) was deleted from the WT and the deamidated αB mutant (i.e., αB N146D) using PCR-based mutagenesis in order to generate N-terminal domain- or C-terminal extension-deleted mutants. The following four mutants were generated: (i) αB-NT (N-terminally truncated [-NT]), (ii)

αB N146D-NT, (iii) αB-CT (C-terminally truncated [-CT]), and (iv) αB N146D-CT. Briefly, 25 ng of template was used under the following PCR conditions: pre-denaturing at 95°C for 30 s, followed by 30 cycles of denaturing at 95°C for 30 s, annealing at 60-64°C for 30 s (depending on the T_m of the primers), and extension/elongation at 72°C for 1 min, with a final extension at 72°C for 10 min. The PCR products were ligated to the pET 100 Directional TOPO vector (Invitrogen) per the manufacturer's instructions, and the positive clones were identified by restriction analysis using Bam HI and Sac I. The desired deletions were confirmed by DNA sequencing (Genomics Core Facility of the University of Alabama at Birmingham).

Expression and Extraction of WT and Mutant Proteins in Soluble and Inclusion Bodies

Positive PCR amplicons were transformed into *E. coli* BL21 (DE3) cells using a standard *E. coli* transformation technique, as previously described [22, 23]. The proteins were over-expressed by addition of IPTG (final concentration of 1 mM), and the cell cultures were incubated further at 37°C for 4 h. The cells were harvested and resuspended in lysis buffer [25 mM Tris-HCl (pH 7.8), 50 mM NaCl, 0.9% glucose, 1 mM EDTA, containing lysozyme (0.25 mg/mL) and protease inhibitor cocktail (Sigma)] and sonicated while kept on ice. DNA was degraded by treatment with DNase I (10 μg/ml) for 30 min on ice. The soluble fraction was separated by centrifugation at 8000 × g for 10 min at 4°C, and the insoluble fraction was resuspended in a detergent buffer (DB) [0.5 M NaCl, 1% (w/v) sodium deoxycholate, 1% NP-40, and 20 mM Tris-HCl, pH 7.5]. The detergent-soluble fraction was separated by centrifugation at 5000 × g for 10 min at 4 °C. The resultant pellet was washed with 0.5% Triton X-100 and centrifuged as stated above.

Washing of the pellet was repeated as necessary to remove bacterial debris from the inclusion bodies. The final pellet was resuspended in denaturating binding buffer (DBB) [8M urea, 0.5 M NaCl, and 20 mM sodium phosphate, pH 7.8].

Purification of WT and Mutant Proteins

Depending on the expression of the desired mutant proteins in either soluble fractions or in inclusion bodies (insoluble fractions), each protein was purified under either native or denaturing conditions. In case the desired protein was expressed as partly soluble form (i.e., present in both soluble fraction and inclusion bodies), the soluble protein fraction was selectively used for its purification. All purification steps, including refolding of proteins, were carried out at 4°C unless otherwise indicated. Each protein was purified by affinity chromatography using Invitrogen ProBond Ni^{2+}-chelating columns according to the manufacture's instructions. Briefly, under native conditions, the column was equilibrated and a protein preparation was applied to the column using a native binding (NB) buffer [20 mM sodium phosphate containing 0.5 M NaCl, pH 7.8], followed by washing with NB buffer containing 20 mM imidazole (pH 7.8) and elution of column-bound protein with NB containing 250 mM imidazole (pH 7.8). Under denaturing conditions, the column was equilibrated with DBB. Following the application of desired protein preparation, the unbound proteins were eluted by a first wash with DBB, followed by a second and third wash with DBB at pH 6.0 and pH 5.3, respectively. Finally, bound proteins were eluted with DBB containing 250 mM imidazole (pH 7.8).

SDS-PAGE analysis [31] was used to analyze the fractions recovered from Ni^{2+}-affinity column chromatography that contained the desired protein after purification.

Proteins purified under native conditions were dialyzed against 50 mM phosphate buffer (pH 7.8) at 4°C, and stored at -20 °C until they were used. The proteins purified under denaturing conditions were refolded using a previously published method [32] briefly described below.

Refolding of Proteins Purified Under Denaturating Conditions

Proteins purified under denaturing conditions were refolded by dialysis for 24 h at 4 °C against 50 mM sodium phosphate (pH 7.5) containing 1 mM DTT and decreasing urea concentrations from 8 M to 4 M, and finally in a urea-free phosphate buffer.

Characterization of Structural/Functional Properties of WT αB-Crystallin and Its Deamidated and Deamidated Plus Deleted Mutants

Circular Dichroism (CD) Spectroscopy

To investigate the conformational changes in purified WT αB and the N146D deamidated or deamidated plus deleted mutant proteins, their far-UV CD spectra were recorded at room temperature over a range of 195 – 260 nm on a Jasco J815 CD spectrometer using 0.2 mg/mL of protein in 50 mM sodium phosphate buffer (pH 7.8), as previously described [Chaves 2008]. A quartz cell of 0.5 mm path length was used, and the reported spectra are the average of five scans, which were corrected for the buffer blank and smoothed. The secondary structural contents of WT and mutant proteins were determined using the SELCON3 analysis program.

Fluorescence Studies

All fluorescence spectra were recorded in corrected spectrum mode using a Shimadzu RF-5301PC spectrofluorometer with excitation and emission bandpasses set at 5 and 3 nm, respectively. The intrinsic Trp fluorescence intensities of the WT αB, the N146D deamidated mutant, and the deamidated plus C-terminal extension-deleted mutants (0.2 mg/mL of protein in 50 mM sodium phosphate buffer, pH 7.8) were recorded with excitation at 295 nm and emission between 300-400 nm. Because human αB crystallin contains Trp residues at positions 9 and 60 that were lost during deletion of the N-terminal domain (residue no. 1-66), the total fluorescence intensities of the N-terminally deleted mutants (i.e., αB-NT and αB N146D-NT) were recorded with excitation at 290 nm and emission between 300-400 nm.

ANS Binding and Fluorescence Spectroscopy

The binding of a hydrophobic probe, 8-anilino-1-naphthalene sulfonate (ANS), to WT αB, deamidated, or deamidated plus N- or C-terminally deleted αB-mutants was determined by recording fluorescence emission spectra between 400-600 nm after excitation at 390 nm, as previously described (Gupta JBC 2004, IOVS 2004). In these experiments, 15 μl of 0.8 mM ANS (dissolved in methanol) was added to 0.2 mg/mL of protein dissolved in 50 mM phosphate buffer (pH 7.8), mixed thoroughly, and incubated at 37°C for 15 min prior to spectroscopy.

Oligomer Size Determination by Dynamic Light Scattering

A multiangle laser light scattering instrument (Wyatt Technology, Santa Barbara, CA) coupled to HPLC system was used to determine the absolute molar mass of the WT protein and its mutant proteins. Prior to their analysis, protein samples in 50 mM sodium phosphate (pH 7.8) were filtered through a 0.22 μm filter. Results were acquired using 18 different angles, which were normalized with the 90º-angle detector.

Chaperone Activity Assay

Chaperone activity of homoaggregates of WT αB, αB N146D, αB-NT, αB N146D-NT, αB-CT, and αB N146D-CT mutants was determined using methods previously described [23]. The aggregation of insulin by reduction with 20 mM DTT at 20°C, either in absence or at varying concentrations of different αB-crystallin species, was determined. Aggregation was monitored using light scattering at 360 nm as a function of time using a Shimadzu UV-VIS scanning spectrophotometer (model UV2101 PC) equipped with a six-cell positioner and a temperature controller (Shimadzu model CPS-260).

Results

Confirmation of Site-Specific Deletions in αB-Crystallin Mutants

WT αB-crystallin and a deamidated αB mutant (i.e., αB N146D), previously generated in the laboratory [23], were used as templates to generate four N-terminal domain-deleted or C-terminal extension-deleted mutants (see Methods). The N-terminally deleted (- NT) and deamidated plus N-terminally deleted mutants are referred

to in the text as αB-NT and αB N146D-NT, respectively, whereas the C-terminally deleted (- CT) and deamidated plus C-terminally deleted mutants are referred to in the text as αB-CT and αB N146D-CT, respectively. DNA sequencing results confirmed the desired deletions: αB-NT and αB N146D-NT (residues no. 67-175), and αB-CT and αB N146D-CT (residues no. 1-150).

Expression and Purification of WT αB-Crystallin and Mutant Proteins

WT αB and mutant protein expression was induced in the BL21 (DE3) expression cell line using 1 mM IPTG for 4 h, as previously described [23], and proteins were recovered in either the soluble fraction, insoluble fraction (inclusion bodies), or both fractions (Table 2). WT αB, αB N146D, αB-NT, and αB N146D-NT proteins were recovered in the soluble fraction, whereas αB-CT and αB N146D-CT proteins were recovered in the insoluble fraction. These results were consistent with the known solubility properties of the N-terminal domain and C-terminal extension. Therefore, upon deletion of the hydrophobic N-terminus, the proteins remained soluble, however, on deletion of the hydrophilic C-terminus, the proteins were insoluble.

Following over-expression of proteins in *E. coli* at 37°C, each protein was purified to almost homogeneity using Ni^{2+}-affinity columns under native or denaturing conditions (see Methods). On SDS-PAGE analysis, the purified His-tagged WT αB-crystallin and deamidated mutant proteins (residues 1-175) showed molecular weights (M_r) of ~27 kDa (Figure 2, lane 2 and 3), whereas His-tagged N-terminally deleted (residues no. 67-175) and C-terminally deleted (residues no 1-150) species showed lower M_r's of ~15 and ~20 kDa, respectively (Figure 2, lanes 4-7). As seen by SDS-PAGE

analysis, WT αB and its mutant proteins were recovered in highly purified forms and showed M_r's higher than expected due to the addition of six His residues.

Comparison of Properties of WT αB, Deamidated and Deamidated Plus Deleted Mutants

Circular Dichroism Spectral Studies

In order to evaluate the effects of deletion of the N-terminal domain or C-terminal extension on the secondary structure of WT αB and a deamidated mutant protein, far-UV CD spectra and secondary structural content were determined (Figure 3, Table 3). As seen in Table 3, SELCON3 software analysis of secondary structural content showed that WT αB contained predominantly β-sheet structure with 19.3% α-helix, 48.7% β-sheet, 12.4% β-turn, and 19.6% random coil. Conversely, the αB N146D mutant showed 6.1% α-helix, 64.2% β-sheet, 5.5% β-turn, and 24.2% random coil, suggesting that deamidation at N146 considerably alters α-helical and β-sheet content (Figure 3, Table 3). Likewise, deletion of either the N-terminal domain or C-terminal extension alone resulted in increased β-sheet content and decreased α-helical content relative to WT αB. αB-NT showed greater reduction in α-helix (i.e., 3.0% α-helix, 69.7% β-sheet, 16.9% β-turn, and 10.6% random coil), while αB-CT showed minimal reduction in α-helix (i.e., 11.7% α-helix, 62.2% β-sheet, 10.5% β-turn, and 17.1% random coil) (Figure 3B and C, Table 3). However, both αB-NT and αB-CT showed similar increases in β-sheet content. With N-terminal domain deletion of the deamidated αB-crystallin, α-helical and β-sheet contents were similar to the content of the deamidated alone species (i.e., αB N146D-NT showed 5.9% α-helix, 62.5% β-sheet, 5.5% β-turn, and 24.4% random coil), suggesting

that NT truncation alone exhibits relatively greater structural changes than the N146 deamidation. On C-terminal extension deletion of the deamidated αB-crystallin, α-helical content substantially increased while β-content decreased relative to both WT and the deamidated alone species (i.e., 47.5% α-helix, 31.7% β-sheet, 6.8% β-turn, and 14.8% random coil). This suggested that the combination of N146 deamidation and C-terminal deletion had greater affect on secondary structural content than C-terminal deletion alone. Therefore, whereas the combination of N146 deamidation and N-terminal domain deletion exhibited secondary structure similar to the deamidated alone species, N146 deamidation and C-terminal extension deletion together produced substantial changes compared to deamidation alone, and all species differed from WT αB.

Intrinsic Trp Fluorescence and Total Fluorescence

The tertiary structure of a protein can be altered by changes in its secondary structure, therefore it is necessary to determine if such changes have occurred given the changes in secondary structural content observed above. One way to do this is by examining the alterations in fluorescence spectra of hydrophobic residues such as Trp. The N-terminal domain of WT αB-crystallin (residues no. 1-66) contains two Trp residues at positions 9 and 60. However, on deletion of the N-terminal domain, these two residues were deleted. Therefore, the intrinsic Trp fluorescence spectra of species containing both Trp residues (i.e., WT αB, αB N146D, αB-CT, and αB N146D-CT) and the total fluorescence spectra of species lacking the Trp residues (i.e., αB-NT and αB N146D-NT) were recorded from 300 – 400 nm with excitation at 295 nm and 290 nm, respectively (Figure 4A and B). On intrinsic Trp fluorescence, recorded by excitation at

295 nm, WT αB and the αB N146D species showed identical fluorescence with λ_{max} peak at 341 nm, though αB N146D emission intensity was slightly increased relative to WT αB (Figure 4A and B). On C-terminal extension deletion, both αB-CT and αB N146D-CT showed noticeably diminished fluorescence intensity compared to WT αB, but minimal to no shift in λ_{max} with λ_{max} peaks at 342 nm and 341 nm, respectively (Figure 4B). This suggested that C-terminal extension deleted species showed almost no change in microenvironment around the Trp residues, but their Trp residues were relatively less exposed. On total fluorescence determined by excitation at 290 nm, αB-NT showed a 3 nm red shift with λ_{max} at 344 nm and a substantial decrease in fluorescence intensity, however αB N146D-NT showed a 2 nm blue shift with λ_{max} 339 nm and the maximum decrease in fluorescence intensity of all the species. These results suggest that N-terminal domain deletion also causes a change in microenvironment, with the most notable change occurring with the combination of both deamidation and N-terminal deletion. Taken together, the results suggest that N-terminal domain deletion caused greater changes in secondary structure, compared to the C-terminal extension deletion or deamidation at N146 alone.

Surface Hydrophobicity

In light of previous studies suggesting that binding of target proteins during chaperone function is associated with exposed hydrophobic surfaces of the chaperone molecule [33-35], we investigated exposed surface hydrophobic surfaces of the WT αB-crystallin and mutant proteins using a hydrophobic fluorescence probe, ANS (Figure 5). ANS is a useful surface hydrophobicity probe because it remains non-fluorescent in

aqueous solutions until bound to hydrophobic surfaces, therefore its fluorescence correlates to its binding. On ANS binding, both WT αB and the αB N146D mutant exhibited fluorescence with λ_{max} peak at 510 nm (Figure 5A and B), but a relative 14 nm blue shift with increased fluorescence on N146 deamidation. The N-terminal domain deleted mutant exhibited a 9 nm red shift with λ_{max} at 519 nm and decreased fluorescence intensity compared to WT (Figure 5A). However, with the combination of N146 deamidation plus N-terminal domain deletion, the αB N146D-NT mutant showed a 5 nm red shift with λ_{max} at 515 nm, with a decrease in fluorescence intensity similarly observed in the αB-NT mutant (Figure 5A). This suggested that, compared to WT, the N-terminal domain deletion alone resulted in a relatively relaxed structure with greater exposure of hydrophobic surfaces but decreased ANS binding intensity, whereas NT deletion plus N146 deamidation exhibited decreased surface exposure. Conversely, mutants with deletion of the C-terminal extension and C-terminal extension deletion plus N146 deamidation showed a similar blue shift in λ_{max} (i.e., λ_{max} at 496 nm and at 494 nm) and similar fluorescence intensity as WT. Both exhibited a blue shift compared to WT but retained similar fluorescence intensity (Figure 5B). This suggested that the C-terminal extension deletion reduced binding intensity to ANS and produced a relatively more compact structure, which became slightly more compact on N146 deamidation. Taken together, the results suggest that N146 deamidation and C-terminal extension deletion had greater effect on surface hydrophobicity compared to WT, causing larger shifts in fluorescence peaks, whereas deamidation alone cause an increase in binding intensity, not seen in any other mutant. These shifts in fluorescence peaks and changes in intensity

suggest alterations in the microenvironments surrounding hydrophobic residues, and in turn changes in the tertiary structures of these mutants compared to WT αB-crystallin.

Determination of Molecular Mass by Dynamic Light Scattering

To determine whether WT αB-crystallin and its mutants were able to oligomerize and form homomers, their molecular masses were determined using HPLC-coupled multi-angle light scattering (MALS) analysis (Wyatt Technology) (Table 4). While WT αB displayed a mass of 5.8×10^5, the deamidated species (αB N146D) showed an increased mass of 3.1×10^6. On deletion of the N-terminal domain (αB-NT) and N-terminal domain deletion plus deamidation (αB N146D-NT), increased masses of 3.0×10^6 and 5.4×10^6, respectively, were observed. Likewise, C-terminal extension deletion (αB-CT) and C-terminal extension deletion plus deamidation (αB N146D-CT) showed relative increase in mass of 1.2×10^6 and 1.5×10^6, respectively. Taken together, all mutants formed larger oligomers compared to WT αB, decreasing in size in the following order: αB N146D-NT > αB N146D > αB-NT > αB N146D-CT > αB-CT > WT αB. These results also suggest that the N-terminally deleted mutants form larger oligomers than the C-terminally deleted mutants. In both cases, however, presence of the N146 deamidation produced greater increases in oligomer size than the N- or C-terminally deleted mutants alone.

Chaperone Activity of WT αB and Its Mutants

In order to determine if the above observed structural changes also alter the functional property of the αB mutants relative to the WT protein, chaperone activities

were determined using insulin (100 μg) as the target protein in a 1:1 ratio (target: αB protein), as previously described [23]. Light scattering caused by DTT-induced aggregation of insulin B chain was measured at 360 nm in the presence and absence of chaperone proteins, and the activity was represented as the percent protection against aggregation provided by the crystallin species (Figure 6). WT αB provided about 90% protection against DTT-induced insulin aggregation. N146 deamidation of αB-crystallin reduced the protection to about 10%, as previously reported [23]. On N-terminal domain deletion, αB-NT provided about 20% protection, whereas on C-terminal extension deletion, αB-CT only about 12% protection was observed. However, with the combination of deamidation plus N- or C-terminal deletion, chaperone activity increased to roughly 24% in αB N146D-NT and about 40% in αB N146D-CT. Chaperone activity across all αB species decreased in the following order: WT αB > αB N146D-CT > αB N146D-NT > αB-NT > αB-CT > αB N146D. These results suggest that deamidation alone greatly diminishes chaperone function. However, the C-terminal deletion alone is more harmful to chaperone function than N-terminal deletion. Addition of N146 deamidation enhances chaperone function more so on C-terminal extension deletion than on N-terminal domain deletion.

Discussion

Although studies have identified deamidation [11,15-23, 30] and truncation of crystallins [36-43] as the most abundant PTMs in aging and cataractous human lenses, the relative effects of these two PTMs, either individually or in combination, on structural and functional properties of the crystallins are not yet fully determined. Our recent report

showed that deamidation alone had greater affect on the chaperone activity of αA-crystallin than deletion of the N-terminal domain or C-terminal extension [30]. This study also showed that although the N123 residue of αA-crystallin plays a crucial role in maintaining its chaperone function, both the N-terminal domain and C-terminal extension are equally important for chaperone activity. The conclusion was based on results showing that the chaperone activity lost by the αA-N123D mutant was partially or fully recovered following either of the above two deletions. In the present study we have taken a similar approach to determine the changes to the structural and functional properties of N146 deamidated and/or N-terminal domain or C-terminal extension deleted mutants relative to WT αB-crystallin. αB contains two deamidation sites at N78 and N146, and we chose to focus on N146 in the present study because our previous work has shown that, among the two, N146D had a more profound effect on the chaperone activity of αB-crystallin [23].

The major findings of the comparative studies of WT αB and its mutant proteins are as follows: (1) The homomers of the C-terminal extension (residues no. 151-175) deleted αB (αB-CT) and its deamidated form (αB N146D-CT) became water insoluble (i.e., recovered in the inclusion bodies), whereas the deamidated αB (αB N146D), N-terminal domain (residues no. 1-66) deleted αB species (αB-NT), and deamidated plus N-terminal deleted (αB N146D-NT) species remained water soluble. (2) Relative to a molecular mass of 5.8×10^5 Da of WT αB, all the αB-mutants showed even higher molecular mass ranging from 1.2×10^6 Da to 3.1×10^6 Da. This suggested that, like WT αB, all mutants also formed oligomers even after the above-described deamidation, deletion of either N-terminal domain or C-terminal extension, or combination of the two

PTMs. (3) Chaperone activity across all αB species decreased in the following order: WTαB > αB N146D-CT > αB N146D-NT > αB-NT > αB-CT > αB N146D. Specifically, relative to WT αB with 90% protection against DTT-induced aggregation of insulin, substantial losses in chaperone activity (only 10% to 20% protection) were seen in αB N146D, N-terminal domain-deleted or C-terminal extension-deleted mutants. However, in the species with the combination of deamidation plus N- or C-terminal deletion, the percent protection increased to about 24% in αB N146D-NT and about 40% in αB N146D-CT. These results suggested the critical importance of the non-deamidated N146 residue, N-terminal domain and C-terminal extension in maintenance of chaperone activity of αB, as was also suggested in our previous work [23, 30]. Additionally, the above results suggested that the N-terminal domain is relatively more important than the C-terminal extension for the chaperone function of αB. (4) CD spectroscopic studies showed that, relative to WT αB, the mutants with deletion of the above-described N- and C-regions or deamidation showed increased β-sheet and decreased α-helical content, with the exception of αB N146D-CT, which showed a substantial increase in α-helix and decrease in β-sheet content. (5) Results of intrinsic Trp fluorescence suggested little change in Trp microenvironment of αB N146D relative to WT αB, but substantial alterations on deletion of C-terminal extension or a combination of this deletion plus deamidation. Because both Trp residues at positions 9 and 60 were lost on deletion of the N-terminal domain (residues no. 1-66), the total fluorescence spectra of the N-terminal domain-deleted mutants were recorded with excitation at 290 nm and emission spectra between 300 to 400 nm instead of intrinsic Trp fluorescence. A substantial decrease in absorption at 344 nm in αB-NT and at 339 nm in αB N146D-NT suggested major

changes in microenvironment due to altered absorption of their aromatic amino acids. (6) The results of ANS binding studies to probe hydrophobic patches showed that relative to the WT αB structure, the N146 deamidation, C-terminal extension deletion or a combination of this deamidation and deletion resulted in a relatively compact structure (a blue shift), whereas the N-terminal domain deletion and a combination of this deletion plus deamidation showed a relaxed structure (a red shift).

On comparison of the above structural and functional changes of αB mutants with our similar earlier study of αA mutants relative to their WT proteins [22, 30], several notable similarities were observed. For instance, like above findings of αB, the previous study showed insolubilization of αA on deletion of the C-terminal extension, a substantially reduced chaperone activity on deamidation of αA-N123 to D, increased β-sheet content on deletion of N-terminal domain or C-terminal extension, and a slight red shift in the intrinsic Trp fluorescence on deletion of C-terminal extension. However, certain differences between the two studies were also observed, which included an opposite effect on the ANS binding to the two crystallin species, as seen by a blue shift in αA in contrast to red shift in αB on N-terminal domain deletion. These differences were expected because, although αA- and αB-crystallins originated via gene duplication and have 57% sequence homology [44], our results show that individually isolated proteins containing either the N-terminal domain, core region or C-terminal extension of both αA- and αB-crystallins differed in their structural and functional properties (Asomugha, Gupta and Srivastava, manuscript in preparation). These differences in the two crystallins were also noted in previous studies. Some such examples are: recombinant αA- and αB-crystallins differ in their secondary and tertiary structures, and relative to αA, αB showed

a greater hydrophobicity and 4X more chaperone activity [45]; αA-crystallin was more stable to gamma irradiation relative to αB [46]; and although αA- and αB-crystallins can each form oligomers independently, together or with other crystallins, their interactions with each other were 3X greater than their interactions with βB2 and γC-crystallins [47].

Several studies have shown in vivo deamidation of α-, β-, and γ-crystallins [10,21,48-50]. We have identified deamidation of N146 in a fragment of human αB-crystallin isolated from normal and cataractous lenses of 60- to 80-year-old donors [21]. Such deamidation of N146 has also been reported in bovine αB-crystallin [51], but its effect on the structural and functional properties of the crystallin was unknown until our present study, which describes such effects for the first time.

Like other small heat shock proteins (sHSPs), α-crystallin also contains a highly conserved sequence of 80 to 100 residues (residues 64-142 in αA-crystallin and 67-146 in αB-crystallin) called the α-crystallin domain [5,52]. Based on similarities with the structure of other HSPs, it is believed that the N-terminal region (residue 1-63 in αA-crystallin and 1-66 in αB-crystallin) of α-crystallin forms an independently folded domain, whereas the C-terminal extension (residues 143-173 in αA- and 147-175 in αB-crystallin) is flexible and unstructured [5]. As stated above, the deamidation at N146 is within the α-crystallin domain (residues 67-146) of αB-crystallin. Several past studies have demonstrated altered structural and functions properties of αA- and αB-crystallins following mutations in the N-terminal domain, α-crystallin domain or C-terminal extension. The α-crystallin domain is believed to engage in subunit–subunit interactions, because recombinant αB-crystallin containing only the α-crystallin core domain formed a dimer [53]. Also, two disease-related point mutations of a highly conserved Arg at

equivalent positions in αA (R116C) and αB (R120G), located in the α-crystallin domain, caused structural changes that lead to hereditary cataracts [25,26,54,55]. Deletion of the last 17 amino acids of the C-terminal extension from human αB-crystallin caused precipitation, with reduced chaperone activity [56], and similarly a deletion of 25 residues from the C-terminus in *Xenopus* Hsp30C reduces its solubility and impairs chaperone activity [57]. On removal of N-terminal residues (partial or 1-56 residues of N-terminus) and the C-terminal extension (partial or 32-34 residues of C-terminus) of αA- and αB-crystallins, the proteins showed improper folding, reduced chaperone activity, and formation of trimers or tetramers [13,58-60]. Residues 42-57 and residues 60-71 (located either in or near the N-terminal domain) of αB-crystallin interact with αA-crystallin [61,62]. Pin-array analysis has further shown that five peptide sequences of αB-crystallin (i.e., residues 37-54 [in the N-terminal domain], residues 75-82,131-138, 141-148 [form β-strands in the conserved α-crystallin domain], and residues 155-166 [in the C-terminal extension]) interact with αA-crystallin [63]. Together these studies suggested that the N-terminal domain, α-crystallin domain and C-terminal extension of αB crystallin are not only important for chaperone activity but also for interaction and oligomerization with αA-crystallin. In spite of these studies, the individual amino acids in the αA and αB subunits that interact with target proteins during chaperone activity have not been fully identified.

In conclusion, our study identified several structural changes in αB-crystallin following deamidation at N146D, deletion of N-terminal domain, deletion of C-terminal extension or a combination of the deamidation and either of the two deletions, and correlated these structural changes to their effect on the chaperone activity of the

crystallin. Further, deamidation may serve as a signal for proteolysis as has been suggested by past studies [28,64]. Whether this signal is used during age- and cataract-related truncations of αA- and αB-crystallins and other crystallins remains to be determined. We are presently attempting to find answers to these questions. In addition, our future studies will be focused on whether these post-translational modifications lead to cataract development in transgenic animals.

Acknowledgments

The work presented was supported by grants from NIH (EY-06400 and P30-EY03039) and by the EyeSight Foundation of Alabama.

References

1. Bloemendal H, de Jong WW, Jaenicke R, Lubsen NH, Slingsby C, Tardieu A. Ageing and vision: structure, stability and function of lens crystallins. Prog Biophys Mol Biol 2004; 86:407-85.
2. Andley UP. Crystallins in the eye: function and pathology. Prog Retin Eye Res 2007; 26:78-98.
3. Klemenz R, Fröholi E, Steiger RH, Schäfer R, Aoyama A. αB-Crystallin is a small heat shock protein. Proc Natl Acad ScI USA 1991 May; 88:3652-56.
4. Bhat SP, Nagineni CN. αB subunit of lens-specific protein α-crystallin is present in other ocular and non-ocular tissues. Biochem Biophys Res Commun 1989; 158:319-25.
5. de Jong WW, Caspers GJ, Leunissen JA. Genealogy of the alpha-crystallin-small heat-shock protein superfamily. Int J Biol Macromol 1998; 14:7363-76.
6. Renkawek K, Vooter CE, Bosman GJ, van Workum FP, de Jong WW. Expression of alpha B-crystallin in Alzheimer's disease. Acta Neuropathol 1994; 87(2):155-60.
7. Renkawek K, Stege GJ, Bosman GJ. Dementia, gliosis and expression of the small heat shock proteins hsp27 and alpha B-crystallin in Parkinson's disease. Neuroreport 1999 Aug 2; 10:2273-6.
8. Horwitz J. α-Crystallin can function as a molecular chaperone. Proc Natl Acad Sci USA 1992 Nov; 89:10449-53.

9. Mchaourab HS, Godar JA, Stewart PL. Structure and mechanism of protein stability sensors: chaperone activity of small heat shock proteins. Biochemistry 2009; 48:3828-37.

10. Hanson SRA, Hasan A, Smith DL, Smith JB. The major in vivo modifications of the human water-insoluble lens crystallins are disulfide bonds, deamidation, methionine oxidation and backbone cleavage. Exp Eye Res 2000; 71:195-207.

11. Lund AL, Smith JB, Smith DL. Modifications of the water-insoluble human lens α-crystallins. Exp Eye Res 1996; 63:661-72.

12. Groenen PJ, Merk KB, de Jong WW, Bloemendal H. Structure and modifications of the junior chaperone α-crystallin. From lens transparency to molecular pathology. Eur J Biochem 1994 Oct 1; 225(1):1-19.

13. Bova MP, Mchaourab HS, Han Y, Fung BK. Subunit exchange of small heat shock proteins. Analysis of oligomer formation of αA-crystallin and Hsp27 by fluorescence resonance energy transfer and site-directed truncations. J Biol Chem 2000 Jan 14; 275(2):1035-42.

14. Pasta SY, Raman B, Ramakrishna T, Rao CM. Role of C-terminal extensions of α-crystallins. Swapping the C-terminal extension of αA-crystallin to αB-crystallin results in enhanced chaperone activity. J Biol Chem 2002 Nov 29; 277(48):45821-8.

15. Lapko VN, Purkiss AG, Smith DL, Smith JB. Deamidation in human γS-crystallin from cataractous lenses is influenced by surface exposure. Biochemistry 2002; 41:8638-48.

16. Harms MJ, Wilmarth PA, Kapfer DM, Steel EA, David LL, Bächinger HP, Lampi KJ. Laser light-scattering evidence for an altered association of βB1-crystllin deamidated in the connecting peptide. Protein Sci 2004 Mar; 13(3):678-86.

17. Wilmarth PA, Tanner S, Dasari S, Nagalla SR, Rifiere MA, Bafna V, Pevzner PA, David LL. Age-related changes in human crystallins determined from comparative analysis of post-translational modifications in young and aged lens: does deamidation contribute to crystallin insolubility? J Proteome Res 2006 Oct; 5(10):2554-66.

18. Lampi KJ, Amyx KK, Ahmann P, Steel EA. Deamidation in human lens βB2-crystallin destabilizes the dimmer. Biochemistry 2006; 45:3146-53.

19. Hains PG, Truscott RJW. Post-translational modifications in the nuclear region of young, aged, and cataract human lenses. J Proteome Res 2007 Oct; 6(10):3935-43.

20. Hains PG, Truscott RJW. Age-dependent deamidation of life-long proteins in the human lens. Invest Ophthalmol Vis Sci 2010 Jun; 51(6):3107-14.

21. Srivastava OP, Srivastava K. Existence of deamidated αB-crystallin fragments in normal and cataractous human lenses. Mol Vis 2003; 9:110-8.

22. Gupta R, Srivastava OP. Deamidation affects structural and functional properties of human αA-crystallin and its oligomerization with αB-crystalln. J Biol Chem 2004 Oct 22; 279(43):44258-69.

23. Gupta R, Srivastava OP. Effect of deamidation of asparagine 146 on functional and structural properties of human lens αB-crystallin. Invest Ophthalmol Vis Sci 2004 Jan; 45(1):206-14.

24. Plater ML, Goode D, Crabbe MJ. Effects of site-directed mutations on the chaperone-like activity of αB-crystallin. J Biol Chem 1996 Nov 8; 271(45):28558-66.

25. Kumar LV, Ramakrishna T, Rao CM. Structural and functional consequences of the mutation of a conserved arginine residue in αA and αB crystallins. J Biol Chem 1999 Aug 20; 274(34):24137-41.

26. Liu Y, Zhang X, Luo L, Wu M, Zeng R, Cheng G, Hu B, Liu B, Liang JJ, Shang F. A novel αB-crystallin mutation associated with autosomal dominant congenital lamellar cataract. Invest Ophthalmol Vis Sci 2006 Mar; 47(3):1069-75.

27. Robinson NE, Robinson AB. Molecular clocks. Proc Natl Acad Sci USA 2001 Jan 30; 98(3):944-9.

28. Robinson NE. Protein deamidation. Proc Natl Acad Sci USA 2002 Apr 16; 99(8):5283-8.

29. Selcen D, Engel AG. Myofibrillar myopathy caused by novel dominant negative αB-crystallin mutations. Ann Neurol 2003 Dec; 54(6):804-10.

30. Chaves JM, Srivastava K, Gupta R, Srivastava OP. Structural and functional roles of deamidation and/or truncation of N- or C-termini in human αA-crystallin. Biochemistry 2008; 47:10069-83.

31. Laemmli UK. Cleavage of structural proteins during the assembly of the head of bacteriophage T4. Nature 1970; 227:680-5.

32. Reddy MA, Bateman OA, Chakarova C, Ferris J, Berry V, Lomas E, Sarra R, Smith MA, Moore AT, Bhattacharya SS, Slingsby C. Characterization of the

G91del CRYBA1/3-crystallin protein: a cause of human inherited cataract. Hum Mol Genet 2004 May 1; 13(9):945-53.

33. Reddy GB, Kumar PA, Kumar MS. Chaperone-like activity and hydrophobicity of α-crystallin. IUBMB Life 2006 Nov; 58(11):643-41.

34. Kundu B, Shukla A, Chaba R, Guptasarma P. The excised heat-shock domain of αB-crystallin is folded, proteolytically susceptible trimer with significant surface hydrophobicity and a tendency to self-aggregate upon heating. Protein Expr Purif 2004 Aug; 36(2):263-71.

35. Kumar MS, Kapoor M, Sinha S, Reddy GB. Insights into hydrophobicity and the chaperone-like function of αA- and αB-crystallins. J Biol Chem 2005 Jun 10; 280(23):21726-30.

36. Srivastava OP. Age-related increase in concentration and aggregation of degraded polypeptide in human lenses. Exp Eye Res 1988 Oct; 47(4):525-43.

37. Srivastava OP, Srivastava K, Harrington V. Age-related degradation of βA3/A1-crystallin in human lenses. Biochem Biophys Res Commun 1999 May 19; 258(3):632-8.

38. Srivastava OP, Srivastava K. βB2-crystallin undergoes extensive truncation during aging in human lenses. Biochem Biophys Res Commun 2003 Jan 31; 201(1):44-9.

39. Harrington V, McCall S, Huynh S, Srivastava K, Srivastava OP. Crystallins in water soluble-high molecular weight protein fractions and water insoluble protein fractions in aging and cataractous human lenses. Mol Vis 2004 Jul 19; 10:476-89.

40. Harrington V, Srivastava OP, Kirk M. Proteomic analysis of water insoluble proteins from normal and cataractous human lenses. Mol Vis 2007 Sep 14; 13:1680-94.

41. Srivastava OP, Srivastava K. Degradation of γD- and γs-crystallins in human lenses. Biochem Biophys Res Commun 1998 Dec 18; 253(2):288-94.

42. Srivastava OP, Srivastava K, Silney C. Levels of crystallin fragments and identification of their origin in water soluble high molecular weight (HMW) proteins of human lenses. Curr Eye Res. 1996 May; 15(5):511-20.

43. Srivastava K, Chaves JM, Srivastava OP, Kirk M. Multi-crystallin complexes exist in the water-soluble high molecular weight protein fractions of aging normal and cataractous human lenses. Exp Eye Res 2008 Oct; 87(4):356-66.

44. Horwitz J. Alpha-crystallin. Exp Eye Res 2003 Feb; 76(2): 145-53.

45. Sun T-X, Das BK, Liang JJ-N. Conformational and functional differences between recombinant human lens αA- and αB-crystallin. J Biol Chem 1997 Mar 7; 272:6220-5.

46. Fujii N, Nakamura T, Sadakane Y, Saito T, Fujii N. Differential susceptibility of alpha A- and alpha B-crystallin to gamma-ray irradiation. Biochim Biophys Acta 2007 Mar; 1774(3):345-50.

47. Fu L, Liang JJ-N. Detection of protein-protein interactions among lens crystallins in a mammalian two-hybrid system assay. J Biol Chem 2002 Feb 8; 277:4255-60.

48. Takemoto L. Increased deamidation of asparagine-101 from alpha-A crystallin in the high molecular weight aggregate of the normal human lens. Exp Eye Res 1999 May; 68(5):641-5.

49. Lampi KJ, Kim YH, Bächinger HP, Boswell BA, Lindner RA, Carver JA, Shearer TR, David LL, Kapfer DM. Decreased heat stability and increased chaperone requirement of modified human βB1-crystallins. Mol Vis 2002 Sep 25; 8:359-66.

50. Lampi KJ, Oxford JT, Bächinger HP, Shearer TR, David LL, Kapfer DM. Deamidation of human βB1 alters the elongated structure of the dimer. Exp Eye Res 2001 Mar; 72(3): 279-88.

51. Groenen PJ, van Dongen M, Voorter CE, Bloemendal H, de Jong WW. Age-dependent deamidation of αB-crystallin. FEBS Lett 1993 May 3; 322(1):69-72.

52. Caspers GJ, Leunissen JA, de Jong WW. The expanding small heat-shock protein family, and structure predictions of the conserved "alpha-crystallin domain". J Mol Evol 1995 Mar; 40(3):238-48.

53. Feil IK, Malfois M, Hendle J, van Der Zandt H, Svergun DI. A novel quaternary structure of the dimeric α-crystallin domain with chaperone-like activity. J Biol Chem 2001; 276:12024-29.

54. Bova MP, Yaron O, Huang Q, Ding L, Haley DA, Stewart PL, Horwitz J. Mutation R120G in αB-crystallin, which is linked to a desmin-related myopathy, results in an irregular structure and defective chaperone-like function. Proc Natl Acad Sci USA 1999 May 25; 96(11):6137-42.

55. Cobb BA, Petrash JM. Structural and functional changes in the αA-crystallin R116C mutant in hereditary cataracts. Biochemistry 2000 Dec 26; 39(51):15791-8.

56. Smulders RHPH, Carver JA, Lindner RA, van Boekel MA, Bloemendal H, de Jong WW. Immobilization of the C-terminal extension of bovine αA-crystallin reduces chaperone-like activity. J Biol Chem 1996 Nov 15; 271(46):29060-6.

57. Fernando P, Heikkila JJ. Functional characterization of Xenopus small heat shock protein, Hsp30C: the carboxyl end is required for stability and chaperone activity. Cell Stress Chaperones 2000 Apr; 5(2):148-59.

58. Takemoto L, Emmons T, Horwitz J. The C-terminal region of alpha-crystallin: involvement in protection against heat-induced denaturation. Biochem J 1993 Sep1; 294(Pt 2):435-8.

59. Aziz A, Santhoshkumar P, Sharma KK, Abraham EC. Cleavage of the C-terminal serine of human αA-crystallin produces αA_{1-172} with increased chaperone activity and oligomeric size. Biochemistry 2007; 46(9):2510-19.

60. Andley UP, Shashank M, Griest TA, Petrash JM. Cloning, expression, and chaperone-like activity of human αA-crystallin. J Biol Chem 1996 Dec 13; 271(50):31973-80.

61. Sreelakshmi Y, Santhoshkumar P, Bhattacharyya J, Sharma KK. αA-crystallin interacting regions in the small heat shock protein, αB-crystallin. Biochemistry 2004 Dec 21; 43(50):15785-95.

62. Sreelakshmi Y, Sharma KK. The interaction between αA- and αB-crystalllin is sequence-specific. Mol Vis 2006 May 24; 12:581-7.

63. Ghosh JG, Clark JI. Insights into the domains required for dimerization and assembly of human αB-crystallin. Protein Sci 2005 Mar; 14(3):684-95.

64. Inaba M, Gupta KC, Kuwabara M, Takahashi T, Benz EJ Jr, Maede Y. Deamidation of human erythrocyte protein 4.1: possible role in aging. Blood 1992 Jn 15; 79(12):3355-61.

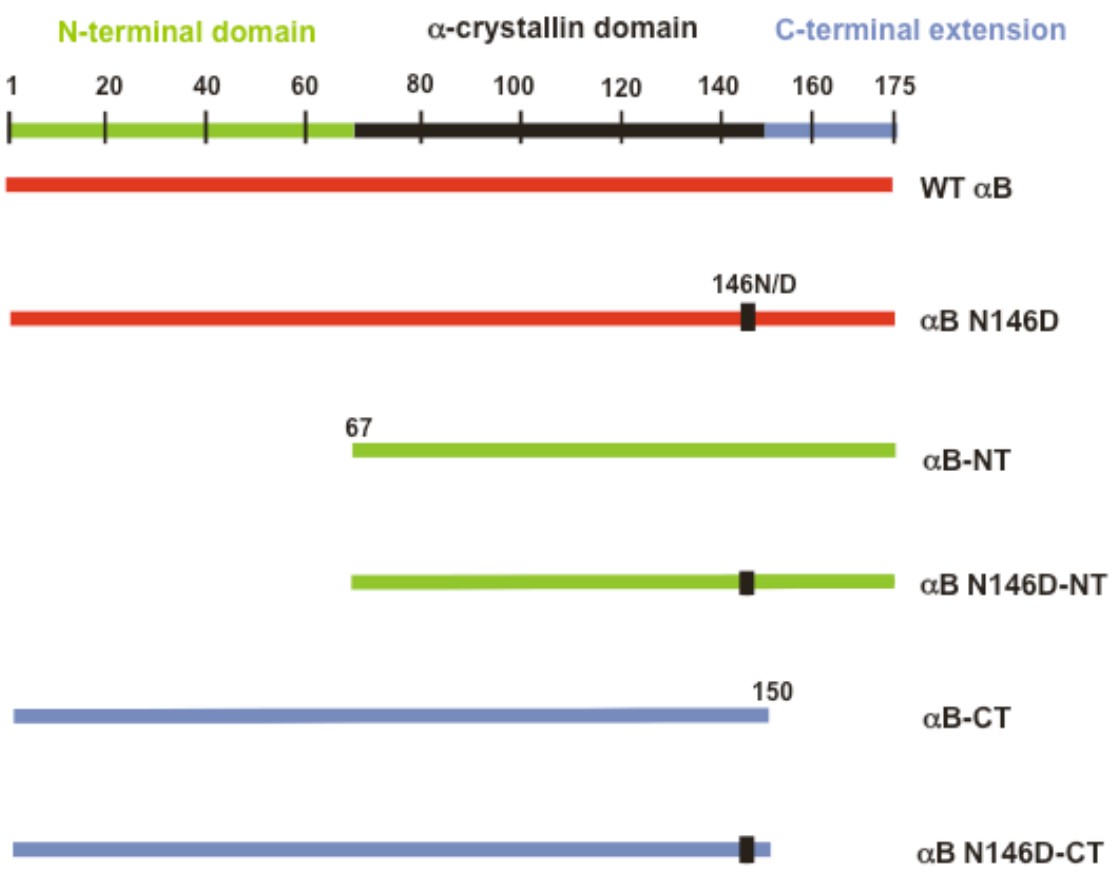

Figure 1. Schematic diagram showing the deamidation sites, regions and residue numbers of the N-terminal domain, α-crystallin domain, and C-terminal extension of WT αB and its mutants. WT αB is a full-length protein containing all residues from 1-175. Residue N146 was deamidated (i.e., N to D) in the deamidated mutants. N-terminal domain deleted mutants (αB-NT and αB N146D-NT) are missing residues no. 1-66, while C-terminal extension deleted mutants (αB-CT and αB N146D-CT) are missing residues no. 151-175.

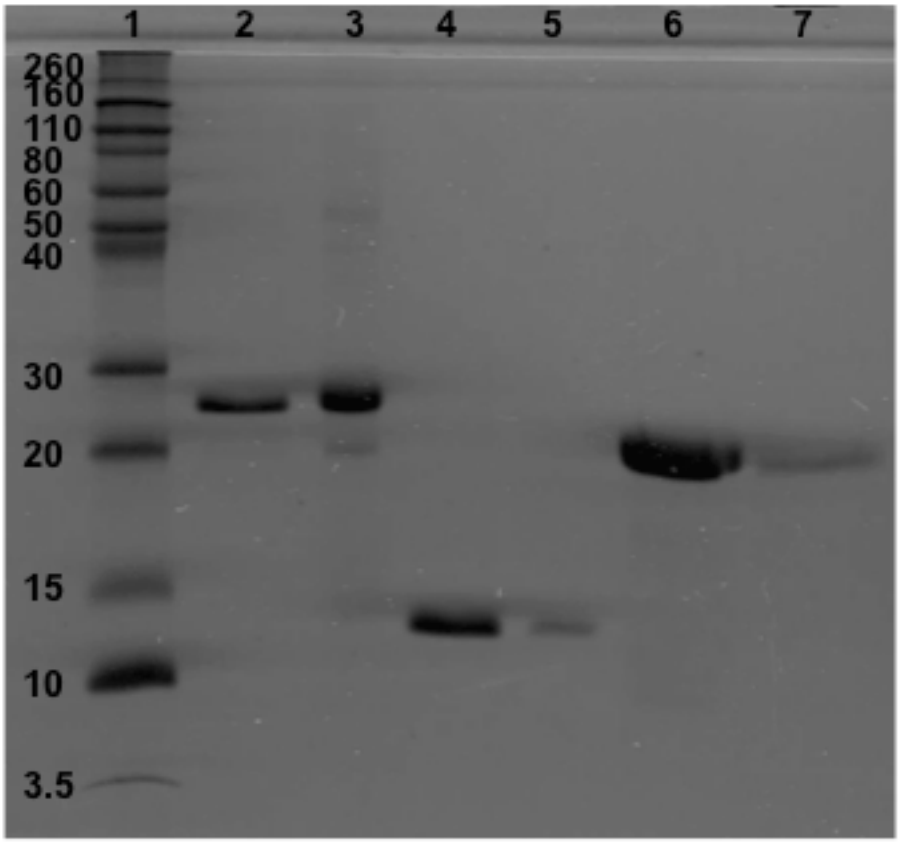

Figure 2. SDS-PAGE analysis of purified, His-tagged WT αB and its deamidated, N- or C-terminally deleted mutants, and deamidated plus deleted mutants, following Ni^{2+}-affinity column purification (see Methods). Lane 1 – molecular weight marker; Lane 2 – WT αB; Lane 3 – αB N146D; Lane 4 – αB-NT; Lane 5 – αB N146D-NT; Lane 6 – αB-CT; αB N146D-CT.

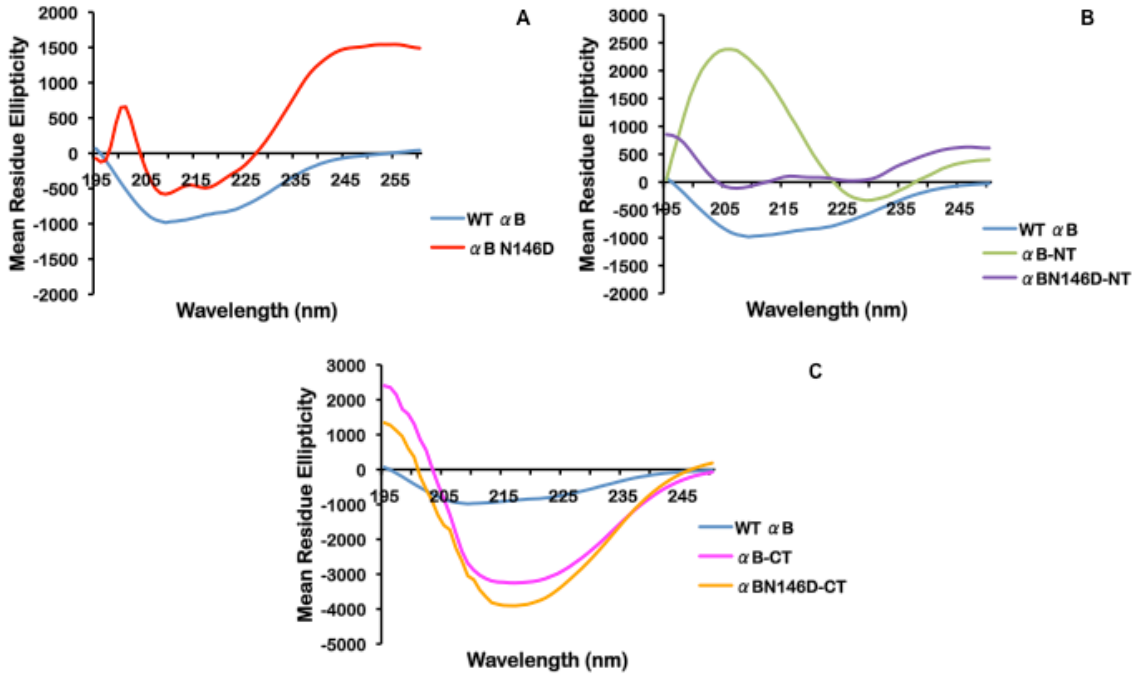

Figure 3. Far-UV CD spectra of WT αB and its mutant proteins. Spectra were recorded using protein preparations of 0.2 mg/ml, dissolved in 50 mM sodium phosphate buffer (pH 7.8), and a cell path length of 0.5 mm. The reported spectra are the average of 5 scans corrected for the buffer blank and smoothed. A, WT αB and the deamidated mutant. B, WT αB and N-terminal domain deleted mutatnts. C, WT αB and C-terminal extension deleted mutants.

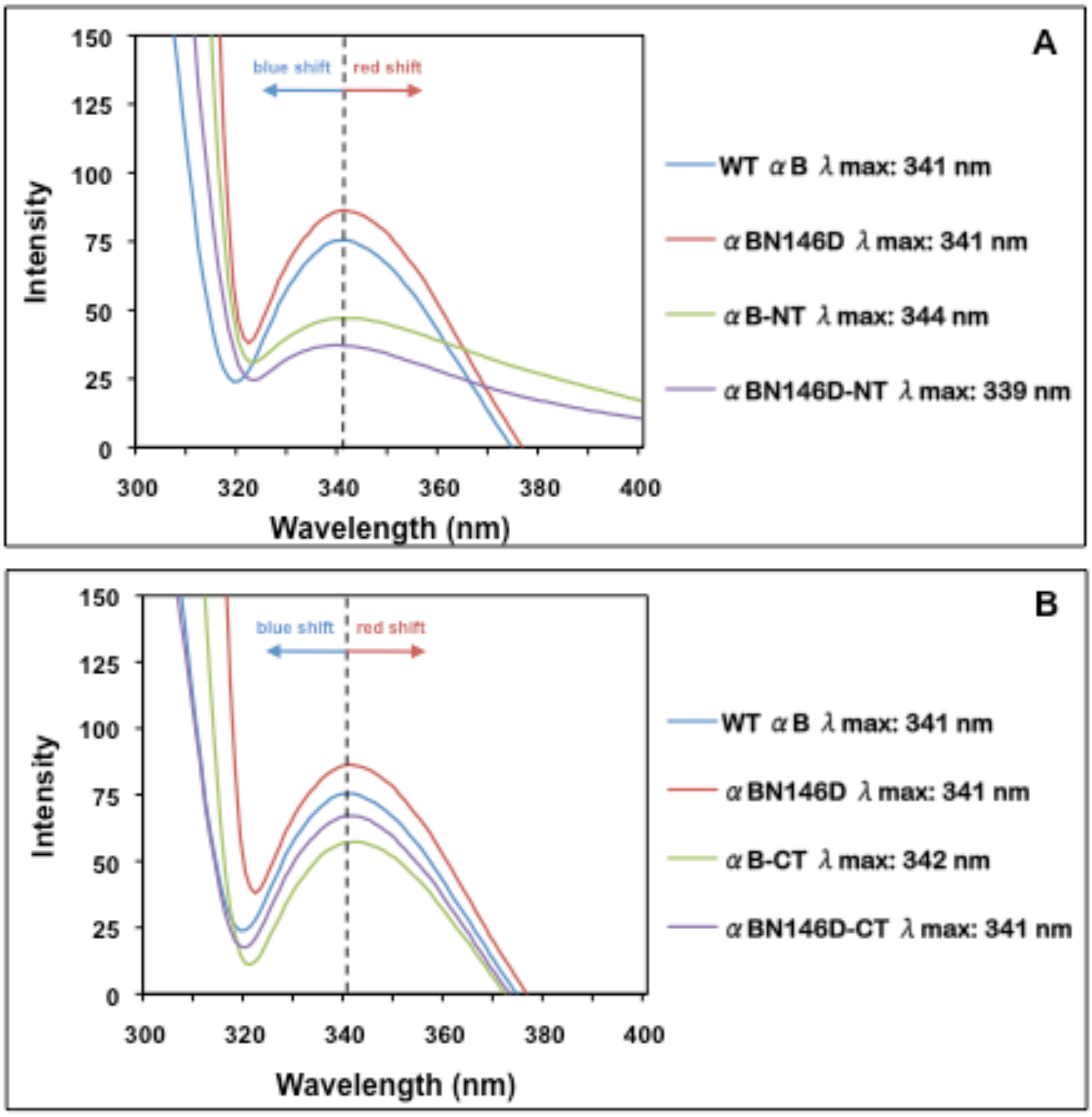

Figure 4: Intrinsic Trp and total fluorescence spectra of WT αB and its mutant proteins. A, Total fluorescence spectra (Ex 290 nm, Em 300-400 nm) were recorded for the N-terminal domain deleted mutants because Trp residues 9 and 60 are deleted along with the deletion of this domain. B, Intrinsic Trp fluorescence spectra (Ex 295 nm, Em 300-400 nm) were recorded for mutants containing the N-terminal domain. The dotted lines indicate the wavelength of maximum peak fluorescence (λ_{max}) observed in WT αB, used to determine whether a blue or red shift in wavelength occurred.

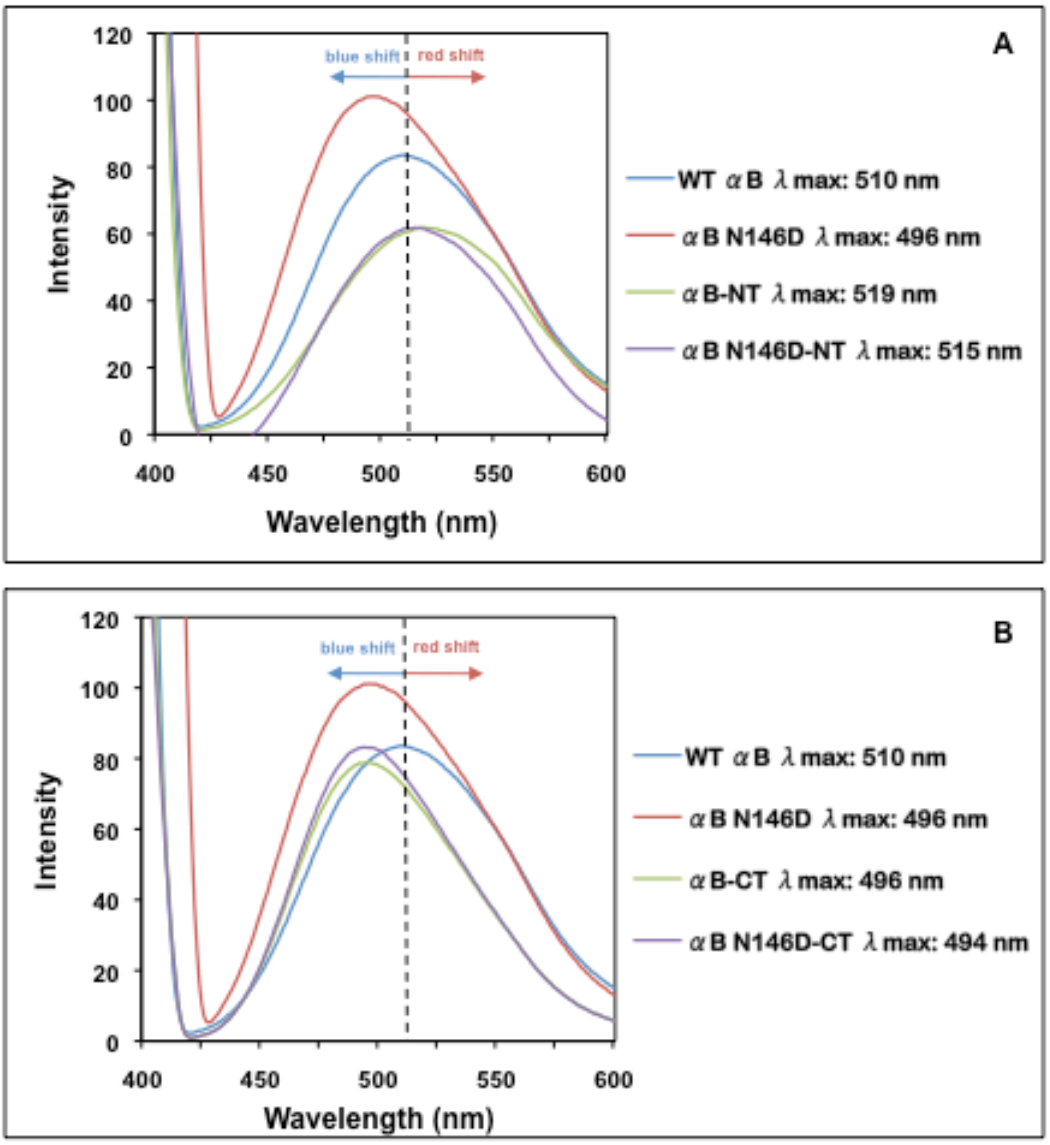

Figure 5: Fluorescence spectra of WT αB and its mutants following ANS biding. Spectra were recorded by excitation at 390 nm and emission from 400-600 nm using 0.2 mg/ml protein preparations mixed with 15 mL of 0.8 mM ANS (dissolved in methanol) and incubated at 37 °C for 15 min. A, WT αB and its deamidated and N-terminal domain deleted mutants. B, WT αB and its deamidatd and C-terminal extension deleted mutants. The dotted lines indicated the wavelength of maximum peak fluorescence (λ_{max}) observed in WT αB, used to determine whether a blue or a red shift in wavelength occurred.

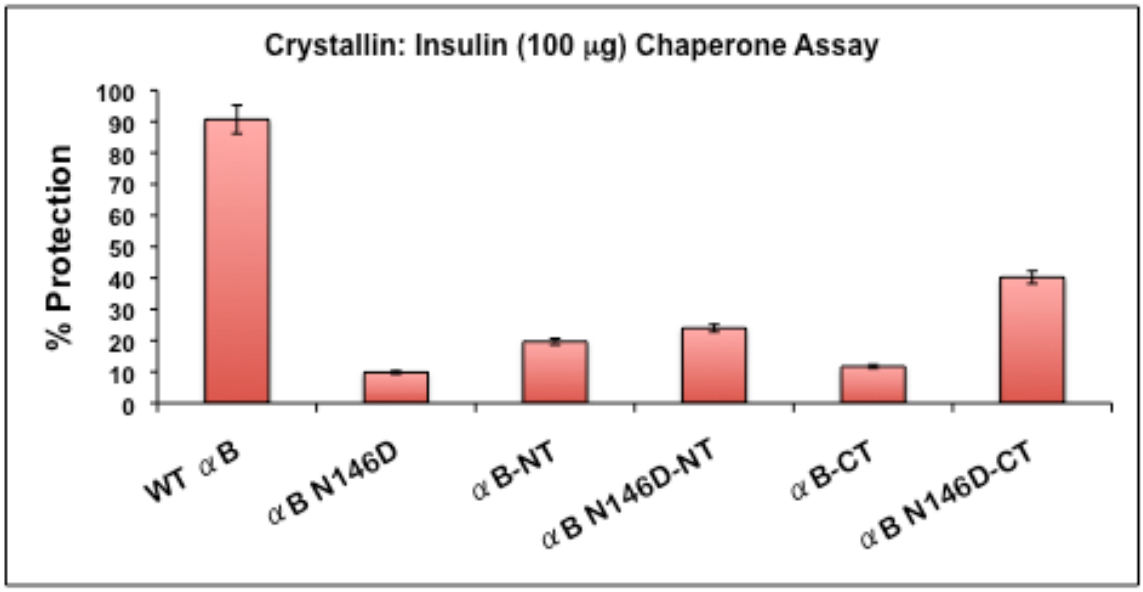

Figure 6. Comparison of chaperone activity of WT αB and its mutant proteins. The chaperone activity, calculated as % protections, was assayed by measuring DTT-induced insulin (100 μg) aggregation in the presence of a chaperone/insulin ration (1:1) at 25 C. Error bars = Percent Error (+/- 1%).

Table 1. Oligonucleotide Primers used for subcloning WT αB and deamidated αB species, and generating truncated αB mutant proteins using PCR-based mutagenesis.

Mutant Constructs		Primers (5' – 3')
WT αB	forward	CACCATGGACATCGCCATCCACCACCCCTG
	reverse	CTATTTCTTGGGGGCTGCGGTGACAGC
αB N146D	forward	CACCATGGACATCGCCATCCACCACCCCTG
	reverse	CTATTTCTTGGGGGCTGCGGTGACAGC
αB-NT	forward	CACCCGCCTGGAAAAGGACAGGTTCTCTG
	reverse	CTATTTCTTGGGGGCTGCGGTGACAGC
αBN146D-NT	forward	CACCCGCCTGGAAAAGGACAGGTTCTCTG
	reverse	CTATTTCTTGGGGGCTGCGGTGACAGC
αB-CT	forward	CACCATGGACATCGCCATCCACCACCCCTG
	reverse	TTATTTCCTTGGTCCATTCACAGTGAG
αBN146D-CT	forward	CACCATGGACATCGCCATCCACCACCCCTG
	reverse	TTATTTCCTTGGTCCATTCACAGTGAG

NT and CT denote the N-terminally truncated and C-terminally truncated mutant proteins, respectively.

Table 2. Presence of WT αB and its deamidated, N-terminal domain or C-terminal extension deleted, and deamidated plus deleted mutants in the soluble fraction or inclusion bodies.

WT αB and Mutant Crystallin Species	Soluble Fraction	Inclusion Bodies
WT αB	+	-
αB N146D	+	-
αB-NT	+	-
αB N146D-NT	+	-
αB-CT	-	+
αB N146D-CT	-	+

The + sign indicates presence of the protein as observed on SDS-PAGE following centrifugation.

Table 3. Secondary structural content of WT αB and its mutants. Percentages were determined by analysis of the Far-UV spectra (Figure 3) using the SELCON3 analysis program.

Crystallin Species	α Helix (+/- 1%)	β Sheet (+/- 1%)	β Turn (+/- 1%)	Random Coil (+/- 1%)
WT αB	19.3	48.7	12.4	19.6
αB N146D	6.1	64.2	5.5	24.2
αB-NT	3.0	69.7	16.9	10.6
αB N146D-NT	5.9	62.5	5.5	24.4
αB-CT	11.7	62.2	10.5	17.1
αB N146D-CT	47.5	31.7	6.8	14.8

Table 4. Molar mass determination of WT αB and its mutants using the dynamic light scattering method (MALS).

Crystallin Species	Molecular Mass (Da)
WT αB	**5.8×10^5**
αB N146D	**3.1×10^6**
αB-NT	**3.0×10^6**
αB N146D-NT	**5.4×10^6**
αB-CT	**1.2×10^6**
αB N146D-CT	**1.5×10^6**

CHARACTERIZATION OF PROPERTIES OF N-TERMINAL DOMAIN, CORE DOMAIN, AND C-TERMINAL EXTENSION OF αA- AND αB-CRYSTALLINS

by

CHINWE O. ASOMUGHA, RATNA GUPTA, OM P. SRIVASTAVA

In preparation for *Molecular Vision*

Format adapted for dissertation

Abstract

Purpose

The purpose of the present study was to determine the biophysical properties of the N-terminal domain, core domain and C-terminal extensions of human αA- and αB-crystallins and correlate these properties to their chaperone activity.

Methods

Wild type (WT) αA- and αB-crystallins, previously cloned in pET 100D TOPO vector, were used as templates to generate different constructs encoding specific regions (N-terminal domain [NTD], core domain [CD], and C-terminal extension, [CTE]). The specific regions amplified by PCR using plasmid DNA from WT αA and WT αB were: αA NTD (residues 1-63), αA CD (residues 64-142), αA CTE (residues 143-173), αB NTD (residues 1-66), αB CD (residues 67-146), and αB CTE (residues 147-175). Resultant blunt-end PCR products were ligated to a pET100 Directional TOPO vector. DNA sequencing confirmed the desired constructs. Positive clones were transformed into the BL21 Star (DE3) expression cell line, and expression and solubility of the proteins were confirmed by SDS-PAGE and Western Blot analysis using a monoclonal antibody against a 6X His-tag epitope. Proteins were purified using Ni^{2+}-affinity column chromatography, under native or denaturing conditions, and used for biophysical and chaperone function analyses.

Results

A total of five constructs were successfully generated: αA NTD, αA CD, αB NTD, αB CD, and αB CTE. SDS-PAGE and Western blot analyses showed that αA CD

and αB CD were present in both the soluble and insoluble fractions, whereas species with NTD alone became insoluble and species with CTE alone became soluble. Confirmed constructs showed alterations in biophysical properties and chaperone function compared to WT α-crystallins. αA NTD and αB CTE exhibited the most notable changes in secondary structural content. Also, αA NTD and all constructs of αB-crystallin showed altered surface hydrophobicity compared to their respective WT α-crystallins.

Conclusions

Although the individual α-crystallin regions (i.e., N-terminal domain, core domain, and C-terminal extension) exhibited varied biophysical properties, each region alone retained some level of chaperone function.

Introduction

Crystallin proteins are the major components of the mammalian lens fiber cells and are subdivided into three classes, α, β, and γ. The crystallins help to increase the refractive power of the lens and maintain lens transparency by forming high concentrations of soluble oligomers and participating in short-range interactions amongst themselves [1,2]. Of the crystallins, α-crystallin accounts for almost half of the total lens protein and its two homologous subunits, αA and αB, oligomerize to form hetero-oligomers of ~800 kDa in a 3:1 ratio in vivo [2-4]. α-Crystallin is also a member of the small heat shock protein (sHSP) family, which are stress-induced proteins of 12-40 kDa subunits containing a conserved α-crystallin domain of ~90 amino acids and flanked on either side by a variable hydrophobic N-terminal domain and a short, hydrophilic unstructured C-terminal extension with a conserved sequence motif [3-8].

Like other sHSPs, α-crystallins posses chaperone function [9], whereby they recognize and bind destabilized and improperly folded proteins [7,8]. However, α-crystallins are ATP-independent chaperones, and cannot refold proteins [6], but sequester aberrant proteins to prevent subsequent formation of light-scattering aggregates. Because there is no protein turnover in mature fiber cells of the lens [10], crystallins must survive the lifetime of the lens and transparency must be maintained despite environmental insults and post-translational modifications (PTMs) that occur with age. In this manner, α-crystallins play a critical role in the maintenance of lens transparency.

It has been well established that chaperone activity of α-crystallins is dependent upon oligomerization of α-crystallins and substrates through hydrophobic contacts between accessible hydrophobic surfaces of α-crystallin and exposed hydrophobic surfaces of unfolding proteins [9,11]. However, the mechanism of chaperone binding is still not fully understood and studies have been undertaken to determine which sites of α-crystallin are involved in its chaperone function. Many have attributed chaperone binding to hydrophobic sequences in the α-crystallin domain, as well as in the N-terminal domain [Reviews 3,6,7]. Specifically, studies suggest a functional chaperone substrate-binding site resides in residues 70-88 of αA-crystallin [12], as well as residues 73-92 of αB-crystallin [13]. It has also been suggested that residues 54-61 of αB-crystallin play an essential role in αB chaperone activity, though unessential for target protein binding [14]. However, others have identified several substrate-binding sites in αB-crystallin, including two N-terminal domain sequences, four α-crystallin domain sequences, and one C-terminal extension sequence, using protein pin arrays [15].

Mutagenesis, in general, has been used as a tool to identify regions of α-crystallin necessary for chaperone function. Studies have generated "point mutations" as well as "truncation" mutations mimicking naturally occurring PTMs to study their affects on crystallin structure and function [16,17]. It has been shown that hereditary point mutations in αA (R116C) and αB (R120G) cause structural and functional alterations that lead to congenital cataract and desmin-related myopathy, respectively [18,19]. Using mutagenesis, we mimicked commonly occurring age-related deamidations in αA- and αB-crystallins and demonstrated that N123D deamidation in αA and N146D deamidation in αB-crystallin are crucial for chaperone activity [20,21]. We also carried out a comprehensive study comparing two PTMs, deamidation and truncation, and showed that N123 deamidation in αA [21] and N146 deamidation in αB [Unpublished data], as well as truncation of N- and C-termini, were detrimental to chaperone function. Whether mutations in the N-terminal domain, α-crystallin core domain, or C-terminal extension of α-crystallin [23-27] affect both structure and function of the protein remains unclear. Previous studies have reported that removal/ swapping of residues/regions from either the N-terminal domain or the C-terminal extension in both αA- and αB-crystallins cause improper folding and reduced chaperone activity [28-31], however none of these studies have explored the structural/functional stability of the individual regions of α-crystallin (i.e., N-terminus, core domain and C-terminus).

With all the variations in results in the literature, it is still unclear where the chaperone activity resides. In an attempt to better understand this phenomena of which region is most important for chaperone activity of αA- and αB-crystallins, we looked at each region (N-terminal domain, core domain, and C-terminal extension) individually.

The following constructs: αA N-terminal domain (αA NTD, residues 1-63), core domain (αA CD, residues 64-142) and αB N-terminal domain (αB NTD, residues 1-66), core domain (αB CD, residues 67-146), and C-terminal extension (αB CTE, residues 147-175) were generated and used to determine the structure and function of the individual regions and narrow down which region is most pertinent to chaperone function. Our results reveal that despite structural alterations in proteins representing the N-terminal domain, core domain, and C-terminal extension, compared to wild-type (WT) αA- and αB- crystallins, each protein individually displayed some level of chaperone activity, though activity was variable.

Methods

Materials

Molecular mass protein markers and DNA markers were purchased from Invitrogen (Carlsbad, CA) and Promega (Madison, WI), respectively. Primers used in the study were obtained from Sigma-Aldrich (St. Louis, MO). Anti-Histidine-tagged mouse monoclonal primary antibody and goat anti-mouse IgG (H+L) horseradish peroxidase-conjugated secondary antibody were obtained from Calbiochem-EMD Biosciences (La Jolla, CA) and Thermo Scientific (Rockford, IL), respectively. Molecular biology-grade chemicals were purchased from either Sigma or Fisher Scientific (Fair Lawn, NJ), unless otherwise stated.

Bacterial Strains and Plasmids

The *Escherichia coli* One Shot® TOP 10 cells and BL21 Star (DE3) bacterial strain were obtained from Invitrogen. TOP10 cells were used for propagation and BL21 cells were used for expression. Plasmids containing human wild-type (WT) αA- and αB-crystallin genes, previously generated, were already present in the laboratory.

Generation of αA- and αB-crystallin Constructs

Plasmids containing human WT αA-crystallin gene in pET 100D TOPO vector (Invitrogen) [22] were used as a template for generating the desired constructs of αA-crystallin. WT αB-crystallin gene was subcloned into pET 100D TOPO vector (Invitrogen) [21] and was used as a template for generating the desired constructs of αB-crystallin. Cloning in the pET 100 Directional TOPO vector added a six His-tag at the N-terminus of the protein, which allowed us to purify cloned proteins in a single affinity chromatographic step using a Ni^{2+}- affinity column. PCR-based deletion was used to generate the desired constructs, using specific complimentary primer pairs (Table1). The following constructs were generated by PCR-directed mutagenesis: (i) N-terminal domain consisting of residues no. 1-63 of αA and residues no. 1-66 of αB, (ii) Core domain consisting of residues no. 64-142 of αA and residues no. 67-146 of αB, and (iii) C-terminal extension consisting of residues no. 143-173 of αA and residues no. 147-175 of αB. Briefly, 25 ng of template was used under the following PCR conditions: pre-denaturation at 95 °C for 5 min, followed by 30 cycles of denaturation at 95 °C for 1 min, annealing at 62-68 °C for 45 s (depending on the T_m of the primers), and extension/elongation at 72 °C for 1 min, with a final extension at 72 °C for 10 min. PCR

products were ligated into the pET 100 Directional TOPO vector as per the manufacturer's instructions, and the deletions at desired sites were confirmed by DNA sequencing (Genomics Core Facility of the University of Alabama at Birmingham) at the transcriptional level, and by Western Blot analysis using a monoclonal anti-His tag antibody at the translational level. Positive clones were transformed into *E. coli* BL21 Star (DE3) cells, and selected using ampicillin.

Expression and Extraction of Proteins in Soluble and Inclusion Bodies

PCR amplicons were transformed into *E. coli* BL21 Star (DE3) cells, as previously described, using a standard *E. coli* transformation technique [20]. IPTG, at a final concentration of 1 mM, was added in order to over-express the proteins, and cell cultures were incubated for 4 h at 37 °C. Cells were harvested, resuspended in lysis buffer [25 mM Tris-HCl (pH 7.8), 50 mM NaCl, 0.9% glucose, 1 mM EDTA, containing lysozyme (0.25 mg/mL) and protease inhibitor cocktail (Sigma)] and sonicated while kept on ice. DNA was degraded by treatment with DNase I (10 mg/mL) for 30 min on ice. The soluble fraction was separated by centrifugation at 8000 × g for 10 min at 4 °C, and the insoluble fraction was resuspended in detergent buffer (DB) [0.5 M NaCl, 1% (w/v) sodium deoxycholate, 1% NP-40, and 20 mM Tris-HCl, pH 7.5]. Further, the detergent-soluble fraction was separated by centrifugation at 5000 × g for 10 min at 4 °C. The resultant pellet was washed with 0.5% Triton X-100 and centrifuged, as stated above, and the wash step was repeated as necessary to remove bacterial debris from the inclusion bodies. The final pellet was resuspended in denaturating binding buffer (DBB) [8M urea, 0.5 M NaCl, and 20 mM sodium phosphate, pH 7.8].

Purification of WT αA- and WT-αB-crystallins and their Constructs

Depending on the presence of expressed proteins in soluble fractions or inclusion bodies (insoluble fractions), each protein was purified under native or denaturing conditions. All purification steps were carried out at 4 °C, unless otherwise stated, including refolding steps. Proteins samples were adsorbed on an Invitrogen ProBond Ni^{2+}-chelating column according to the manufacturer's instructions. Under native conditions, the column was equilibrated and loaded with the protein sample using a native binding (NB) buffer [20 mM sodium phosphate containing 0.5 M NaCl, pH 7.8], washed with NB buffer containing 20 mM imidazole (pH 7.8), and eluted with NB buffer containing 250 mM imidazole (pH 7.8). Under denaturing conditions, the column was equilibrated with DBB, and following the application of desired protein preparation, the unbound proteins were eluted by a first wash with DBB; followed by a second and third wash with DBB at pH 6.0 and pH 5.3, respectively. Finally, the bound proteins were eluted with DBB containing 250 mM imidazole (pH 7.8).

Fractions recovered from Ni^{2+}-affinity column chromatography and containing a desired protein, purified under native or denaturing conditions, were analyzed by SDS-PAGE [32]. Those purified under native conditions were dialyzed against 50 mM phosphate buffer (pH 7.8) at 4 °C, and stored at -20 °C until needed. Proteins purified under denaturing conditions were refolded using a previously published method [33] briefly described below. Purity of WT αA- and αB-crystallins and their constructs was examined by SDS-PAGE and their identities were confirmed by Western Blot analyses [34] using an anti-His-tagged monoclonal antibody. Protein concentrations were

determined by absorbance at 280 nm using a NanoDrop 2000 spectrophotometer (Thermo Scientific).

Refolding of Proteins Purified Under Denaturing Conditions

Proteins purified under denaturing conditions were refolded by 24 h dialysis at 4°C against 50 mM sodium phosphate (pH 7.5) containing 1 mM DTT and decreasing urea concentrations from 8 M to 4 M, and finally in a urea-free phosphate buffer.

Characterization of Structural/Functional Properties of WT αA- and WT αB-Crystallins and their Contstructs

Circular Dichroism (CD) Spectroscopy

The far-UV CD spectra of purified WT αA- and WT αB-crystallins and their constructs were recorded at room temperature over a range of 190 – 260 nm on a Jasco J815 CD spectrometer using 0.2 mg/mL of protein in 50 mM sodium phosphate buffer (pH 7.8), as described previously [22]. A quartz cell of 0.5 mm path length was used, and the reported spectra are an average of five scans baseline-corrected for the buffer blank and smoothed. The secondary structural contents of WT proteins and constructs were determined by analysis of the CD spectra using SELCON3 analysis program.

ANS Binding and Fluorescence Spectroscopy

Binding of a hydrophobic probe, 8-anilino-1-naphthalene sulfonate (ANS), to WT αA- and WT αB-crystallins and their constructs was measured by recording fluorescence

emission spectra at 400 – 600 nm with excitation at 390 nm, as previously described [20, 21]. For this, 15 mL of 0.8 mM ANS (dissolved in methanol) was added to 0.2 mg/mL of protein in 50 mM sodium phosphate buffer (pH 7.8), mixed thoroughly, and incubated for 15 min at 37 °C prior to spectroscopy.

Oligomer Size Determination by Dynamic Light Scattering

A multiangle laser light scattering instrument (Wyatt Technology, Santa Barbara, CA) coupled to an HPLC system was used to determine the absolute molar mass of the WT proteins and their constructs. Prior to their analysis, protein samples in 50 mM sodium phosphate (pH 7.8) were filtered through a 0.22 μm filter. Results were acquired using 18 different angles, which were normalized with the 90º detector.

Chaperone Activity Assay

In order to assess the ability of different α-crystallin constructs to prevent DTT-induced insulin aggregation, chaperone activity was determined following methods previously described [21]. Aggregation of insulin by reduction with 20 mM DTT at 20°C, either in absence or at varying concentrations of different αA- and αB-crystallin species in 1mL reaction volumes containing 50 mM sodium phosphate (pH 7.8) was determined. Aggregation was monitored by measuring light scattering at 360 nm as a function of time using a Shimadzu UV-VIS scanning spectrophotometer (model UV2101 PC) equipped with a six-cell positioner and a temperature controller (Shimadzu model CPS-260).

Results

Confirmation of Site-Specific Deletions in α-Crystallin Constructs

WT αA- and WT αB-crystallins, already present in the laboratory, were used as templates to generate constructs of individual α-crystallin domains (see Methods). The individual N-terminal domain, core domain, and C-terminal extension constructs of both αA- and αB-crystallins were generated using PCR-based mutagenesis and are referred to as αA NTD, αA CD, αB NTD, αB CD, and αB CTE in the text (Figure1). DNA sequencing confirmed the desired constructs: αA NTD (residues no. 1-63), αA CD (residues no. 64-142), αB NTD (residues no. 1-66), αB CD (residues no. 67-146), and αB CTE (residues no. 147-175).

Expression and Purification of WT α-Crystallins and Constructs

Expression of WT αA, WT αB and their crystallin constructs was induced in the BL21 Star (DE3) expression cell line using 1 mM IPTG for 4 h, as previously described [20], and proteins were recovered in either the soluble fraction, insoluble fraction (inclusion bodies), or both fractions (Table 2). WT αA, WT αB and αB CTE proteins were recovered in the soluble fraction, whereas αA NTD and αB NTD proteins were recovered in the insoluble fraction. These results were expected considering the hydrophobic nature of the N-terminal domain and hydrophilic nature of the C-terminal extension. However, the αA CD and αB CD proteins were recovered in both the soluble and insoluble fractions, suggesting their partial solubility property. The expression and solubility of individual proteins were also confirmed by Western blot analysis using a specific monoclonal antibody against a 6X His-tag epitope (data not shown).

Each protein was over-expressed in *E. coli* at 37 °C and purified to almost homogeneity, under native or denaturing conditions, using Ni^{2+}-affinity columns (see Methods). On SDS-PAGE analysis, the molecular weights (M_r) of purified His-tagged WT αA, WT αB and their constructs ranged between 7 and 27 kDa (Figure 2). WT αA and WT αB showed M_r of ~25-27 kDa (Figure 2, lanes 2 and 5), while M_r of N-terminal domain constructs (αA residues 1-63 and αB residues 1-66) were ~11-13 kDa, core domain constructs (αA residues 64-142 and αB residues 67-146) were ~13-14 kDa, and the C-terminal extension construct (αB residues 147-175) was ~7kDa (Figure 2, lanes 3, 4, 6-8). The SDS-PAGE gel showed the highly purified nature of these proteins, and Western blot analysis using a monoclonal anti-His antibody confirmed their identity as His-tagged α-crystallin proteins (data not shown).

Comparative Properties of Individual α-Crystallin Domains and WT α-Crystallins

Circular Dichroism Spectral Studies

To evaluate the effect of deletion/truncation of specific regions, leaving only a single domain, on the secondary structure of the α-crystallin constructs, far-UV CD spectra and secondary structural content were determined (Figure 3, Table 3). As evident, the constructs exhibited varied CD spectra (Figure 3 A and B) compared to WT αA- and WT αB-crystallins. Based on secondary structural content, as determined using the SELCON3 analysis software, WT αA exhibited 21.6% α-helix, 46.6% β-sheet, 13.4% β-turn, and 17.6% random coil. In contrast, the αA NTD construct showed a marked difference in secondary structure with 80.5% α-helix, 7.9% β-sheet, 3.2% β-turn, and

8.4% random coil, suggesting that the N-terminal domain of αA-crystallin by itself assumes a more helical structure (Figure 3A, Table 3). The αA CD construct varied slightly from WT αA with 37.9% α-helix, 42.7% β-sheet, 10.7% β-turn, and 9.6% random coil, suggesting that αA CD alone retains a secondary structure similar to WT (Figure 3A, Table 3). Based on SELCON3 analysis, WT αB exhibited 19.3% α-helix, 48.7% β-sheet, 12.4% β-turn, and 19.6% random coil. However, αB NTD differed in secondary structural content with 29.9% α-helix, 41.3% β-sheet, 9.1% β-turn, and 19.4% random coil. The increase in α-helical content and slight decrease in β-sheet of αB NTD produced a readily visible difference in spectra compared to WT (Figure 3B). Like αA CD, αB CD also exhibited only a slight difference in its CD spectra relative to WT αB (Figure 3B). αB CD showed 20.6% α-helix, 48.1% β-sheet, 14.3% β-turn, and 18.7% random coil (Table 3). Among the αB-crystallin constructs, αB CTE showed the most marked difference in secondary structure compared to WT, with 5.9% α-helix, 66.6% β-sheet, 4.3% β-turn, and 23.5% random coil. αB CTE also exhibited more random coil structure than all other constructs (Table 3). This noticeable decrease in α-helical content and increase in β-sheet suggests that, by itself, the C-terminal extension of αB-crystallin has more β-sheet structure. Taken together, the results suggested that, individually, the domains flanking the α-crystallin core domain display greater alterations in secondary structure than the core domains when compared to their respective WT proteins. The most notable changes were that the N-terminal domain construct of αA-crystallin showed greater α-helical content compared to WT, while the C-terminal extension of αB-crystallin showed a substantial decrease in α-helical content and increase in β-sheet content.

Surface Hydrophobicity

Changes to the secondary structure of a protein likely affect its tertiary structural conformation as well. Previous studies have implicated the exposed hydrophobic surfaces of α-crystallins in the binding of target proteins during chaperone function [7,33,35]. In light of the altered secondary structures of the individual domains of αA- and αB-crystallins, we investigated surface hydrophobicity binding, among WT proteins and their constructs, by using a hydrophobic fluorescence probe, ANS (Figure 4). ANS is a useful probe for assaying surface hydrophobicity because it is non-fluorescent in aqueous solutions, but fluoresces when bound to hydrophobic surfaces, so its fluorescence correlates to its binding. On ANS binding, WT αA exhibited fluorescence with λ_{max} peak at 497 nm, and similarly, αA CD showed a fluorescence peak at 497 nm with identical intensity. However, with a peak at 507 nm, αA NTD exhibited a 10 nm red shift relative to WT αA, and it was coupled with a decrease in fluorescence intensity (Figure 4A). The results suggest that, relative to WT αA, the N-terminal domain construct showed a relatively relaxed structure with a greater exposure of hydrophobic surfaces but decreased binding intensity, while the αA core domain retained its surface hydrophobicity property. On binding to ANS, WT αB exhibited a fluorescence peak with λ_{max} at 517 nm. However, αB NTD, CD, and CTE all showed a blue shift compared to WT, as well as reduced fluorescence intensity, with peaks at 495 nm, 488 nm, and 510 nm, respectively (Figure 4B). The differences in λ_{max} peaks of the αB-crystallin constructs relative to WT αB were as follows: a 22 nm shift in the αB NTD peak, a 29 nm shift in αB CD peak, and a 7 nm shift in αB CTE peak. Of all the constructs, the C-terminal extension construct showed a substantial decrease in fluorescence intensity, compared to WT αB.

The results suggest that, compared to WT, the individual αB-crystallin domain constructs displayed relatively compact structures with both decreased exposure of hydrophobic surfaces and decreased binding intensity. Taken together, shifts in fluorescence peaks and changes in intensity suggest changes in the microenvironments surrounding the hydrophobic residues and imply changes to the tertiary structures of these proteins compared to their WT crystallins.

Determination of Molecular Mass by Dynamic Light Scattering

To determine whether the individual crystallin domain constructs were able to oligomerize, the molecular masses of WT αA, WT αB and their constructs were determined by HPLC multi-angle light scattering (MALS) analysis (Wyatt Technology). Table 4 shows the molecular mass of each protein. Compared to WT αA, which had a mass of 6.8×10^5 D, the αA NTD and αA CD constructs showed a mass of 1.6×10^4 D and 3.0×10^4 D, respectively. Individually, the N-terminal domain and core domain of αA-crystallin form smaller oligomers, though the core domain forms slightly larger oligomers than the N-terminal domain. Similar to WT αA, WT αB had a mass of 5.8×10^5 D. Compared to WT αB, αB NTD displayed a mass of 2.6×10^3 D, however, both αB CD and αB CTE showed increases in mass of 8.4×10^7 D and 1.0×10^6 D, respectively. Individually, the N-terminal domain forms smaller oligomers, while the core domain and C-terminal extension both form much larger oligomers compared to WT αB.

Chaperone Activity of WT α-Crystallins and Individual Domain Constructs

To determine if the individual α-crystallin domains retain functionality, the chaperone activity of these constructs was assayed. The chaperone activities of WT αA and WT αB and their individual domain constructs were determined using insulin (100 mg) as the target protein in a 1:1 ratio. Light scattering at 360 nm was used to measure aggregation of the insulin B chain by reduction with DTT in the presence and absence of chaperone proteins. Chaperone activity was represented as the percent protection provided by the crystallins (Figure 5). WT αA exhibited about 90% protection against DTT-induced insulin aggregation, whereas both αA NTD and αA CD constructs showed a decrease in chaperone activity, providing about 65% and 60% protection, respectively. Similar to WT αA, WT αB exhibited about 95% protection against insulin aggregation. However, both αB NTD and αB CD constructs showed decreased chaperone activity compared to WT. αB NTD showed the greatest protection at about 85%, while αB CD showed about 70%. αB CTE provided only minimal protection to insulin at about 25%. In general, amongst the constructs, chaperone activity decreased as follows: NTD > CD > CTE. More specifically, chaperone activity across all proteins decreased in the following order: WT αB > WT αA > αB NTD > αB CD > αA NTD > αA CD > αB CTE (Figure 5). Taken together, the results suggested that isolating the individual domains of both αA- and αB-crystallins, particularly the N-terminal domains, affected the chaperone activity of the proteins, but did not completely deplete their function.

Discussion

The purpose of the present study was to generate individual constructs of N-terminal domain, core domain, and C-terminal extension of both αA- and αB-crystallins

and utilize them for comparative structural and functional analyses to ascertain which region is most pertinent to chaperone function. For this purpose, two constructs of αA-crystallin (i.e., αA N-terminal domain [αA NTD, residues 1-63] and core domain [αA CD, residues 64-142]) and three constructs of αB-crystallin (i.e., αB N-terminal domain [αB NTD residues 1-66], core domain [αB CD, residues 67-146], and C-terminal extension [αB CTE, residues 147-175]) were generated. One construct, αA C-terminal extension [αA CTE, residues 143-173] could not be successfully generated even after five attempts and utilizing variable conditions. This could be due to a small αA CTE region (containing only 90 bp) relative to other regions of both αA- and αB-crystallins. Our failure could also be due to other reasons, which are presently unknown to us.

The reason for selectively utilizing the three regions (i.e., N-terminal domain, core domain, and C-terminal extension) of αA- and αB-crystallins for the comparative structural and functional study was because several past reports have described effects of either partial deletion or mutation in the three regions, but never examined the properties of each individual region.

Each of the above constructs was confirmed by DNA sequencing. Similarly, the specific protein products of the constructs were confirmed by their expected M_r's following SDS-PAGE analysis, and by immunoreactivity to an anti-His-tag antibody during Western blot analysis. Each of the His-tagged proteins was purified by one step Ni^{2+}-affinity column chromatography, and SDS-PAGE analysis showed their recovery in highly purified forms (Figure 2).

The following were the major findings of the study: (1) In contrast to the high content of 46.6% β-sheet and only 21.6% α-helix in WT αA, αA NTD showed high α-

helix (80.5%) and substantially low (7.9%) β-sheet content. Similarly, the αA CD construct showed 37.9% α-helix and 42.7% β-sheet content, suggesting that both the N-terminal domain and core domain alone of αA-crystallin assume a more helical structure than WT αA (Figure 3A, Table 3). (2) Relative to 19.3% α-helix and 48.7% β-sheet content of WT αB, αB NTD also showed a higher α-helical content of 29.9%, and a lower β-sheet content of 41.3%. However, αB CD showed 20.6% α-helix and 48.1% β-sheet, which was similar to WT αB-crystallin. In contrast, αB CTE showed only 5.9% α-helix and 66.6% β-sheet, which was the most marked difference in secondary structure compared to WT αB. (3) On determination of hydrophobicity by ANS-binding, WT αA and αA CD exhibited λ_{max} fluorescence peaks at 497 nm with identical intensity, whereas αA NTD exhibited a 10 nm red shift with a λ_{max} peak at 507 nm, suggesting that the secondary structure was relatively relaxed with greater exposed hydrophobic surfaces. On a similar ANS binding, WT αB showed λ_{max} at 517 nm, whereas αB NTD, αB CD, and αB CTE showed blue shifts compared to WT with λ_{max} peaks at 495 nm, 488 nm, and 510 nm, respectively. Therefore, relative to WT αB, the differences in λ_{max} peaks of the αB-crystallin constructs were as follows: a 22 nm shift in the αB NTD peak, a 29 nm shift in the αB CD peak, and a 7 nm shift in the αB CTE peak. Together, the results suggest that compared to WT, the individual αB constructs displayed relatively compact structures with a decrease in both exposure of hydrophobic surfaces and binding intensity. (4) The MALS results showed that relative to a M_r of 6.8×10^5 Da of WT αA oligomers, its constructs also oligomerized but exhibited lower molecular mass (i.e., αA NTD and αA CD M_r of 1.6×10^4 Da and $3.0\text{x}10^4$ Da, respectively). Similarly, relative to the M_r of $5.8\text{x}10^5$ Da of WT αB, the αB NTD construct showed a substantially lower M_r

of $2.6x10^3$ Da, while the other two constructs showed higher M_r (i.e., αB CD and αB CTE displayed $8.4x10^7$ Da and $1.0x10^6$ Da, respectively). Therefore, relative to the N-terminal domain of αB, both the core domain and C-terminal extension of αB formed much larger oligomers, which were even bigger than the oligomers of WT αB. (5) WT αA and WT αB exhibited almost the same levels of about 90% protection against DTT-induced insulin aggregation. However, both N-terminal and core domain constructs of αA also showed 65% and 60% protection, respectively. Similarly, αB NTD, αB CD and αB CTE exhibited protection at about 85%, 70% and 25%, respectively. Together, the results show a greater chaperone activity of the N-terminal domain of αB relative to N-terminal domain of αA, but similar levels of activity of core domain of the two crystallins. The C-terminal extension construct of αB exhibited substantially low (25%) chaperone activity relative to all other regions of both αA and αB-crystallins. We anticipate a similar low level of chaperone activity of αA CTE.

The above differences in the structural and functional properties in the three regions of αA and αB were seen in spite of their origin via gene duplication and having ~57% sequence homology [36]. Some other examples showing differences in the two crystallins include: recombinant αA- and αB-crystallins differ in their secondary and tertiary structures, and relative to αA, αB showed a greater hydrophobicity and 4X more chaperone activity [37]. Other reports showed that αA-crystallin was more stable to gamma irradiation relative to αB [38], and although αA- and αB-crystallins can each form oligomers independently, together or with other crystallins, their interactions with each other were 3X greater than their interactions with βB2 and γC-crystallins [39]. Both crystallins also exhibit varied expression in different diseases. While αA is lens specific,

αB-crystallin is widely expressed in other tissues, most prominently in astrocytes [40] and muscles [41]. αB has also been detected in the brain and associated with neurological diseases such as Alzheimer's [42], Parkinson's [43], Creutzfeldt-Jakob disease [44], Alexander disease [45] and diffuse Lewy body disease [46].

As stated above, like other sHSPs, α-crystallin also contains a highly conserved sequence of 80-100 residues called the α-crystallin domain [2,29]. Based on similarities with the structures of other HSPs, it is believed that the N-terminal region of both αA- and αB-crystallins form an independently folded domain, whereas the C-terminal region is flexible and unstructured [2,29]. Our CD spectra results also suggest that the N-terminal domain of αA indeed formed an independently folded domain with high content of α-helix (80.5%) and low β-sheet (7.9%) compared to 46.6% β-sheet and 21.6% α-helix in WT αA. Similarly, αB-NTD with 29.9% α-helix and 41.3% β-sheet also exhibited distinct secondary structure compared to WT αB with 19.3% α-helix, and 48.7% β-sheet. Because of the absence of data regarding the secondary structure of αA CTE, we could only compare the secondary structural data of αB CTE (5.9% α-helix, 66.6% β-sheet) with WT αB (19.3% α-helix, 48.7% β-sheet). The results show that αB CTE assumes a greater β-sheet structure relative to WT αB. αA NTD showed drastic differences in secondary structure because of significant increase in α-helical content and concurrent decrease in β-sheet content. The results of altered secondary structures of N-terminal domains of αA and αB compared to their WT proteins were also supported by their ANS binding results and molecular mass determined by the MALS method. Relative to WT αA (λ_{max} at 497 nm), αA NTD exhibited a λ_{max} peak at 507 nm with a 10 nm red shift whereas, compared to WT αB (λ_{max} at 517 nm), αB NTD showed λ_{max} of

495 nm with a 22 nm blue shift. Therefore, both αA NTD and αB NTD exhibited altered hydrophobicity relative to their WT proteins, but the former acquired a relatively relaxed structure and the latter a compact structure. Additionally, relative to molecular mass of 6.8×10^5 Da of WT αA and 5.8×10^5 Da of WT αB, both αA NTD and αB NTD exhibited oligomers with mass of 1.6×10^4 Da and 2.6×10^3 Da, respectively. The lower molecular mass of αB NTD compared to αA NTD supports their blue and red shifts during ANS binding, respectively. On ANS binding, both WT αA and αA CD exhibited λ_{max} fluorescence peaks at 497 nm with identical intensity, however, the molecular mass of αA CD (3.0×10^4 D) was significantly lower than that of WT αA (6.8×10^5 D). Both αB CD and αB CTE showed a blue shift with λ_{max} of 488 and 510 nm, respectively. These results clearly showed changes in the microenvironment of hydrophobic patches of αB CD and αB CTE. However, in spite of compact structure, both αB CD and αB CTE displayed higher molecular mass of 8.4×10^7 D and 1.0×10^6 D, respectively, compared to WT αB. Together, the results show a greater tendency of αB CD and αB CTE to form oligomers of bigger sizes compared to those αA NTD, αB NTD and αACD. Further, interestingly, each region of both αA and αB could form oligomers in the same manner as full-length α-crystallins.

The present study showed that all three regions of both αA- and αB-crystallins are involved in varied levels of chaperone activity. While both WT αA and WT αB exhibited almost the same levels (~90%) protection against DTT-induced insulin aggregation, the higher level of chaperone activity of the N-terminal domains of both crystallins relative to their core domains and C-terminal extension suggest that it is most relevant among the three regions for the chaperone activity. This is supported by previous

reports that showed that, primarily, the residues within the N-terminal domain or near it are involved in chaperone substrate binding, i.e. residues 70-88 of αA-crystallin [12], as well as residues 73-92 of αB-crystallin [13]. Similarly, residues 54-61 of αB-crystallin are essential for its chaperone activity although unessential for target protein binding [14].

Reports have suggested that, as in other sHSPs, the N-terminal domain of αA-crystallin is important for chaperone activity, self-assembly into oligomers, and structural stability. Our previous report has shown that the deletion of the N-terminal domain of αA resulted in altered structure with properties such as increased hydrophobic patches, β-sheet content, and subunit exchange rate with WT-αB, but reduced oligomer mass and chaperone activity [22]. Residues 12-21 and 70-88 in the N-terminal domain of αA were identified as substrate binding sites [12]. Similarly, two bis-ANS binding sites at residues 50-54 and 79-99 were also identified [47]. Deletion of 1-63 amino acid residues in bovine α-crystallin resulted in the formation of only a tetrameric species [48], suggesting severely diminished oligomerization property. This is consistent with the peptide scan results, which showed that residues 42-57 and 60-71 of αA play a role in oligomerization and subunit interactions [49]. Further, both the N-terminal domain and C-terminal extension were shown to be important in the self-interaction of αA-crystallin.

Although our study showed little chaperone activity in the C-terminal extension of αB-crystallin, a previous study showed that on the removal of N-terminal residues (partial or 1-56 residues of N-terminus) and C-terminal extension residues (partial or 32-34 residues of C-terminus) of αA- and αB-crystallins, the proteins showed improper

folding, reduced chaperone activity and formation of trimers or tetramers [2,12,22,29,45-47].

In summary, we have taken an alternative approach in this study than the previously published reports that examined whether mutation or deletion of three regions of both αA- and αB-crystallins have effects on their structural and functional properties. The most intriguing finding of the present study was that although the three different regions (i.e., N-terminal domain, core domain, and C-terminal extension) of both αA- and αB-crystallins have different secondary structures, surface hydrophobicity and oligomerization properties, they individually retain variable levels of chaperone activity.

Acknowlegements

This work was supported by NIH grants EY06400 and P30-EY03039.

References

1. Delaye M, Tardieu A. Short-range order of crystalline proteins accounts for eye lens transparency. Nature 1983; 302:415-7.
2. Bloemendal H, de Jong W, Jaenicke R, Lubsen NH, Slingsby C, Tardieu A. Ageing and vision: structure, stability and function of lens crystallins. Prog Biophys Mol Biol 2004; 86:407-85.
3. Augusteyn RC. α-Crystallin: a review of its structure and function. Clin Exp Optom 2004; 87:356-66.
4. Andley UP. Crystallins in the eye: function and pathology. Prog Retin Eye Res 2007; 26:78-98.
5. de Jong WW, Caspers GJ, Leunissen JA. Genealogy of the α-crystallin – small heat-shock protein superfamily. Int J Biol Macromol 1998; 22:151-62.
6. Narberhaus F. α-Crystallin-type heath shock proteins: socializing minichaperones in the context of a multichaperone network. Microbiol Molec Biol Rev 2002; 66:64-93.
7. Reddy GB, Kumar PA, Kumar MS. Chaperone-like activity and hydrophobicity of α-crystallin. IUBMB Life 2006 Nov; 58(11):643-41.
8. Mchaourab HS, Godar JA, Stewart PL. Structure and mechanism of protein stability sensors: chaperone activity of small heat shock proteins. Biochemistry 2009; 48:3828-37.
9. Horwitz J. α-Crystallin can function as a molecular chaperone. Proc Natl Acad Sci USA 1992 Nov; 89:10449-53.

10. Lynnerup N, Kjeldsen H, Heegaard S, Jacobsen C, Heinemeier J. Radiocarbon dating of the human eye lens crystallines reveal proteins without carbon turnover throughout life. PLoS One 2008 Jan; 3(1)e1529.

11. Proctor CJ, Sóti C, Boys RJ, Gillespie CS, Shanley DP, Wilkinson DJ, Kirkwood TBL. Modelling the actions of chaperones and their role in ageing. Mech Ageing Dev 2005 Jan; 126(1):119-31.

12. Sharma K, Kumar RS, Kumar GS, Quinn PT. Synthesis and characterization of a peptide identified as a functional element in αA-crystallin. J Biol Chem 2000; 275:3767-771.

13. Bhattacharyya J, Udupa EGP, Wang J, Sharma KK. Mini-αB-crystallin: a functional element of αB-crystallin with chaperone-like activity. Biochemistry 2006; 45:3069-76.

14. Santhoshkumar P, Murugesan R, Sharma KK. Deletion of ^{54}FLRAPSWF^{61} residues decreases the oligomeric size and enhances the chaperone function of αB-crystallin. Biochemistry 2009; 48:5066-73.

15. Ghosh JG, Estrada MR, Clark JI. Interactive domains for chaperone activity in the small heat shock protein, human αB crystallin. Biochemistry 2005 Nov 15; 44(45):14854-69.

16. Derham BK, van Boekel MAM, Muchowski PJ, Clark JI, Horwitz J, Hepburn-Scott HW, de Jong WW, Crabbe MJC, Harding JJ. Chaperone function of mutant versions of αA- and αB-crystallin prepared to pinpoint chaperone binding sites. Eur J Biochem 2001; 268:713-21.

17. Muchowski PJ, Wu GJS, Liang JJN, Adman ET, Clark JI. Site-directed mutations within the core "α-crystallin" domain of the small heat-shock protein, human αB-crystallin, decrease molecular chaperone functions. J Mol Biol 1999 Jun4; 289(2): 397-411.

18. Bova MP, Yaron O, Huang Q, Ding L, Haley DA, Stewart PL, Horwitz J. Mutation R120G in αB-crystallin, which is linked to a desmin-related myopathy, results in an irregular structure and defective chaperone-like function. Proc Natl Acad Sci USA 1999; 96:6137-42.

19. Kumar LV, Ramakrishna T, Rao CM. Structural and functional consequences of the mutation of a conserved arginine residue in αA and αB crystallins. J Biol Chem 1999 Aug 20; 274(34):24137-41.

20. Gupta R, Srivastava OP. Deamidation affects structural and functional properties of human αA-crystallin and its oligomerization with αB-crystalln. J Biol Chem 2004 Oct 22; 279(43):44258-69.

21. Gupta R, Srivastava OP. Effect of deamidation of asparagine 146 on functional and structural properties of human lens αB-crystallin. Invest Ophthalmol Vis Sci 2004 Jan; 45(1):206-14.

22. Chaves JM, Srivastava K, Gupta R, Srivastava OP. Structural and functional roles of deamidation and/or truncation of N- or C-termini in human αA-crystallin. Biochemistry 2008; 47:10069-83.

23. Feil IK, Malfois M, Hendle J, van Der Zandt H, Svergun DI. A novel quaternary structure of the dimeric α-crystallin domain with chaperone-like activity. J Biol Chem 2001; 276:12024-29.

24. Aziz A, Santhoshkumar P, Sharma KK, Abraham EC. Cleavage of the C-terminal serine of human αA-crystallin produces $\alpha A_{1\text{-}172}$ with increased chaperone activity and oligomeric size. Biochemistry 2007; 46(9):2510-19.

25. Langowsky A, Benesch JLP, Landau M, Ding L, Sawaya MR, Cascio D, Huang Q, Robinson CV, Horwitz J, Eisenberg D. Crystal structures of truncated alpha A and alpha B crystallins reveal structural mechanisms of polydispersity important for eye lens function. Protein Sci 2010; 19:1031-43.

26. Cheng C, Xia C, Huang Q, Ding L, Horwitz J, Gong X. Altered chaperone-like activity of α-crystallins promotes cataractogenesis. J Biol Chem 2010 Dec 24; 285(52): 41187-93.

27. Andley UP, Shashank M, Griest TA, Petrash JM. Cloning, expression, and chaperone-like activity of human αA-crystallin. J Biol Chem 1996 Dec 13; 271(50):31973-80.

28. Bova MP, Mchaourab HS, Han Y, Fung BK. Subunit exchange of small heat shock proteins. Analysis of oligomer formation of α-crystallin and Hsp27 by fluorescence resonance energy transfer and site-directed truncations. J Biol Chem 2000 Jan14; 275(2):1035-42.

29. Pasta SY, Raman B, Ramakrishna T, Rao CM. Role of C-terminal extensions of α-crystallins. Swapping the C-terminal extension of αA-crystallin to αB-crystallin results in enhanced chaperone activity. J Biol Chem 2002 Nov 29; 277(48):45821-8.

30. Kundu B, Shukla A, Chaba R, Guptasarma P. The excised heat-shock domain of αB-crystallin is folded, protoelytically susceptible trimer with significant surface

hydrophobicity and a tendency to self-aggregate upon heating. Protein Expr Purif 2004 Aug; 36(2):263-71.

31. Zhang X, Dudek EJ, Liu B, Ding L, Fernandes AF, Liang JJ, Horwitz J, Taylor A, Shang F. Degradation of C-terminal truncated αA-crystallins by the ubiquitin-proteasome pathway. Invest Ophthalmol Vis Sci 2007 Sep; 48(9):4200-8.

32. Laemmli UK. Cleavage of structural proteins during the assembly of the head of bacteriophage T4. Nature 1970; 227:680-5.

33. Reddy MA, Bateman OA, Chakarova C, Ferris J, Berry V, Lomas E, Sarra R, Smith MA, Moore AT, Bhattacharya SS, Slingsby C. Characterization of the G91del CRYBA1/3-crystallin protein: a cause of human inherited cataract. Hum Mol Genet 2004 May 1; 13(9):945-53.

34. Towbin H, Staehelin T, Gordon J. Electrophoretic transfer of proteins from polyacrylamide gels to nitrocellulose sheets: procedure and some applications. Proc Natl Acad Sci USA 1979 Sep; 79(9):4350-4.

35. Kumar MS, Kapoor M, Sinha S, Reddy GB. Insights into hydrophobicity and the chaperone-like function of αA- and αB-crystallins. J Biol Chem 2005 Jun 10; 280(23):21726-30.

36. Horwitz J. Alpha-crystallin. Exp Eye Res. 2003 Feb; 76(2):145-53.

37. Sun T-X, Das BK, Liang JJ-N. Conformational and functional differences between recombinant human lens αA- and αB-crystallin. J Biol Chem 1997 Mar 7; 272:6220-5.

38. Fujii N, Nakamura T, Sadakane Y, Saito T, Fujii N. Differential susceptibility of alpha A- and alpha B-crystallin to gamma-ray irradiation. Biochim Biophys Acta 2007 Mar; 1774(3):345-50.

39. Fu L, Liang JJ-N. Detection of protein-protein interactions among lens crystallins in a mammalian two-hybrid system assay. J Biol Chem 2002 Feb 8; 277:4255-60.

40. Iwaki T, Iwaki A, Liem RK, Goldman JE. Expression of alpha B-crystallin in the developing rat kidney. Kidney Int 1991 Jul; 40(1):52-6.

41. Kato K, Shinohara H, Kurobe N, Inaguma Y, Shimizu K, Ohshima K. Tissue distribution and developmental profiles of immunoreacitve alpha B crystallin in the rat determined with a sensitive immunoassay system. Biochim Biophys Acta 1991 May 24; 1074(1):201-8.

42. Renkawek K, Vooter CE, Bosman GJ, van Workum FP, de Jong WW. Expression of alpha B-crystallin in Alzheimer's disease. Acta Neuropathol 1994; 87(2):155-60.

43. Renkawek K, Stege GJ, Bosman GJ. Dementia, gliosis and expression of the small heat shock proteins hsp27 and alpha B-crystallin in Parkinson's disease. Neuroreport 1999 Aug 2; 10:2273-6.

44. Renkawek K, de Jong WW, Merck KB, Frenken CW, van Workum FP, Bosman GJ. Alpha B-crystallin is present in reactive glia in Creutzfeldt-Jakob disease. Acta Neuropathol 1992; 83(3):324-7,

45. Goldman JE, Corbin E. Rosenthal fibers contain ubiquitinated alpha B-crystallin. Am J Pathol 1991 Oct; 139(4):933-8.

46. Lowe J, McDermott H, Pike I, Spendlove I, Landon M, Mayer RJ. Alpha B crystallin expression in non-lenticular tissues and selective presence in ubiquitinated inclusion bodies in human disease. J Pathol 1992 Jan; 166(1):61-8.

47. Sharma KK, Kumar GS, Murphy AS, and Kester K. Identification of 1,1'-bi(4-anilino)naphthalene-5,5'-disulfonic acid binding sequences in α-crystallin. J Biol Chem 1998 Jun 19; 273(25):15474-8.

48. Kantorow M, Horwitz J, van Boekel MA, deJong WW, Piatigorsky J. Conversion from oligomers to tetramers enhances autophosphorylation by lens αA-crystallin. Specificity between αA- and αB-crystallin subunits. J Biol Chem 1995 Jul 21; 270(29):17215-20,.

49. Sreelakshmi Y, Sharma KK. The interaction between αA- and αB-crystalllin is sequence-specific. Mol Vis 2006 May 24; 12:581-7.

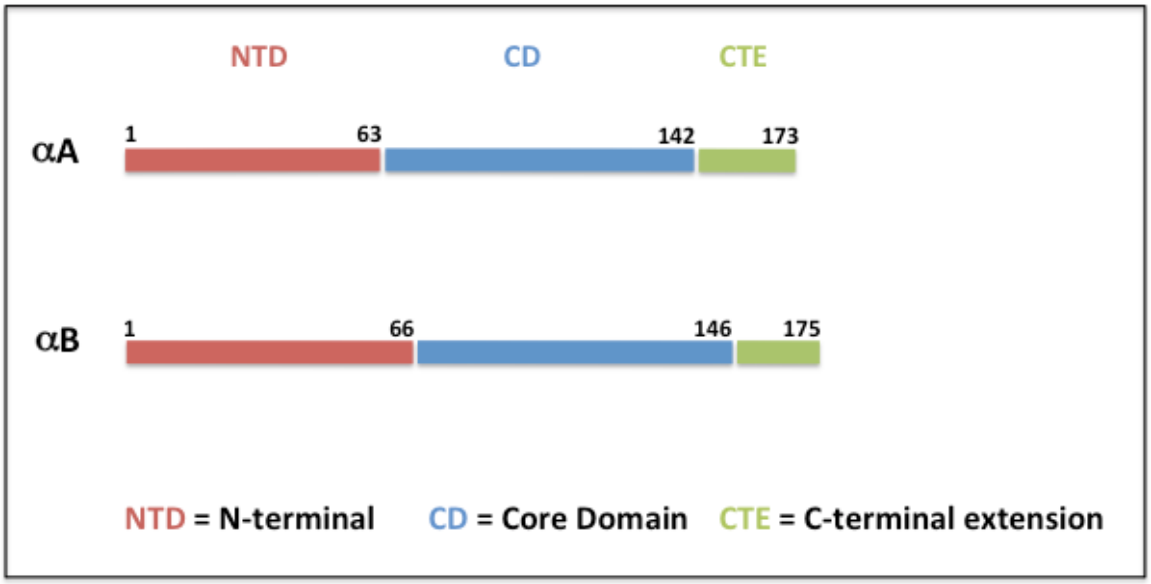

Figure 1. Schematic diagram showing the regions and residue numbers forming the N-terminal domain (NTD), core domain (CD), and C-terminal extension (CTE) of αA- and αB-crystallins in the current study. The residues spanned by each domain were as follows: αA NTD (residues no.1-63), αA CD (residues no. 64-142), αA CTE (residues no. 143-173), αB NTD (residues no. 1-66), αB CD (residues no. 67-146), and αB CTE (residues no. 167-175).

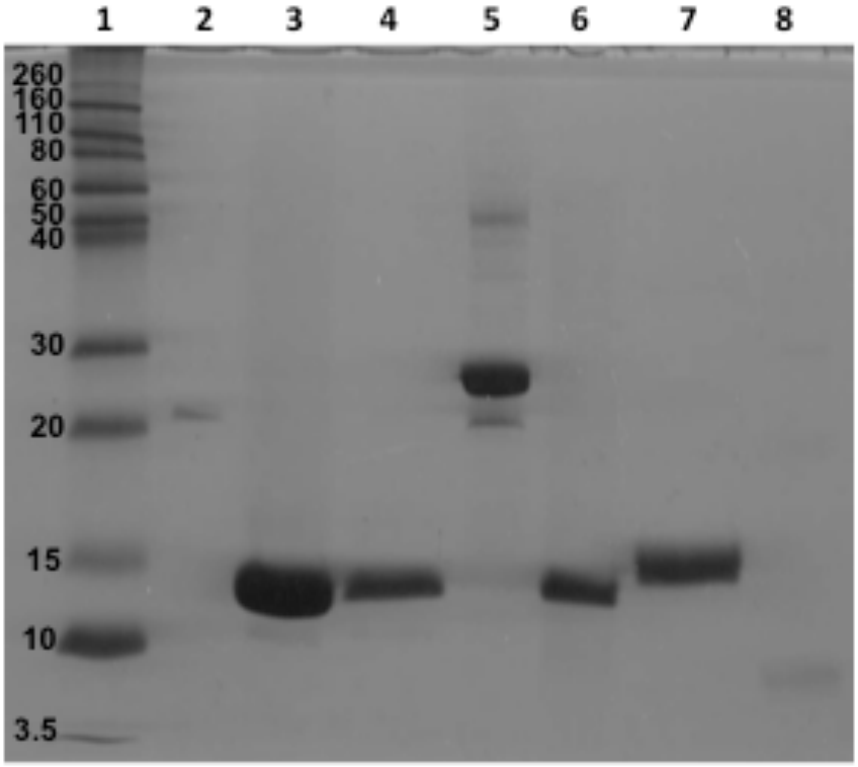

Figure 2. SDS-PAGE analysis of purified WT αA, WT αB and their individual domain constructs following purification. Protein purification was performed using Ni^{2+}-affinity column chromatography (see Methods). Lane 1 – molecular weight marker; Lane 2 – WT αA; Lane 3 – αA NTD; Lane 4 – αA CD; Lane 5 – WT αB; Lane 6 – αB NTD; Lane 7 – αB CD; and Lane 8 – αB CTE.

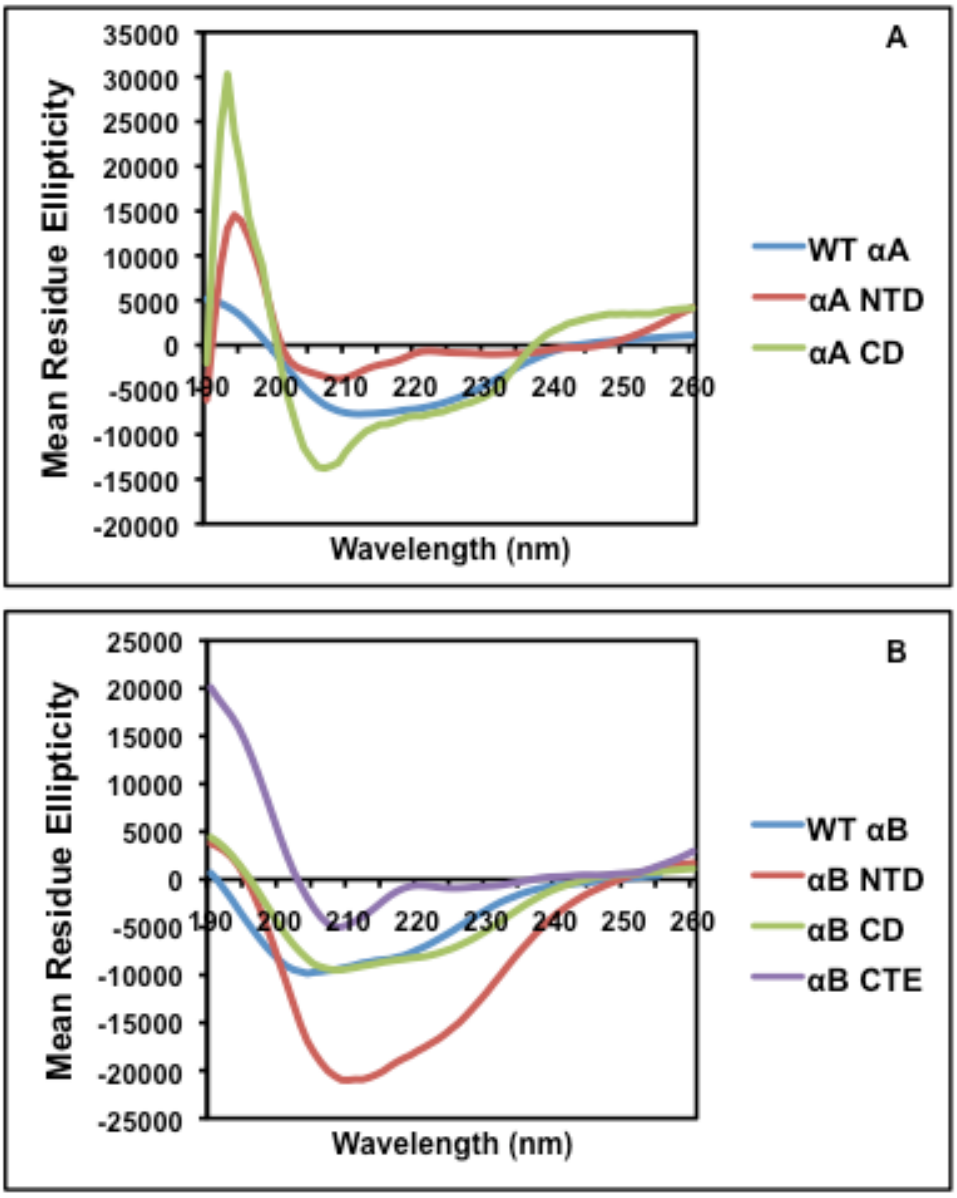

Figure 3. Far-UV CD spectra of WT αA, WT αB and their individual domain constructs. Spectra were recorded using protein preparations of 0.2 mg/ml, dissolved in 50 mM sodium phosphate buffer (pH 7.8), and a cell path length of 0.5 mm. The reported spectra are the average of 5 scans, corrected for the buffer blank, and smoothed. A, WT αA, N-terminal domain, and core domain constructs. B, WT αB, N-terminal domain, core domain, and C-terminal extension constructs.

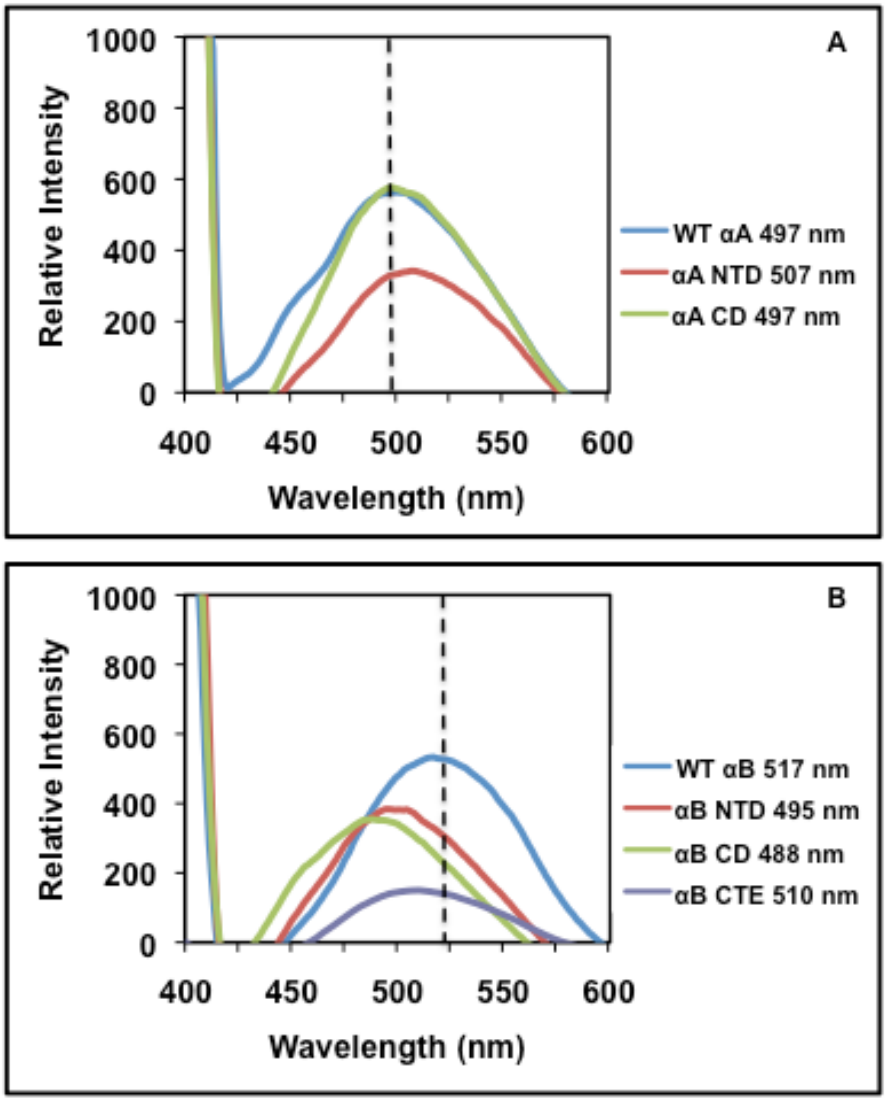

Figure 4. Fluorescence spectra of WT αA, WT αB and their individual domain constructs following ANS binding. Fluorescence spectra were recorded by excitation at 390 nm and emission from 400-600 nm, with protein preparations (0.2 mg/ml) mixed with 15 mL of 0.8 mM ANS (dissolved in methanol) and incubated at 37 °C for 15 min. A, WT αA, N-terminal domain, and core domain constructs. B, WT αB, N-terminal domain, core domain, and C-terminal extension constructs. Dotted lines indicate the maximum peak wavelength (λ_{max}) of the respective WT α-crystallins, used to determine whether a blue or red shift in wavelength occurred.

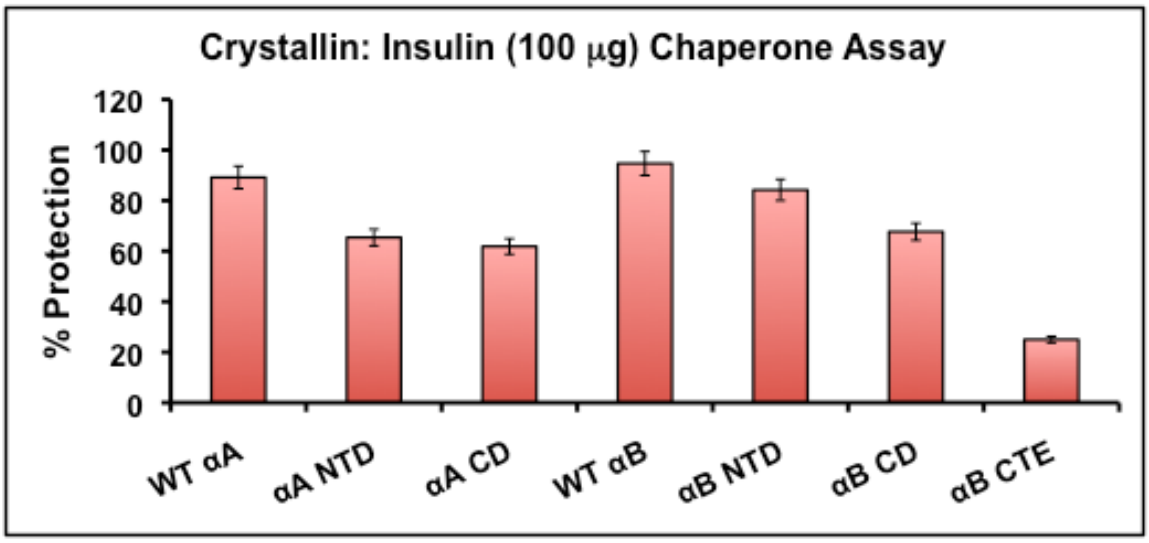

Figure 5. Chaperone activity comparison of WT αA, WT αB and their individual domain constructs. The chaperone activity, calculated as % protection, was assayed by measuring DTT-induced insulin (100 μg) aggregation in the presence of chaperone/insulin ration (1:1) at 25 °C. Error bars = Percent Error (+/- 1%).

Table 1. Oligonucleotide primers used for generation of individual domain constructs of αA- and αB-crystallins using PCR-based mutagenesis.

Mutant Constructs		Primers (5'-3')
αA NTD	Fwd	CACCATGGACGTGACCATCCAGCACCCC
	Rev	TTACTCAGAGATGCCGGAGTCCAGCACGGT
αA CD	Fwd	CACCGTTCGATCCGACCGGGACAAGTTCGTC
	Rev	TTAACAGAAGGTCAGCATGCCATCGGCAGA
αA CTE	Fwd	CACCGGCCCCAAGATCCAGACTGGCCTGGAT
	Rev	TTAGGACGAGGGAGCCGAGGTGGGGTTCTC
αB NTD	Fwd	CACCATGGACATCGCCATCCACCACCCC
	Rev	TTATGAGAGTCCAGTGTCAAACCAGCT
αB CD	Fwd	CACCGAGATGCGCCTGGAAAAGGACAGG
	Rev	TTAATTCACAGTGAGGACCCCATCAGA
αB CTE	Fwd	CACCGGACCAAGGAAAGAGGTCTCTGGC
	Rev	CTATTTCTTGGGGGCTGCGGTGAC

Table 2. Presence of WT αA, WT αB, and the N-terminal, core domain, and C-terminal extension constructs in the soluble fraction and/or inclusion bodies.

Crystallin Species	Soluble Fraction	Inclusion Bodies
WT αA	+	-
αA NTD	-	+
αA CD	+	+
αA CTE	**ND***	**ND***
WT αB	+	-
αB NTD	-	+
αB CD	+	+
αB CTE	+	-

+ Indicates presence of protein in given fraction on SDS-PAGE
***ND: Not Determined**

Table 3. Secondary structural content of WT αA, WT αB and their individual domain constructs. Percentages were determined by analysis of the Far-UV spectra (Figure3) using the SELCON3 analysis program.

Crystallin Species	α-Helix (+/- 1%)	β-Sheet (+/- 1%)	β-Turn (+/- 1%)	Random Coil (+/- 1%)
WT αA	**21.6**	**46.6**	**13.4**	**17.6**
αA NTD	**80.5**	**7.9**	**3.2**	**8.4**
αA CD	**37.9**	**42.7**	**10.7**	**9.6**
WT αB	**19.3**	**48.7**	**12.4**	**19.6**
αB NTD	**29.9**	**41.3**	**9.1**	**19.4**
αB CD	**20.6**	**48.1**	**14.3**	**18.7**
αB CTE	**5.9**	**66.6**	**4.3**	**23.5**

Table 4. Molar mass determination of WT αA, WT αB and their individual domain constructs using the dynamic light scattering method (MALS).

Crystallin Species	Molecular Mass (Da)
WT αA	**6.8×10^5**
αA NTD	**1.6×10^4**
αA CD	**3.0×10^4**
WT αB	**5.8×10^5**
αB NTD	**2.6×10^3**
αB CD	**8.4×10^7**
αB CTE	**1.0×10^6**

CONCLUSIONS

Specific Aim I

The goal of the initial study was to map the *in situ* protein profile and post-translational modifications in cortical and nuclear regions of normal aging human lenses. As an alternative approach to *in vitro* studies, and to better correlate to *in vivo* events, a combination of LCM, 2D-DIGE, and mass spectrometric analyses were used for the first time to identify the regional distributions of crystallins and their PTMs. LCM allowed for one-step, computer-monitored microdissection and acquisition of specific cells/tissues from specified regions of frozen human lens sections, without compromise of tissue integrity or morphology. Therefore, proteins from the cortical and nuclear regions were successfully recovered. The 2D-DIGE method allowed for labeling of proteins from the cortical and nuclear regions with fluorescent CyDyes, including an internal control pooled from individually labeled samples. These samples could then be electrophoresed on a single 2-D gel, which subjected them to the same running conditions and minimized gel-to-gel variation. Using this effective method, the comparative distribution of proteins recovered from two regions of the lens was determined. Further, ESI-QTRAP LC-MS/MS identified various crystallin species and intermediate filaments, as well as their PTMs.

Results from this study showed that crystallin fragments (M_r <20 kDa) were present in both the cortical and nuclear regions of the lens, suggesting that the

truncation of crystallins began in the cortical region and continued in the nucleus. Conversely, HMW aggregates (M_r >35 kDa) of crystallins and filament proteins were found to be more prevalent in the nuclear region, suggesting greater aggregation and/or cross-linking occurred in the nuclear region. This is likely a result of conformational changes in these modified crystallin and filament proteins that increase exposure of hydrophobic surfaces, allowing aggregation. These nuclear HMW complexes largely contained more truncated and modified β-crystallins than α- and γ-crystallins, as well as two intermediate filament proteins, CP49 and filensin. Modified α-crystallins were in low abundance in the nuclear region compared to the cortical region; therefore their chaperone function was possibly compromised due to truncation and subsequent aggregation with other crystallins. In turn, this could potentially have resulted in the insolubilization of unchaperoned β- and γ-crystallins since modified β- and γ-crystallins were more abundant in the nuclear region. Overall, several different PTMs were identified in crystallins, CP49, and filensin, and some were reported here for the first time.

In summary, the results from this study were that crystallin truncation was initiated in the cortical region and progressed to the nuclear region, where most aggregates were found. Deamidation, a commonly occurring modification, was observed at several sites in α-, β-, and γ-crystallins. However, deamidated α-crystallins were absent from the HMW complexes, though present as crystallin fragments (M_r >20 kDa). This is relatively significant, since our further studies show that though deamidation alters α-crystallin structure, its function is not completely depleted, therefore deamidated α-crystallins may still be able to chaperone other

proteins. It is also possible that deamidation serves as a signal to initiate further modifications. These results also suggest that the apparent loss of α-crystallin chaperone function with aging may leave β- and γ-crystallins in a vulnerable state and more susceptible to degradation and aggregation. Taken together, these PTMs may disrupt the structural and functional properties of the crystallins, leading to protein degradation and/or aggregation. Future studies would be aimed at confirming whether these relative changes between the cortical and nuclear layers are universal, by examining lenses from younger age groups. Also, examination of cataractous lenses would help distinguish any changes that are solely age-related versus cataractogenic.

Specific Aim II

In the second study, a more focused approach was taken to examine specific changes in the structure and function of αB-crystallins occurring as a result of deamidation and/or truncation. Several studies from this laboratory had previously established the prevelance of αB-crystallin fragments with Asn deamidations *in vivo* (Srivastava, 2003), and had confirmed that N146 deamidation had greater effects on structural and functional properties of αB than N78 deamidation (Gupta 2004a). Likewise, a similar comparative study examined the effects of deamidation and/or truncation on αA-crystallin (Chaves, 2008). Therefore, this study focused on the relative effects of deamidation at Asn 146, deletion of the N-terminal domain (residues no. 1-66) or the C-terminal extension (residues no. 151-175), or deamidation plus N- or C-terminal deletion on the structural and functional properties of αB-crystallin.

Results from this study showed definite changes in structural properties of αB mutants. The N146 deamidated and the N-terminally deleted αB mutants remained soluble, whereas the C-terminally deleted mutants became insoluble. However, these results were consistent with the known solubility properties of the hydrophobic N-terminal domain and the hydrophilic C-terminal extension of αB-crystallin.

All mutants showed changes in structural properties and increased in oligomer size. αB N146D decreased in α-helical content, while increasing β-sheet content. However, compared to other mutants, minimal changes in microenvironment occurred with this mutant, as seen by increases in intensity on Trp fluorescence and ANS binding studies.

N-terminal domain deletion in αB caused decreased α-helical content and increased β-sheet content, whereas C-terminal extension deletion plus deamidation caused noticeable increase in α-helical content and decrease in β-sheet content. Trp fluorescence spectroscopic studies revealed greater changes in the microenvironments of N-terminally deleted mutant, as seen by a red shift compared to WT αB λ_{max} and substantial decrease in fluorescence intensity. ANS binding studies also revealed changes in surface hydrophobicity of N-terminally deleted mutants, as evidenced by decreases in binding intensity. C-terminally deleted αB mutants showed more similarities to WT during Trp fluorescence, though they exhibited mildly decreased fluorescence intensities. ANS binding studies revealed changes in surface hydrophobicity, as well, as evidenced by larger blue shifts compared to WT αB.

Determination of the functional properties of these αB mutants revealed that deamidation of N146 alone was most harmful to chaperone function, followed closely

by the C-terminal extension deletion. However, the combination of N146 deamidation plus N- or C-terminal deletion seemed to recover some of the chaperone function lost by these deletions alone.

Taken together, these results show that on mimicking modifications that occur *in vivo* in these *in vitro* studies, the structural properties of αB-crystallin are altered. These results also confirm that multiple factors determine αB-crystallin's ability to function as a chaperone protein. Further, these results also suggest that residue number 146 is of great importance to interactions between αB and target protein during chaperone binding, and future studies may seek to investigate the molecular mechanism of such interactions. Molecular modeling may help visualize and understand the conformational changes in αB due to deamidation and N- and C-terminal truncation.

Specific Aim III

The third study took an even closer look at specific structural and functional properties of individual regions of αA- and αB-crystallins (i.e., the N-terminal domain [NTD], core domain [CD], and C-terminal extension [CTE]). Although it is well established that α-crystallins posses chaperone function (Horwitz, 1992) and bind improperly folded proteins to prevent their aggregation, the regions involved and the mechanism of chaperone binding is still not fully understood. Chaperone binding has been found to be dependent on oligomerization of α-crystallins and substrates through hydrophobic interactions, and the subunit exchange rate between αA and αB. However, there is a discrepancy in the literature about which regions of αA and αB

are involved in chaperone function, with hydrophobic sequences in all three regions identified as essential sites for chaperone binding. In light of this, this study sought to explore the structural and functional properties of three individual regions of αA and αB (NTD, CD, and CTE), in an attempt to better understand which region is most important for chaperone activity. The following constructs were successfully generated and used for this purpose: αA NTD (residues no. 1-63), αA CD (residues no. 64-142), αB NTD (residues no. 1-66), αB CD (residues no. 67-146), and αB CTE (residues no. 147-175).

Results from this study revealed changes in the structural and functional properties of these constructs. WT αA, WT αB, and the CTE proteins were recovered in the soluble fraction, while both NTD proteins were recovered in the insoluble fraction. Again, these results were as expected considering the hydrophobic nature of the N-terminal domain and the hydrophilic nature of the C-terminal extension of these proteins. However, both CD constructs were found in both the soluble and insoluble fractions, suggesting this region is partially soluble.

Findings from this study showed that these individual regions showed altered structural and functional properties relative to their WT proteins. Compared to WT αA, αA NTD was noticeably high in α-helical content and low in β-sheet content, and αA CD also showed an increase in α-helix and decrease in β-sheet, though not as drastic. This suggested that both the N-terminal domain and core domain of αA-crystallin assume a more helical structure when individually isolated. On the other hand, αB NTD showed an increase in α-helical content and a decrease in β-sheet content, whereas αB CD retained secondary structural content relatively similar to

WT αB. The most marked difference in secondary structure was seen with αB CTE, which showed a substantial decrease in α-helix and increase in β-sheet compared to WT αB, suggesting the C-terminal extension alone assumes greater β-sheet structure. ANS binding studies revealed that αB constructs exhibited greater changes in surface hydrophobicity than αA constructs, as seen by their relatively larger blue shifts, and were relatively compact structures with decreased binding intensity. However, αA NTD displayed a small red shift, suggesting a more relaxed structure, while αA CD retained surface hydrophobicity and binding intensity similar to WT αA. Changes in oligomer size were seen in all contructs, with most constructs displaying decreased oligomer size relative to WT, except for αB CD and αB CTE, which showed increased oligomer sizes.

All constructs retained some level of chaperone function. αB NTD and αB CD showed the greatest percent protection, followed by αA NTD and αA CD. Surprisingly, αB CTE also showed chaperone activity, though minimal compared to other constructs.

Taken together, these results suggest that a greater portion of chaperone binding sites reside in the N-terminal domain of αA and αB, since this region provided the greatest protection in both. However, the fact that αB CTE also had some chaperone activity also suggests residues in this region are also involved in chaperone binding as well. Apparently, the appropriate conformation brings certain residues in each of these regions in close proximity to form a fully functional chaperone-binding site for a target protein. Future studies will need to establish if αA CTE also retains some chaperone activity. Again, molecular modeling would be

beneficial to visualize and understand the conformational changes in these three individual regions of αA- and αB-crystallins.

GENERAL LIST OF REFERENCES

Andley UP. (2007). Crystallins in the eye: function and pathology. *Prog Retin Eye Res*, 26(1), 79-98.

Banks RE, Dunn MJ, Forbes MA, Stanley A, Pappin D, Naven T, Gough M, Harnden P, Selby PJ. (1999). The potential use of laser capture microdissection to selectively obtain distinct populations of cells for proteomic analysis – preliminary findings. *Electrophoresis*, 20, 689-700.

Bhat SP, Nagineni CN. (1989). αB subunit of lens-specific protein α-crystallin is present in other ocular and non-ocular tissues. *Biochem Biophys Res Commun*, 158:319-25.

Bhattacharyya J, Udupa EGP, Wang J, Sharma KK. (2006). Mini-αB-crystallin: a functional element of αB-crystallin with chaperone-like activity. *Biochemistry*, 45, 3069-76.

Bloemendal H, de Jong W, Jaenicke R, Lubsen NH, Slingsby C, Tardieu A. (2004). Ageing and vision: structure, stability and function of lens crystallins. *Prog Biophys Mol Biol*, 86(3), 407-485.

Bova MP, Yaron O, Huang Q, Ding L, Haley DA, Stewart PL, Horwitz J. (1999). Mutation R120G in αB-crystallin, which is linked to a desmin-related myopathy, results in an irregular structure and defective chaperone-like function. *Proc Natl Acad Sci USA*, 96, 6137-42.

Boyle DL, Takemoto LJ. (1997). Confocal microscopy of human lens membranes in aged normal and nuclear cataracts. *Invest Ophthalmol Vis Sci*, 38(13), 2826-2832.

Chaves JM, Srivastava K, Gupta R, Srivastava OP. (2008). Structural and functional roles of deamidation and/or truncation of N- or C-termini in human αA-crystallin. *Biochemistry*, 47(38), 10069-10083.

Cornett DS, Mobley JA, Dias EC, Andersson M, Arteaga CL, Sanders ME, Caprioli RM. (2006). A novel histology-directed strategy for MALDI-MS tissue profiling that improves throughput and cellular specificity in human breast cancer. *Mol Cell Proteomics*, 5(10), 1975-1983.

Derham BK, van Boekel MAM, Muchowski PJ, Clark JI, Horwitz J, Hepburn-Scott HW, de Jong WW, Crabbe MJC, Harding JJ. (2001). Chaperone function of mutant versions of αA- and αB-crystallin prepared to pinpoint chaperone binding sites. *Eur J Biochem*, 268, 713-21.

Duncan G, Wormstone IM, Davies PD. The aging human lens: structure, growth, and physiological behaviour. (1997) *Br J Ophthalmol*, 81, 818-823.
Espina V, Wulfkuhle JD, Calvert VS, VanMeter A, Zhou W, Coukos G, Geho DH, Petricoin EF 3rd, Liotta LA. (2006). Laser-capture microdissection. *Nat Protoc*, 1(2), 586-603.

Ghosh JG, Estrada MR, Clark JI. (2005). Interactive domains for chaperone activity in the small heat shock protein, human αB crystallin. *Biochemistry*, 44(45), 14854-69.

Grey AC, Schey KL. (2008). Distribution of bovine and rabbit lens α-crystallin products by MALDI imaging mass spectrometry. *Mol Vis*, 14, 171-179.

Gupta R, Srivastava K, Srivastava OP. (2006). Truncation of motifs III and IV in human lens βA3-crystallin destabilizes the structure. *Biochemistry*, 45(33), 9964-9978.

Gupta R, Srivastava OP. (2004a). Deamidation affects structural and functional properties of human αA-crystallin and its oligomerization with αB-crystallin. *J Biol Chem*, 279(43):44258-44269.

Gupta R, Srivastava OP. (2004b). Effect of deamidation of asparagines 146 on functional and structural properties of human lens αB-crystallin. *Invest Ophthalmol Vis Sci*, 45(1), 206-214.

Hains PG, Truscott RJW. (2007). Post-translational modifications in the nuclear region of young, aged, and cataract human lenses. *J Proteome Res*, 6(10), 3935-3943.

Han J, Schey KL. (2006). MALDI tissue imaging of ocular lens α-crystallin. *Invest Opthalmol Vis Sci*, 47(7), 2990-2996.

Hanson SR, Hasan A, Smith DL, Smith JB. (2000). The major in vivo modifications of the human water-insoluble lens crystallins are disulfide bonds, deamidation, methionine oxidation, and backbone cleavage. *Exp Eye Res*, 71(2), 195-207.

Harding CV, Chylack Jr. LT, Susan SR, Lo W, Bobrowski WF. (1983). Calcium-containing opacities in the human lens. *Invest Ophthalmol Vis Sci*, 24(9), 1194-1202.
Harding JJ. (1997). Lens. *Biochemistry of the Eye*. Ed. JJ Harding. London: Chapman & Hall, pp. 94-134.

Harding JJ. (2002). Viewing molecular mechanisms of ageing through a lens. *Ageing Res Rev*, 1, 465-479.

Harms M, Wilmarth PA, Kapfer DM, Steel EA, David LL, Bächinger HP, Lampi KJ. (2004). Laser light-scattering evidence for an altered association of βB1-crystallin deamidated in the connecting peptide. *Protein Sci*, 13(3), 678-686.

Harrington V, McCall S, Huynh S, Srivastava K, Srivastava OP. (2004). Crystallins in water soluble-high molecular weight protein fractions and water insoluble protein fractions in aging and cataractous human lenses. *Mol Vis*, 10, 476-489.

Harrington V, Srivastava OP, Kirk M. (2007). Proteomic analysis of water insoluble proteins from normal and cataractous human lenses. *Mol Vis*, 13, 1680-1694.
Horwitz J. (1992) α-Crystallin can function as a molecular chaperone. *Proc Natl Acad Sci*, 89(21), 10449-10453.

Kondo T, Hirohashi S. (2007). Application of highly sensitive fluorescent dyes (CyDye DIGE Fluor saturation dyes) to laser microdissection and two-dimensional difference gel electrophoresis (2D-DIGE) for cancer proteomics. *Nat Protoc*, 1(6), 2940-2956.

Kumar LV, Ramakrishna T, Rao CM. (1999). Structural and functional consequences of the mutation of a conserved arginine residue in αA and αB crystallins. *J Biol Chem*, 274(34), 24137-41.

Lampi KJ, Amyx KK, Ahmann P, Steel EA. (2006). Deamidation in human lens βB2-crystallin destabilizes the dimmer. *Biochemistry*, 45(10), 3146-3153.

Lampi KJ, Ma Z, Hanson SR, Azuma M, Shih M, Shearer TR, Smith DL, Smith JB, David LL. (1998). Age-related changes in human lens crystallins identified by two-dimensional electrophoresis and mass spectrometry. *Exp Eye Res*, 67(1), 31-43.

Lapko VN, Purkis AG, Smith DL, Smith JB. Deamidation in human γS-crystallin from cataractous lenses is influenced by surface exposure. *Biochemistry*, 41(27), 8638-8648.

Liu Y, Zhang X, Luo L, Wu M, Zeng R, Cheng G, Hu B, Liu B, Liang JJ, Shang F. (2006). A novel αB-crystallin mutation associated with autosomal dominant congenital lamellar cataract. *Invest Ophthalmol Vis Sci*, 47(3), 1069-75.

Lund Al, Smith JB, Smith DL. (1996). Modifications of the water-insoluble human lens α-crystallins. *Exp Eye Res*, 63(6), 661-672.

Ma Z, Hanson SRA, Lampi KJ, David LL, Smith DL, Smith JB. (1998). Age-related changes in human lens crystallins identified by HPLC and mass spectrometry. *Exp Eye Res*, 67(1), 21-30.

Muchowski PJ, Wu GJS, Liang JJN, Adman ET, Clark JI. (1999). Site-directed mutations within the core "α-crystallin" domain of the small heat-shock protein, human αB-crystallin, decrease molecular chaperone functions. *J Mol Biol*, 289(2), 397-411.

Narberhaus F. (2002). α-Crystallin-type heath shock proteins: socializing minichaperones in the context of a multichaperone network. *Microbiol Molec Biol Rev*, 66, 64-93.

Reddy GB, Kumar PA, Kumar MS. (2006). Chaperone-like activity and hydrophobicity of α-crystallin. *IUBMB Life*, 58(11), 643-41.

Sharma K, Kumar RS, Kumar GS, Quinn PT. (2000). Synthesis and characterization of a peptide identified as a functional element in αA-crystallin. *J Biol Chem*, 275, 3767-771.

Simone NL, Bonner RF, Gillespie JW, Emmert-Buck MR, Liotta LA. (1998). Laser-capture microdissection: opening the microscopic frontier to molecular analysis. *Trends in Genetics*, 14(7), 272-276.

Simone NL, Paweletz CP, Charboneau L, Petricoin III EF, Liotta LA. (2000). Laser capture microdissection: beyond functional genomics to proteomics. *Mol Diagn*, 5(4), 301-307.

Smith JB, Sun Y, Smith DL, Green B. (1992). Identification of the posttranslational modifications of bovine lens αB-crystallin by mass spectrometry. *Protein Sci*, 1, 601-608.

Srivastava OP, Srivastava K. (2003). Existence of deamidated αB-crystallin fragments in normal and cataractous human lenses. *Mol Vis*, 9, 110-118.

Takemoto L, Emmons T, Horowitz J. (1993). The C-terminal region of α-crystallin: involvement in protection against heat-induced denaturation. *Biochem J*, 294, 435-438.

Takemoto LJ, Boyle D. (1998a) Determination of the in vivo deamidation rate of asparagines-101 from alpha-A crystallin using microdissected sections of the aging human lens. *Exp Eye Res*, 67(1), 119-120.

Takemoto LJ. (1998b). Quantitation of asparagines-101 deamidation from alpha-A crystallin during again of the human lens. *Curr Eye Res*, 17, 247-250.

Vermorken AJM, Hilderink JMHC, van de Ven WJM, Bloemendal H. Lens differentiation. (1978) *J Cell Biol*, 76, 175-183.

Wilmarth PA, Tanner S, Dasari S, Nagalla SR, Rifiere MA, Bafna V, Pevzner PA, David LL. (2006). Age-related changes in human crystallins determined from comparative analysis of post-translational modifications in young and aged lens: does deamidation contribute to crystalline insolubility? *J Proteome Res*, 5(10), 2554-2566.

APPENDIX A

APPENDIX 1

Appendix 1: Crystallin species, sequences, and modifications from 2D-DIGE gel of a 69 year-old human lens identified by ESI-QTRAP LC-MS/MS. Underlined residues represent the modified amino acids

Spot number	α-Crystallin	β- and γ-Crystallin	CP49	Filensin
1		γD: #2-10 GKITLYEDR γD: #4-10 ITLYEDR γD: #154-163 YQDWGATNAR	Present only in spots 22 and 28	Present only in spot 35
2	αA: #55-65 TVLDSGISEVR αA: #79-88 HFSPEDLTVK αB: #1-11 MDIAIHHPWIR [Acet(N-term);Oxi(MHW] αB: #12-22 RPFFPFHSPSR αB: #57-69 APSWFDTGLSEMR [Oxi(MHW)] αB: #57-72 APSWFDTGLSEMRLEK αB: #73-82 DRFSVNLDVK αB: #83-90 HFSPEELK αB: #83-92 HFSPEELKVK [Eth(N-term)] αB: #93-103 VLGDVIEVHGK αB: #108-116 QDEHGFISR [Eth(N-term)] αB: #124-149 IPADVDPLTITSSLSSDGVLTVNGPR [Deam(NQ)]			
3	αA: #55-65 TVLDSGISEVR αB: #12-22 RPFFPFHSPSR αB: #57-69 APSWFDTGLSEMR	βA3: #33-44 ITIYDQENFQGK βA3: #33-45 ITIYDQENFQGKR βA3: #96-109 WDAWSGSNAYHIER		

	αB: #57-72 APSWFDTGLSEMRLEK	βA3: #126-137 MTIFEKENFIGR [Oxi(M)]
	αB: #73-82 DRFSVNLDVK	βA3: #197-211 EWGSHAQTSQIQSIR
	αB: #83-90 HFSPEELK	βB3: #26-37 VILYELENFQGK
	αB: #83-92 HFSPEELKVK	βB3: #26-38 VILYELENFQGKR
	αB: #93-103 VLGDVIEVHGK	
4	αB: #1-11 MDIAIHHPWIR [Acet(N-term);Oxi(M)]	βA3: #33-45 ITIYDQENFQGKR
	αB: #12-22 RRFFPFHSPSR	βA3: #96-109 WDAWSGSNAYHIER
	αB: #57-69 APSWFDTGLSEMR [Oxi(MHW)]	βA3: #126-137 MTIFEKENFIGR [Oxi(M)]
	αB: #57-72 APSWFDTGLSEMRLEK	βA3: #197-211 EWGSHAQTSQIQSIR
	αB: #73-82 DRFSVNLDVK	βB1: #151-160 ISLFEGANFK
	αB: #83-90 HFSPEELK	γD: #2-10 GKITLYEDR
	αB: #83-92 HFSPEELKVK [Cam(K)]	γD: #154-163 YQDWGATNAR
	αB: #91-103 VKVLGDVIEVHGK	
	αB: #93-107 VLGDVIEVHGKHEER	
	αB: #108-116 QDEHGFISR [Eth(N-term)]	
	αB: #124-149 IPADVDPLTITSSLSSDGVLTVNGPR [Deam(NQ)]	
	αB: #164-174 EEKPAVTAAPK	
5	αB: #1-11 MDIAIHHPWIR	βA3: #33-45 ITIYDQENFQGKR
	αB: #12-22 RPFFPFHSPSR	βA3: #126-137

		MTIFEKENFIGR [Oxi(M)]
	αB: #57-69 APSWFDTGLSEMR [Oxi(M)]	γD: #2-10 GKITLYEDR
	αB: #57-72 APSWFDTGLSEMRLEK	γD: #60-77 RGDYADHQQWMGLSDSVR
	αB: #73-82 DRFSVNLDVK	γD: #61-77 GDYADHQQWMGLSDSVR
	αB: #83-92 HFSPEELKVK	γD: #143-152 QYLLMPGDYR
	αB: #93-103: VLGDVIEVHGK	γD: #143-153 QYLLMPGDYRR
	αB: #108-116: QDEHGFISR	γD: #154-163 YQDWGATNAR
6	αA: #55-65 TVLDSGISEVR	βA3: #33-44 ITIYDQENFQGK
	αB: #12-22 RPFFPFHSPSR	βA3: #96-109 WDAWSGSNAYHIER
	αB: #57-69 APSWFDTGLSEMR [Oxi(M)]	βA3: #126-137 MTIFEKENFIGR [Oxi(M);Sulph(M)]
	αB: #57-72 APSWFDTGLSEMRLEK	βA3: #197-211 EWGSHAQTSQIQSIR
	αB: #83-90 HFSPEELK	γD: #78-89 SCRLIPHSGSHR
	αB: #83-92 HFSPEELKVK [Meth(H,N-term);Eth(N-term)]	γD: #143-152 QYLLMPGDYR
	αB: #91-103 VKVLGDVIEVHGK	γD: #143-153 QYLLMPGDYRR
	αB: #93-103 VLGDVIEVHGK [Eth(N-term)]	γD: #154-163 YQDWGATNAR
	αB: #93-107 VLGDVIEVHGKHEER	γS: #8-14 ITFYEDK [Eth(K)]
	αB: #158-174 TIPITREEKPAVTAAPK	γS: #73-79 WMGLNDR
7	αA: #13-21 TLGPFYPSR	βA3: #33-44 ITIYDQENFQGK

	αA: #146-157 IQTGLDATHAER	βA3: #33-45 ITIYDQENFQGKR [Cam(K)]
	αB: #1-11 MDIAIHHPWIR [Acet(N-term);Cam(N-term);Oxi(M)]	βA3: #91-95 GEYPR
	αB: #12-22 RPFFPFHSPSR	βA3: #96-109 WDAWSGSNAYHIER [Eth(N-term);Oxi(HW)]
	αB: #57-69 APSWFDTGLSEMR	βA3: #126-137 MTIFEKENFIGR [Cam(K);Deam(NQ);Oxi(M)]
	αB: #57-72 APSWFDTGLSEMRLEK	βA3: #197-211 EWGSHAQTSQIQSIR
	αB: #83-90 HFSPEELK	βB2: #109-120 IILYENPNFTGK
	αB: #83-92 HFSPEELKVK	γB: #4-10 ITFYEDR
	αB: #150-157 KQVSGPER	γB: #60-77 RGEYPDYQQWMGLSDSIR
	αB: #164-174 EEKPAVTAAPK [Cam(N-term)]	γB: #155-164 FLDWGAPNAK
		γS: #8-14 ITFYEDK
		γS: #73-79 WMGLNDR
		γS: #85-95 AVHLPSGGQYK
8	αB: #73-82 DRFSVNLDVK	βA3: #33-44 ITIYDQENFQGK
	αB: #83-92 HFSPEELKVK	βA3: #33-45 ITIYDQENFQGKR
	αB: #93-107 VLGDVIEVHGKHEER	βA3: #197-211 EWGSHAQTSQIQSIR
8B	αB: #73-82 DRFSVNLDVK	βA3: #33-44 ITIYDQENFQGK
	αB: #93-107 VLGDVIEVHGKHEER	βA3: #96-109 WDAWSGSNAYHIER
		βA3: #126-137

		MTIFEKENFIGR [Oxi(M)]
9	αB: #150-157 KQVSGPER	βA3: #33-44 ITIYDQENFQGK
	αB: #158-163 TIPITR	βA3: #33-45 ITIYDQENFQGKR
	αB: #164-174 EEKPAVTAAPK	βA3: #96-109 WDAWSGSNAYHIER
		βA3: #126-131 MTIFEK
		βA3: #126-137 MTIFEKENFIGR
		βA4: #14-25 MVVWDEDGFQGR [Oxi(M)]
		βA4: #107-118 LTIFEQENFLGK
		βA4: #107-119 LTIFEQENFLGKK
10	αA: #1-11 MDVTIQHPWFK [Acet(N-term);Oxi(M)]	βA3: #33-44 ITIYDQENFQGK
	αA: #13-21 TLGPFYPSR	βA3: #96-109 WDAWSGSNAYHIER [Deam(NQ)]
	αA: #55-65 TVLDSGISEVR	βA3: #126-137 MTIFEKENFIGR [Oxi(M)]
	αA: #79-88 HFSPEDLTVK	βA4: #14-25 MVVWDEDGFQGR
	αA: #89-99 VQDDFVEIHGK	βA4: #107-118 LTIFEQENFLGK
	αA: #146-157 IQTGLDATHAER [Meth(N-term,Q,R); Eth(N-term)]	
	αB: #1-11 MDIAIHHPWIR [Acet(N-term;Oxi(M)]	
	αB: #83-92 HFSPEELKVK	
11	αA: #1-11 MDVTIQHPWFK	βA3: #33-44 ITIYDQENFQGK

	[Acet(N-term);Oxi(M)]	
	αA: #13-21 TLGPFYPSR	βA3: #33-45 ITIYDQENFQGKR
	αA: #55-65 TVLDSGISEVR	βA3: #126-137 MTIFEKENFIGR
	αA: #79-88 HFSPEDLTVK	βA4: #107-118
	[Meth(H,N-term);Eth(N-term)]	LTIFEQENFLGK
	αA: #89-99 VQDDFVEIHGK	
	αA: #146-157 IQTGLDATHAER	
	[Meth(H)]	
11B	αA: #1-11 MDVTIQHPWFK	βA4: #14-25
	[Acet(N-term);Oxi(MHW)]	MVVWDEDGFQGR [Oxi(M)]
	αA: #12-21 RTLGPFYPSR	βA4: #107-118
		LTIFEQENFLGK
	αA: #13-21 TLGPFYPSR	
	[Eth(N-term)]	
	αA: #50-65	
	QSLFRTVLDSGISEVR	
	αA: #55-65 TVLDSGISEVR	
	αA: #79-88 HFSPEDLTVK	
	αA: #89-99 VQDDFVEIHGK	
	[Eth(N-term);Meth(N-term,Q)]	
	αA: #146-157 IQTGLDATHAER	
	[Meth(H)]	
	αA: #158-173	
	AIPVSREEKPTSAPSS	
	αB: #1-11 MDIAIHHPWIR	
	αB: #93-103 VLGDVIEVHGK	
12	αA: #13-21 TLGPFYPSR	γS: #8-19 ITFYEDKNFQGR
	αA: #55-65 TVLDSGISEVR	
	αA: #146-157 IQTGLDATHAER	
12B	αB: #83-90 HFSPEELK	βA3: #33-44 ITIYDQENFQGK

		βB1: #203-214 GYQYLLEPGDFR βB2: #91-101 TDSLSSLRPIK βB2: #109-120 IILYENPNFTGK βB2: #173-188 DSSDFGAPHPQVQSVR γC: #4-10 ITFYEDR γS: #8-14 ITFYEDK [Eth(K)] γS: #8-19 ITFYEDKNFQGR γS: #73-79 WMGLNDR γS: #85-95 AVHLPSGGQYK γS: #159-174 KPIDWGAASPAVQSFR [Deam(NQ);Fkyn(W);Oxi(HW)]
13	αA: #55-65 TVLDSGISEVR	βA4: #14-25 MVVWDEDGFQGR [Oxi(M)] βA4: #107-118 LTIFEQENFLGK βB1: #61-72 LVVFELENFQGR βB2: #82-89 WDSWTSSR βB2: #109-120 IILYENPNFTGK βB2: #161-168 GLQYLLEK βB2: #173-188 DSSDFGAPHPQVQSVR γS: #8-19 ITFYEDKNFQGR γS: #85-95 AVHLPSGGQYK [Meth(H)] γS: #149-155 QYLLDKK

	γS: #156-174 EYRKPIDWGAASPAVQSFR [Oxi(HW)]
	γS: #159-174 KPIDWGAASPAVQSFR [Meth(K,N-term);Oxi(HW);FKyn(W);Phos(STY)]
14	βA3: #33-44 ITIYDQENFQGK
	βA3: #33-45 ITIYDQENFQGKR
	βB1: #61-72 LVVFELENFQGR
	γS: #8-19 ITFYEDKNFQGR
	γS: #73-79 WMGLNDR
	γS: #85-95 AVHLPSGGQYK
	γS: #159-174 KPIDWGAASPAVQSFR [Oxi(HW)]
14B	βB2: #69-76 KGEQFVFEK
	βB2: #91-101 TDSLSSLRPIK
	βB2: #109-120 IILYENPNFTGK
	βB2: #109-121 IILYENPNFTGKK
	βB2: #121-140 KMEIIDDDVPSFHAHGYQEK
	βB2: #122-140 MEIIDDDVPSFHAHGYQEK [Oxi(M)]
	βB2: #146-160 VQSGTWVGYQYPGYR

	βB2: #169-188 GDYKDSSDFGAPHPQVQSV R
15	βA3: #33-44 ITIYDQENFQGK βA4: #107-118 LTIFEQENFLGK [Deam(NQ)] βB1: #61-72 LVVFELENFQGR βB2: #69-76 GEQFVFEK βB2: #109-120 IILYENPNFTGK βB2: #161-168 GLQYLLEK βB2: #169-188 GDYKDSSDFGAPHPQVQSV R γS: #8-19 ITFYEDKNFQGR γS: #85-95 AVHLPSGGQYK γS: #159-174 KPIDWGAASPAVQSFR [Deam(NQ);Oxi(HW)]
15B	βA3: #33-44: ITIYDQENFQGK βB2: #109-120 IILYENPNFTGK βB2: #109-120 IILYENPNFTGK βB2: #161-172 GLQYLLEKGDYK βB2: #169-188 GDYKDSSDFGAPHPQVQSV R βB2: #173-188

		DSSDFGAPHPQVQSVR
		γS: #8-19 ITFYEDKNFQGR
		γS: #85-95 AVHLPSGGQYK
		γS: #159-174
		KPIDWGAASPAVQSFR
		[Fkyn(W)]
16	αA: #55-65 TVLDSGISEVR	βB1: #51-60 AAELPPGNYR
		βB1: #61-72
		LVVFELENFQGR
		βB1: #61-73
		LVVFELENFQGRR
		βB1: #74-86
		AEFSGECSNLADR
		βB1: #124-132
		WNTWSSSYR
		βB1: #151-160 ISLFEGANFK
		βB1: #188-202
		VSSGTWVGYQYPGYR
		βB1: #203-214
		GYQYLLEPGDFR
		βB1: #234-252
		DKQWHLEGSFPVLATEPPK
		βB1: #236-252
		QWHLEGSFPVLATEPPK
		βB2: #91-101 TDSLSSLRPIK
		βB2: #109-120
		IILYENPNFTGK
		βB2: #109-121
		IILYENPNFTGKK
		βB2: #146-160
		VQSGTWVGYQYPGYR
		βB2: #161-168 GLQYLLEK

	βB2: #169-188 GDYKDSSDFGAPHPQVQSVR
	βB2: #173-188 DSSDFGAPHPQVQSVR
17	βB1: #51-60 AAELPPGNYR
	βB1: #61-72 LVVFELENFQGR
	βB1: #61-73 LVVFELENFQGRR
	βB1: #74-86 AEFSGECSNLADR
	βB1: #111-118 GEMFILEK
	βB1: #124-132 WNTWSSSYR
	βB1: #188-202 VSSGTWVGYQYPGYR
	βB1: #236-252 QWHLEGSFPVLATEPPK
	βB2: #2-18 ASDHQTQAGKPQSLNPK [Acet(N-term)]
	βB2: #69-81 GEQFVFEKGEYPR [Deam(NQ)]
	βB2: #77-89 GEYPRWDSWTSSR
	βB2: #82-89 WDSWTSSR [Fkyn(W); Oxi(HW)]
	βB2: #90-101 RTDSLSSLRPIK
	βB2: #91-108

TDSLSSLRPIKVDSQEHK
[Deam(NQ)]
βB2: #109-120
IILYENPNFTGK
[2Deam(NQ)]
βB2: #109-121
IILYENPNFTGKK [Eth(N-
term)]
βB2: #121-140
KMEIIDDDVPSFHAHGYQEK
[Oxi(M)]
βB2: #122-140
MEIIDDDVPSFHAHGYQEK
[Deam(NQ);Oxi(M)]
βB2: #146-160
VQSGTWVGYQYPGYR
[Fkyn(W);Oxi(HW)]
βB2: #161-168 GLQYLLEK
βB2: #161-172
GLQYLLEKGDYK
[Deam(NQ)]
βB2: #169-188
GDYKDSSDFGAPHPQVQSV
R
βB2: #173-188
DSSDFGAPHPQVQSVR
18 βB1: #51-60 AAELPPGNYR
βB1: #61-72
LVVFELENFQGR
βB1: #151-160 ISLFEGANFK
βB1: #188-202
VSSGTWVGYQYPGYR
βB1: #234-252

DKQWHLEGSFPVLATEPPK
[Deam(NQ)]
βB2: #2-18
ASDHQTQAGKPQSLNPK
βB2: #82-89 WDSWTSSR
βB2: #90-101
RTDSLSSLRPIK
βB2: #91-101 TDSLSSLRPIK
βB2: #91-108
TDSLSSLRPIKVDSQEHK
βB2: #109-120
IILYENPNFTGK [Eth(N-term)]
βB2: #109-121
IILYENPNFTGKK
[Deam(NQ)]
βB2: #121-140
KMEIIDDDVPSFHAHGYQEK
[Deam(NQ);Eth(N-
term);Oxi(M)]
βB2: #122-140
MEIIDDDVPSFHAHGYQEK
[Deam(NQ); Oxi(M,2HW)]
βB2: #146-160
VQSGTWVGYQYPGYR
[Fkyn(W);Oxi(HW)]
βB2: #161-168 GLQYLLEK
βB2: #161-172
GLQYLLEKGDYK
βB2: #169-188
GDYKDSSDFGAPHPQVQSV
R
βB2: #173-188
DSSDFGAPHPQVQSVR

		[Deam(NQ)] βB2: #173-189 DSSDFGAPHPQVQSVRR
19	αA: #55-65 TVLDSGISEVR	βB1: #61-72 LVVFELENFQGR βB1: #203-214 GYQYLLEPGDFR βB2: #82-89 WDSWTSSR βB2: #90-101 RTDSLSSLRPIK βB2: #91-101 TDSLSSLRPIK βB2: #109-120 IILYENPNFTGK [Deam(NQ)] βB2: #109-121 IILYENPNFTGKK βB2: #146-160 VQSGTWVGYQYPGYR [Oxi(HW)] βB2: #161-168 GLQYLLEK βB2: #169-188 GDYKDSSDFGAPHPQVQSV R βB2: #173-188 DSSDFGAPHPQVQSVR
19B	αA: #1-11 MDVTIQHPWFK [Acet(N-term);Oxi(MHW)] αA: #1-12 MDVTIQHPWFKR αA: #13-21 TLGPFYPSR αA: #55-65 TVLDSGISEVR αA: #79-88 HFSPEDLTVK	βA3: #33-44 ITIYDQENFQGK βA4: #107-118 LTIFEQENFLGK βB2: #109-120 IILYENPNFTGK

[Eth(N-term);Meth(H,N-term)]
αA: #89-99 VQDDFVEIHGK
[Meth(N-term,Q)]
αA: #146-157 IQTGLDATHAER
[Eth(N-term);Meth(H,N-term,Q,R);Oxi(HW)]
αA: #158-173
AIPVSREEKPTSAPSS
αB: #1-11 MDIAIHHPWIR
αB: #12-22 RPFFPFHSPSR
αB: #57-72
APSWFDTGLSEMRLEK
[Oxi(M)]
αB: #83-90 HFSPEELK
αB: #124-149
IPADVDPLTITSSLSSDGVLTVN
GPR [Deam(NQ)]

βA3: #33-44 ITIYDQENFQGK
βB1: #61-72
LVVFELENFQGR
[Deam(NQ)]
βB2: #82-89 WDSWTSSR
βB2: #109-120
IILYENPNFTGK
βB2: #161-168 GLQYLLEK
βB2: #169-188
GDYKDSSDFGAPHPQVQSV
R
βB2: #173-188
DSSDFGAPHPQVQSVR
γS: #8-14 ITFYEDK
γS: #8-19 ITFYEDKNFQGR
[Eth(N-term)]
γS: #73-79 WMGLNDR
γS: #147-154 GRQYLLDK

		γS: #159-174 KPIDWGAASPAVQSFR [Deam(NQ);Eth(N-term);Meth(K,N-term);Oxi(HW)]
21	αA: #13-21 TLGPFYPSR	βA3: #33-44 ITIYDQENFQGK
	αA: #55-65 TVLDSGISEVR	βB1: #51-60 AAELPPGNYR
	αB: #83-90 HFSPEELK	βB1: #61-72 LVVFELENFQGR
	αB: #124-149 IPADVDPLTITSSLSSDGVLTVNGPR [Deam(NQ)]	βB1: #73-86 RAEFSGECSNLADR
		βB1: #188-202 VSSGTWVGYQYPGYR
		βB1: #203-214 GYQYLLEPGDFR
		βB2: #69-81 GEQFVFEKGEYPR
		βB2: #90-101 RTDSLSSLRPIK
		βB2: #91-101 TDSLSSLRPIK
		βB2: #91-108 TDSLSSLRPIKVDSQEHK
		βB2: #109-120 IILYENPNFTGK [Eth(N-term)]
		βB2: #109-121 IILYENPNFTGKK
		βB2: #122-140 MEIIDDDVPSFHAHGYQEK
		βB2: #146-160 VQSGTWVGYQYPGYR [Oxi(HW)]

		βB2: #161-168 GLQYLLEK [Eth(N-term)] βB2: #173-188 DSSDFGAPHPQVQSVR		
22	αA: #55-65 TVLDSGISEVR αA: #79-88 HFSPEDLTVK αA: #89-99 VQDDFVEIHGK		CP49: #201-211 AAEEEINSLYK	
28			CP49: #77-89 ALGISSVFLQGLR CP49: #174-191 LMLQTETIQAGAD DFKER [Oxi(M)]	
35	αA: #55-65 TVLDSGISEVR			Filensin: #78-90 LGELAGPEDALAR

Spot numbers refer to spots in Figure 4. Underlined amino acids mark sites of modification and modifications are shown in brackets. Abbreviations Used: Acet – Acetylation; Cam – Carbamylation; Deam – Deamidation; Eth – Ethylation; Fkyn – Formylkynurenin = Double oxidation of Trp; Kyn – Kynurenine = Triple oxidation of Trp; Meth – Methylation; Oxi – Oxidation=Single oxidation; Phos – Phosphorylation; Sulph - Sulphone

Note: From "Identification of crystallin modifications in the human lens cortex and nucleus using laser capture microdissection and CyDye labeling" by Asomugha et al., 2010, *Mol Vis*, *16*, p. 476. Copyright 2010 by Molecular Vision. Reprinted with permission.

APPENDIX B

INSTITUTIONAL REVIEW BOARD APPROVAL

Project Revision/Amendment Form

Form version: October 28, 2010

In MS Word, click in the white boxes and type your text; double-click checkboxes to check/uncheck.

- **Federal regulations require IRB approval before implementing proposed changes. See Section 14 of the IRB Guidebook for Investigators for additional information.**
- **Change means any change, in content or form, to the protocol, consent form, or any supportive materials (such as the Investigator's Brochure, questionnaires, surveys, advertisements, etc.). See Item 4 for more examples.**

1. Today's Date

2. Principal Investigator (PI)

Name (with degree)	Om P. Srivastava	Blazer ID	srivasta
Department	Vision Sciences	Division (if applicable)	
Office Address	Worrell Bldg., Rm. 638	Office Phone	975-7630
E-mail	srivasta@uab.edu	Fax Number	934-5725

Contact person who should receive copies of IRB correspondence (Optional)

Name		E-Mail	
Phone		Fax Number	
Office Address (if different from PI)			

3. UAB IRB Protocol Identification

3.a. Protocol Number	X000202003
3.b. Protocol Title	Proteinase Inhibitors & Crystallin Fragments in Cataract

3.c. Current Status of Protocol—Check ONE box at left; provide numbers and dates where applicable

☐	Study has not yet begun	No participants, data, or specimens have been entered.
X	In progress, open to accrual	Number of participants, data, or specimens entered: Previously collected human lenses from deceased and cataractous lenses following surgery are being used.
☐	Enrollment temporarily suspended by sponsor	
☐	Closed to accrual, but procedures continue as defined in the protocol (therapy, intervention, follow-up visits, etc.)	Date closed: / Number of participants receiving interventions: / Number of participants in long-term follow-up only:
☐	Closed to accrual, and only data analysis continues	Date closed: / Total number of participants entered:

4. Types of Change

Check all types of change that apply, and describe the changes in Item 5.c. or 5.d. as applicable. To help avoid delay in IRB review, please ensure that you provide the required materials and/or information for each type of change checked.

☐ **Protocol revision (change in the IRB-approved protocol)**
In Item 5.c., if applicable, provide sponsor's protocol version number, amendment number, update number, etc.

☐ **Protocol amendment (addition to the IRB-approved protocol)**
In Item 5.c., if applicable, provide funding application document from sponsor, as well as sponsor's protocol version number, amendment number, update number, etc.

X **Add or remove personnel**
In Item 5.c., include name, title/degree, department/division, institutional affiliation, and role(s) in research, and address whether new personnel have any conflict of interest. See "Change in Principal Investigator" in the IRB Guidebook if the principal investigator is being changed.

- X **Add graduate student(s) or postdoctoral fellow(s) working toward thesis, dissertation, or publication**
  ☐ In Item 5.c., (a) identify these individuals by name; (b) provide the working title of the thesis, dissertation, or publication; and (c) indicate whether or not the student's analysis differs in any way from the purpose of the research described in the IRB-approved HSP (e.g., a secondary analysis of data obtained under this HSP).

☐ **Change in source of funding; change or add funding**
In Item 5.c., describe the change or addition in detail, include the applicable OGCA tracking number(s), and provide a copy of the application as funded (or as submitted to the sponsor if pending). Note that some changes in funding may require a new IRB application.

- ☐ **Add or remove performance sites**
  In Item 5.c., identify the site and location, and describe the research-related procedures performed there. If adding site(s), attach notification of permission or IRB approval to perform research there. Also include copy of subcontract, if applicable. If this protocol includes acting as the Coordinating Center for a study, attach IRB approval from any non-UAB site added.
- ☐ **Add or change a genetic component or storage of samples and/or data component—this could include data submissions for Genome-Wide Association Studies (GWAS)**
  To assist you in revising or preparing your submission, please see the IRB Guidebook for Investigators or call the IRB office at 934-3789.
- ☐ **Suspend, re-open, or permanently close protocol to accrual of individuals, data, or samples (IRB approval to remain active)**
  In Item 5.c., indicate the action, provide applicable dates and reasons for action; attach supporting documentation.
- ☐ **Report being forwarded to IRB (e.g., DSMB, sponsor or other monitor)**
  In Item 5.c., include date and source of report, summarize findings, and indicate any recommendations.
- ☐ **Revise or amend consent, assent form(s)**
  Complete Item 5.d.
- ☐ **Addendum (new) consent form**
  Complete Item 5.d.
- ☐ **Add or revise recruitment materials**
  Complete Item 5.d.
- ☐ **Other (e.g., investigator brochure)**
  Indicate the type of change in the space below, and provide details in Item 5.c. or 5.d. as applicable.
  Include a copy of all affected documents, with revisions highlighted as applicable.

▶

5. Description and Rationale
In Item 5.a. and 5.b, check Yes or No and see instructions for Yes responses.
In Item 5.c. and 5.d, describe—and explain the reason for—the change(s) noted in Item 4.

☐Yes ☐No **5.a. Are any of the participants enrolled as normal, healthy controls?**
If yes, describe in detail in Item 5.c. how this change will affect those participants.

☐Yes ☐No **5.b. Does the change affect subject participation, such as procedures, risks, costs, location of services, etc.?**
If yes, FAP-designated units complete a FAP submission and send to fap@uab.edu. Identify the FAP-designated unit in Item 5.c.
For more details on the UAB FAP, see www.uab.edu/cto.

5.c. Protocol Changes: In the space below, briefly describe—and explain the reason for—all change(s) to the protocol.

▶ (a) Add Chinwe Asomugha, a graduate student in PI's laboratory as an investigator. (b) Working title of thesis: Post-translational modifications, structure and function of human lens crystallins. (c) Chinwe's analysis is part of the overall goal of the project to determine molecular mechanism of human age-related cataract development. For this purpose, human lenses either previously collected and stored in the PI's laboratory or those obtained from a local eye bank are being used. The PI's protocol has been approved by the UAB-IRB. Student had already been added, but thesis title had not been submitted. CLS 3/16/10

5.d. Consent and Recruitment Changes: In the space below,
(a) describe all changes to IRB-approved forms or recruitment materials and the reasons for them;
(b) describe the reasons for the addition of any materials (e.g., addendum consent, recruitment); and
(c) indicate either how and when you will reconsent enrolled participants or why reconsenting is not necessary (not applicable for recruitment materials).

Also, indicate the number of forms changed or added. For new forms, provide 1 copy. For revised documents, provide 3 copies:
- **a copy of the currently approved document (showing the IRB approval stamp, if applicable)**
- **a revised copy highlighting all proposed changes with "tracked" changes**
- **a revised copy for the IRB approval stamp.**

▶

Signature of Principal Investigator Om P. Srivastava Date 03-15-11